ISTANBUL TECHNICAL UNIVERSITY ★ GRADUATE SCHOOL

HIGH SENSITIVE TORQUE CONTROL OF PERMANENT MAGNET SYNCHRONOUS MOTOR FOR NATIONAL MILITARY APPLICATIONS

M.Sc. THESIS

Mehmet Eralp KÖSE

Department of Electronics and Communication Engineering

Electronic Engineering Programme

JULY 2021

ISTANBUL TECHNICAL UNIVERSITY ★ GRADUATE SCHOOL

HIGH SENSITIVE TORQUE CONTROL OF PERMANENT MAGNET SYNCHRONOUS MOTOR FOR MILITARY APPLICATIONS

M.Sc. THESIS

Mehmet Eralp KÖSE
(504181249)

Department of Electronics and Communication Engineering

Electronic Engineering Programme

Thesis Advisor: Assoc.Prof. Dr. Derya Ahmet KOCABAŞ

JULY 2021

İSTANBUL TEKNİK ÜNİVERSİTESİ ★ LİSANSÜSTÜ EĞİTİM ENSTİTÜSÜ

YERLİ ASKERİ UYGULAMALAR İÇİN DAİMİ MIKNATISLI SENKRON MOTORLARDA YÜKSEK HASSASİYETLİ MOMENT KONTROLÜ

YÜKSEK LİSANS TEZİ

Mehmet Eralp KÖSE
(504181249)

Elektronik ve Haberleşme Mühendisliği Anabilim Dalı

Elektronik Mühendisliği Programı

Tez Danışmanı: Doç. Dr. Derya Ahmet KOCABAŞ

TEMMUZ 2021

Mehmet Eralp KÖSE, a M.Sc. student of ITU Graduate School student ID 504181249 successfully defended the thesis entitled "HIGH SENSITIVE TORQUE CONTROL OF PERMANENT MAGNET SYNCHRONOUS MOTOR FOR MILITARY APPLICATIONS", which he prepared after fulfilling the requirements specified in the associated legislations, before the jury whose signatures are below.

Thesis Advisor : **Assoc. Prof. Dr. Derya Ahmet KOCABAŞ** ....
Istanbul Technical University

Jury Members : **Prof. Dr. Ece Olcay GÜNEŞ** ....
Istanbul Technical University

Prof. Dr. Kamuran Nur BEKİROĞLU ....
Yildiz Technical University

Date of Submission : 30 June 2021
Date of Defense : 26 July 2021

To my dear family,

FOREWORD

Firstly, I want to express my sincere thanks to my supervisor Asst. Prof. Dr. Derya Ahmet KOCABAŞ. He always supports and helps me. Thanks to Aselsan Academy for providing this Master's program support and thanks to Aselsan Inc. for laboratory and equipment support. Also, I would like to thank my coworkers. Especially, I am grateful to Mr. Fehmi KAYA and Mr. Erdinç YALVAÇ for their kind support and encouragement during this experiment.
Finally, I would like to thank my dear family and friends.

July 2021 Mehmet Eralp KÖSE

TABLE OF CONTENTS

Page

FOREWORD ..... **ix**
TABLE OF CONTENTS ..... **xi**
ABBREVIATIONS ..... **xiii**
SYMBOLS ..... **xv**
LIST OF TABLES ..... **xvii**
LIST OF FIGURES ..... **xix**
SUMMARY ..... **xxiii**
ÖZET ..... **xxv**
1. INTRODUCTION **1**
1.1 Purpose of Thesis 2
1.2 Literature Review 3
2. ELECTRIC MOTORS AND THEIR PROPERTIES **7**
2.1 Types of Electrical Motors 7
2.1.1 DC motors and their properties 7
2.1.1.1 DC motor structure 8
2.1.1.2 DC Motor Working Principles 12
2.1.1.3 Mathematical model of DC motor 14
2.1.2 AC motor properties and advantages over DC motors 16
2.2 Permanent Magnet Synchronous Motor 16
2.2.1 Operational principles 17
2.2.2 Mathematical model 18
2.2.3 Power and torque calculation 20
2.3 Control of Permanent Magnet Synchronous Motor 21
2.3.1 Scalar control 22
2.3.2 Vector control 23
2.3.2.1 Field oriented control 23
2.3.2.2 Direct torque control 25
2.4 Hardware structure 26
2.4.1 Communication protocols between intelligent units 27
2.4.1.1 SPI protocol 27
2.4.1.2 I2C protocol 28
2.4.1.3 RS232 protocol 29
2.4.1.4 CAN protocol 29
2.5 Military Standards at PMSM Control 30
3. IMPLEMENTATION OF FIELD ORIENTED CONTROL OF PMSM **31**
3.1 d-q Reference Coordinate System and Transformations 31
3.2 SVPWM Production 32
3.3 Torque Control with Field Oriented Control System 36
3.4 Control Cards, Demo boards and MATLAB Programming 37
3.4.1 MATLAB properties and application 37
3.4.2 Model based simulations 38
3.4.3 Hardware in the loop and embedded coder support package 38

3.4.4 Microprocessor, inverter and position manager (encoder) demo board's properties 40
3.4.5 Motor properties 41
3.5 Simulink Model 42
4. PROGRAMMING, TEST AND EXPERIMENTS 45
4.1 Design and Practical Implementations 45
4.1.1 Motor driver block schematic 45
4.1.2 Test setup system and block schematic 46
4.1.3 Absolute encoder integration 48
4.1.4 Motor torque constant verification 50
4.1.5 CAN communication basis and performance analysis 51
4.2 Motor Driver Performance Tests 53
4.3 Temperature Tests For Motor Driver Card 61
4.4 Electromagnetic Compatibility Tests 67
4.4.1 MIL-STD-461 CE102 and CE101 tests 68
4.4.2 CE 102 Setup 68
4.4.2.1 Motor driver noise and improvement studies 69
4.4.3 MIL-STD-461 CE101 test 72
4.5 Comments on the Results 79
5. CONCLUSIONS AND RECOMMENDATIONS 81
REFERENCES 83
APPENDICES 87
APPENDIX A 88
APPENDIX B 96
CURRICULUM VITAE 101

ABBREVIATIONS

AC	: Alternating Current
DC	: Direct Current
PMSM	: Permanent Magnet Synchronous Motor
FOC	: Field Oriented Control
PWM	: Pulse Width Modulation
SVPWM	: Space Vector Pulse Width Modulation
THD	: Total Harmonic Distortion
EMF	: Electromotive Force
BLDC	: Brushless DC
VFD	: Variable Frequency Drive
FOC	: Direct Torque Control
MISO	: Master Input/Slave Output
MOSI	: Master Output/Slave Input
SCLK	: Clock (SPI)
SS/CS	: Slave select/Chip select
SDA	: Data
SCL	: Clock (I2C)
CAN	: Controller Area Network
SPI	: Serial Peripheral Interface
EMI	: Electromagnetic Interference
EMC	: Electromagnetic Compatibility
MOSFET	: Metal Oxide Semiconductor Field
GPIO	: General Purpose Input Output
TI	: Texas Instruments
ADC	: Analog to Digital Converter
DSP	: Digital signal processors
LISN	: Line Impedance Stabilization Network
CE	: Conducted Emission
EUT	: Equipment Under Test
App	: Appendix

Mbps **:** Megabits per second

SSI **:** Synchronous Serial Interface

SYMBOLS

C	: Capacitance
L	: Inductor
$\mathbf{E_c}$	: Inductor Back EMF voltage of the DC motor
$\mathbf{K_b}$	: Back EMF constant
$\boldsymbol{\omega_m}$	: Rotational Speed
$\mathbf{T_e}$	: Electrical Torque
$\mathbf{I_a}$	: Armature Current
$\mathbf{R_a}$	: Armature Resistance
$\mathbf{U_a}$	: Terminal Voltage
B	: Viscous Friction coefficient
$\mathbf{T_L}$	: Load Torque
$\mathbf{E_{ph}}$	: Electromotive force (Volts)
f	: frequency (Hertz)
$\mathbf{Ø_m}$	: flux per pole (Weber)
$\mathbf{T_{ph}}$	: number of turn per phase
$\mathbf{L_a}$	: Armature Inductor
$\mathbf{L_a}$	: Armature Inductor
$\mathbf{L_a}$	: Armature Inductor
$\mathbf{V_d}$	: Direct Axis Voltage
$\mathbf{I_d}$	: Direct Axis Current
$\mathbf{V_q}$	: Quadrature Axis Voltage
$\mathbf{I_q}$	: Quadrature Axis Current
$\boldsymbol{\omega_{re}}$	: Angular Speed
$\boldsymbol{\theta_r}$	: Position
$\mathbf{L_d}$	: Direct Axis Inductance
$\mathbf{L_q}$	: Quadrature Axis Inductance
$\mathbf{R_s}$	: Stator Resistance
$\boldsymbol{\lambda_d}$	: Direct Axis Flux
$\boldsymbol{\lambda_q}$	: Quadrature Axis Flux

T_e : Electromagnetic Torque

T_L : Load Torque

p : Pole Pairs Number

V_k : k^{th} active vector

T_k : time period duration that applied V_k vector

T_{k+1} : time period duration that applied V_{k+1} vector

T_s : time period of PWM switching which corresponds to $T_0+T_k+T_{k+1}$

T_0 : time period duration that applied zero voltage vector

I_a : Phase-A Current

I_b : Phase-B Current

I_c : Phase-C Current

P : Proportional Gain

I : Integral Gain

D : Derivative Gain

LIST OF TABLES

Page

Table 4.1 : Torque values and corresponding RMS currents.............................. 51
Table 4.2 : Torque ripple according to corresponding switching frequency 60

LIST OF FIGURES

Page

Figure 1.1 : Satcom on the move for aircraft, submarine and ship platforms [1]. 2
Figure 1.2 : Satcom on the move for varying land platforms [1]. 3
Figure 2.1 : Electric motor types. 7
Figure 2.2 : Structure of motor [22]. 8
Figure 2.3 : Structure of yoke [22]. 9
Figure 2.4 : Structure of pole [22]. 10
Figure 2.5 : The field winding on the core [22]. 10
Figure 2.6 : Armature core [22]. 11
Figure 2.7 : Armature winding [22]. 11
Figure 2.8 : Commutator ring [22]. 12
Figure 2.9 : A pair of carbon brushes [22]. 12
Figure 2.10 : DC motor working principles [22]. 13
Figure 2.11 : Equivalent Circuit of DC motor [23]. 14
Figure 2.12 : Dynamic equivalent circuit of PMSM with d-q axis. 19
Figure 2.13 : PMSM control strategies. 22
Figure 2.14 : FOC with hysteresis modulation [32]. 24
Figure 2.15 : FOC with space vector modulation [32]. 24
Figure 2.16 : DTC with hysteresis modulation [36]. 25
Figure 2.17 : DTC with space vector modulation [36]. 26
Figure 2.18 : Basically PMSM control hardware structure. 27
Figure 2.19 : SPI protocol [37]. 28
Figure 2.20 : I2C protocol [37]. 28
Figure 2.21 : RS232 protocol [37]. 29
Figure 2.22 : CAN protocol [37]. 30
Figure 3.1 : Clarke transformation logic [40]. 32
Figure 3.2 : Park transformation logic [41]. 32
Figure 3.3 : Voltage source inverter diagram. 33
Figure 3.4 : Basic voltage vectors, reference vector and modulation plane[13]. 34
Figure 3.5 : Two adjacent vectors and resulting reference vector V_{ref} which is associated with space vector V_s [13]. 35
Figure 3.6 : Torque control block diagram with FOC. 36
Figure 3.7 : C2000 toolbox. 39
Figure 3.8 : Torque control blocks at SIMULINK. 42
Figure 3.9 : Clarke, park, control, SWPWM structure. 42
Figure 3.10 : Control PI blocks for Id and Iq. 43
Figure 3.11 : CAN message blocks. 43
Figure 4.1 : Intended motor driver schematic. 45
Figure 4.2 : Motor driver test setup block schematic. 46
Figure 4.3 : Motor driver test setup. 47
Figure 4.4 : Motor, encoder and torque meter. 48
Figure 4.5 : Absolute encoder logic. 49

Figure 4.6 : Absolute encoder and microproccessor connection. 50
Figure 4.7 : Encoder, inverter, PMSM connections...50
Figure 4.8 : Torque vs RMS current graph...51
Figure 4.9 : Simulink project which satisfies receiving and transmitting via CAN communication. 52
Figure 4.10 : Intended torque, proportional and internal gain coefficient blocks. 53
Figure 4.11 : Torque value observation at 10 kHz switching frequency............54
Figure 4.12 : Torque ripple at 10 kHz switching frequency................................54
Figure 4.13 : Iq current characteristic at 10 kHz switching frequency. 54
Figure 4.14 : Step response settling time at 10 kHz switching frequency..........55
Figure 4.15 : Torque value observation at 15 kHz switching frequency............55
Figure 4.16 : Torque ripple at 15 kHz switching frequency................................56
Figure 4.17 : Iq current characteristic at 15 kHz switching frequency. 56
Figure 4.18 : Step response settling time at 15 kHz switching frequency..........56
Figure 4.19 : Torque value observation at 20 kHz switching frequency............57
Figure 4.20 : Torque ripple at 20 kHz switching frequency................................57
Figure 4.21 : Iq current characteristic at 20 kHz switching frequency. 57
Figure 4.22 : Step response settling time at 20 kHz switching frequency..........58
Figure 4.23 : Torque value observation at 25 kHz switching frequency............58
Figure 4.24 : Torque ripple at 25 kHz switching frequency................................58
Figure 4.25 : Iq current characteristic at 25 kHz switching frequency. 59
Figure 4.26 : Step response settling time at 25 kHz switching frequency..........59
Figure 4.27 : Temperature test setup at the oven...61
Figure 4.28 : The oven test...62
Figure 4.29 : Motor driver card in the oven. 63
Figure 4.30 : The temperature of the oven..63
Figure 4.31 : Temperature measurement with the thermistor. 64
Figure 4.32 : Torque characteristic at (-40) degree...65
Figure 4.33 : Torque ripple at (-40) degree...65
Figure 4.34 : Iq current characteristic at (-40) degree..65
Figure 4.35 : Settling time at (-40) degree...66
Figure 4.36 : Torque characteristic at 55 degree...66
Figure 4.37 : Torque ripple at 55 degree...66
Figure 4.38 : Iq current characteristic at 55 degree...67
Figure 4.39 : Settling time at 55 degree..67
Figure 4.40 : CE 102 setup...69
Figure 4.41 : Ambient noise...70
Figure 4.42 : Motor driver noise..70
Figure 4.43 : LC filter. 71
Figure 4.44 : Suppression curve for 100 Hz to 100 kHz. 71
Figure 4.45 : Motor driver noise with LC filter. 72
Figure 4.46 : Setup for CE101 test...73
Figure 4.47 : CE101 limit for aircraft applications..74
Figure 4.48 : 0-1 kHz frequency noise for aircraft platform...............................75
Figure 4.49 : 1-10 kHz frequency noise for aircraft platform.............................75
Figure 4.50 : CE101 limit for surface ships and submarine applications..........76
Figure 4.51 : 0-2.6 kHz frequency noise for submarine and ship platforms. 76
Figure 4.52 : 2.6-10 kHz frequency noise for submarine and ship platforms. ...77
Figure 4.53 : 0-1 kHz frequency noise with LC filter for aircraft platform. 77

Figure 4.54 : 1-10 kHz frequency noise with LC filter for aircraft platform. 78
Figure 4.55 : -2.6 kHz frequency noise with LC lilter for submarine and ship platforms. 78
Figure 4.56 : 2.6-10 kHz frequency noise with LC filter for submarine and ship platforms. 78
Figure A.1: CE101 limit for surface ships and submarine applications, DC. 90
Figure A.2: CE101 limit for surface ships and submarine applications, 60 Hz. 91
Figure A.3: CE101 limit for surface ships and submarine applications, 400 Hz. 92
Figure A.4: CE101 limit for Navy ASW aircraft and Army aircraft (including flight line) applications. 93
Figure A.5: Measurement system check. 94
Figure A.6: Measurement setup. 95
Figure B.1: CE102 limit (EUT power leads, AC and DC) for all applications... 98
Figure B.2: Measurement system check setup. 99
Figure B.3: Measurement system check setup. 100

HIGH SENSITIVE TORQUE CONTROL OF PERMANENT MAGNET SYNCHRONOUS MOTOR FOR NATIONAL MILITARY APPLICATIONS

SUMMARY

Electric motors are systems that convert electrical energy into mechanical energy, and they have a very important place in the industry. DC motors are often preferred for applications that do not require driving precision due to their ease of use and low cost. On the other hand, alternating current motors have many superior features over direct current motors. Alternating current motors have higher efficiency, lower maintenance costs, and high torque to volume ratio. They are more reliable and durable motors.

One of the most important advantages of alternating current motors is that they offer superior motor control opportunities. With these motors, speed and torque control can be done with appropriate control methods. With the appropriate control method, torque control can be done at very low speeds. Because of these features, alternating current motors are preferred in control applications that require precision. With the developing magnet technology, permanent magnet electric motors come to the fore with their high efficiency.

Power electronics and control applications are used together for the control of alternating current motors, and there are different methods and circuit structures in the literature for this. Control methods are basically divided into two as scalar and vector control. In scalar control, the "voltage/frequency" ratio is kept constant so that the flux remains constant, and the speed and torque are adjusted with the change in frequency. In this method, only the magnitudes of flux and current are controlled, rotor position information is not received as feedback and is not included in the control loop. In vector control, in addition to the magnitude of the flux and the current, the angle between them is also controlled, and rotor position information is required as feedback while speed and torque controls are being made. Direct torque control and field oriented control are sub-branches of vector control. In field oriented control, which is the focus of this study, the rotor position is needed. This information can be obtained with sensors, or it can be detected by sensorless estimation methods, and position information is used in control. In this way, while precise speed and torque controls are carried out, a more stable control is provided in a steady state condition.

In this thesis, high precision torque control of permanent magnet synchronous motors for use in military systems has been studied. The main goal is to design motor drivers that are imported and provide torque control in military stabilization systems and to reduce foreign dependency by using domestic and national motor drivers in these systems. Since high precision torque control is aimed even at low speeds in military applications, field oriented control was used. Due to the high military expectations, sensor control was preferred, and an absolute encoder was preferred as position sensor. This method can be applied in many areas with different power and torque requirements. Stabilization systems were chosen as the application. Based on filed oriented control, a national control algorithm has been applied, and an infrastructure adaptable to the power and torque requirements of the application to be used has been established. In this context, TMS320F28069M type numbered processor from Texas Instruments (TI) company, and trial card were used as controller. Inverter design is implemented with modular circuits of TI company, and MOSFET switches are used. Algorithm development studies were carried out in MATLAB/Simulink environment.

An absolute encoder is used to increase sensitivity. With this encoder, absolute position information can be accessed and position information is not lost even if there is a power cut. The position information obtained from here is transferred to the field oriented torque control loop. By carrying out the load test, the moment ripple in the steady state and its performance at the rated load have been determined. Different communication methods have been used to determine the interaction of the performance of the system. Since it was seen that the method called "external mode" which works over Simulink, became insufficient and did not work efficiently as the algorithm became more complex, CAN communication was started, and it was ensured that the instantaneous torque value could be controlled with the P and I coefficients that can be changed instantly via the PI controller. Input and output feedbacks were instantly observed via Simulink, algorithms were written in Simulink, and all hardware was communicated with Simulink via CAN communication. The effect of switching frequency on torque ripple was investigated with appropriate P,I coefficients, and as a result of the optimization, this ripple was reduced below the values expected by the standards.

In the second part of the study, compliance checks were made in terms of military standards, and temperature and electromagnetic compatibility tests were completed. Since a device with a chassis was not aimed directly, mechanical compatibility tests were not needed. Temperature tests were carried out between -40°C and +55°C in accordance with the standards, and the distortions observed in the clock frequency of the processor at values close to the limit temperatures in the first tests were overcome by the use of an external oscillator. Although an increase in torque fluctuation was observed in this test, the maximum value remained below 3%.

In electromagnetic compatibility tests, MIL-STD 461 CE101 and CE102 tests were carried out, and the noise emitted by the device in various frequency ranges was measured. Although the noise remained above the acceptable level in the first CE102 test, the circuit passed the tests successfully with the appropriate filter design. In addition, with the study, infrastructure was created for the selection of materials for further studies.

As a result, within the scope of this thesis, low torque vibration, high precision field oriented torque control of a permanent magnet synchronous motor in accordance with military temperature and EMC standards has been realized. With the output of the thesis, domestic equivalents of hardware and software products supplied from abroad and used in national applications have been obtained, contributing to the country's economy and reducing foreign dependency in this area.

YERLİ ASKERİ UYGULAMALAR İÇİN DAİMİ MIKNATISLI SENKRON MOTORLARDA YÜKSEK HASSASİYETLİ MOMENT KONTROLÜ

ÖZET

Elektrik motorları elektrik enerjisini mekanik enerjiye çeviren sistemlerdir ve endüstride çok önemli bir yere sahiptirler. Doğru akım motorları, sürüş hassasiyeti gerektirmeyen uygulamalar için kullanım kolaylığı, düşük maliyeti gibi sebeplerden dolayı sıklıkla tercih edilmektedir. Bunun yanı sıra, alternatif akım motorları doğru akım motorlarına karşı pek çok üstün özelliğe sahiptir. Alternatif akım motorları daha yüksek verimliliğe sahiptirler, bakım masrafları daha düşüktür, yüksek bir "moment / hacim" oranına sahiptirler. Güvenilirliği ve dayanıklılığı daha yüksek motorlardır. Alternatif akım motorlarının en önemli avantajlarından birisi üstün motor kontrolü fırsatları sunmasıdır. Bu motorlarla uygun kontrol metotları ile hız ve moment kontrolü yapılabilir. Uygun kontrol yöntemi ile çok düşük hızlarda da moment kontrolü yapılabilir. Bu özelliklerden dolayı hassasiyet gerektiren kontrol uygulamalarında alternatif akım motorları tercih edilir. Gelişen mıknatıs teknolojisi ile daimi mıknatıslı elektrik motorları yüksek verimleri ile ön plana çıkmaktadırlar.

Alternatif akım motorlarının kontrolü için güç elektroniği ve kontrol uygulamaları bir arada kullanılır ve bunun için literatürde değişik yöntemler ve devre yapıları yer almaktadır. Kontrol yöntemleri temel anlamda skaler ve vektör kontrol olarak ikiye ayrılmaktadır. Skaler kontrolde akı sabit kalacak şekilde "gerilim/frekans" oranı sabit tutulur ve frekansın da değişimi ile hız ve moment ayarlanır. Bu yöntemde akı ile akımın sadece büyüklükleri kontrol edilir, rotor konum bilgisi geri bildirim olarak alınmaz ve kontrol döngüsüne katılmaz. Vektör kontrolde ise akı ile akımın büyüklüklerinin yanısıra aralarındaki açı da kontrol edilir, hız ve moment kontrolleri yapılırken rotor konum bilgisi de geri bildirim olarak gereklidir. Doğrudan moment kontrolü ve alan yönlendirmeli kontrol vektör kontrolünün alt dallarıdır. Bu çalışmanın odağı olan alan yönlendirmeli kontrolde rotor konumuna ihtiyaç duyulur. Bu bilgi algılayıcılı olarak elde edilebileceği gibi algılayıcısız kestririm yöntemleri ile de tespit edilerek kontrolde kullanılabilir. Bu sayede hassas hız ve moment kontrolleri gerçekleştirilirken sürekli halde daha kararlı bir kontrol sağlanır.

Bu tez kapsamında askeri sistemlerde kullanılmak üzere daimi mıknatıslı senkron motorlarda yüksek hassasiyetli moment kontrolü üzerinde çalışılmıştır. Temel hedef, ithal edilerek temin edilen ve askeri stabilizasyon sistemlerinde moment kontrolü yapan motor sürücülerini tasarlamak, bu sistemlerde yerli ve milli motor sürücü kullanımı ile dışa bağımlılığı azaltmaktır. Askeri uygulamalarda düşük hızlarda dahi yüksek hassasiyetli moment kontrolü hedeflendiğinden alan yönlendirmeli kontrol kullanılmıştır. Askeri beklentilerin yüksek olması sebebiyle algılayıcılı kontrol tercih edilmiş olup, algılayıcı olarak mutlak kod çözücü (absolute encoder) tercih edilmiştir. Bu sayede düşük hızlarda dahi pozisyon bilgisi net ve kesin şekilde alınabilmiş ve işlenmiştir. Bu kontrol yöntemi farklı güç ve moment isterlerine sahip birçok alanda uygulanabilir. Yüksek güç isteyen enerji sistemleri, özellikle son yıllarda önemi giderek artan elektrikli araçlar, daha düşük gücün yeterli olduğu çamaşır makinası ve askeri uygulamalarda büyük öneme sahip sabit konumlandırma (stabilizasyon) sistemleri daimi mıknatıslı elektrik motor kontrolünün yapıldığı uygulama alanlarından bazılarıdır. Bu tez kapsamında uygulama olarak sabit konumlandırma

(stabilizasyon) sistemleri seçilmiştir. Alan yönlendirmeli kontrol temel alınmış ve yerli kontrol algoritması geliştirilerek kullanılacak uygulamanın güç ve moment isterlerine uyarlanabilir bir altyapı tesis edilmiştir. Bu kapsamda kontrolcü olarak Texas Instruments (TI) firmasının TMS320F28069M tip numaralı işlemcisi ve deneme kartı kullanılmıştır. Evirici tasarımı TI firmasının modüler yapıdaki devreleri ile gerçeklenmiş olup MOSFET anahtarlar kullanılmıştır. Algoritma geliştirme çalışmaları MATLAB/Simulink ortamında gerçekleştirilmiştir. Hassasiyeti artırmak amacıyla mutlak kodlayıcı (absolute encoder) kullanılmıştır. Bu kodlayıcı ile mutlak pozisyon bilgisine erişilebilmekte ve güç kesintisi olsa dahi konum bilgisi kaybolmamaktadır. Buradan alınan pozisyon bilgisi alan yönlendirmeli moment kontrolü döngüsüne aktarılmıştır. Algılayıcı kod çözücü ile işlemcinin haberleşmesi için uygun veri dönüşümleri yapılmıştır ve SPI haberleşme protokolü kullanılmıştır. Yük testi yapılarak sürekli halde moment dalgalılığı ve anma yükündeki başarımı tespit edilmiştir. Sistemin performansının etkileşiminin tespit edilebilmesi için farklı haberleşme yöntemleri kullanılmıştır. Simulink üzerinden çalışan “external mode” adı verilen yöntemin algoritma karmaşıklaştıkça yetersiz kaldığı ve verimli çalışmadığı görüldüğünden CAN haberleşmesine geçilmiş ve anlık moment değerinin, PI kontrolcü üzerinden anlık değiştirilebilen P ve I katsayıları ile kontrol edilebilmesi sağlanmıştır. Giriş ve çıkış geri beslemeleri Simulink üzerinden anlık olarak gözlemlenmiş, algoritmalar Simulink’te yazılmış ve tüm donanım CAN haberleşmesi vasıtasıyla Simulink ile haberleştirilmiştir. Uygun P,I katsayılarında anahtarlama frekansının moment dalgalılığı üzerindeki etkisi incelenmiş olup en uygunlaştırma sonucunda bu dalgalılık, standartların beklediği değerlerin altına düşürülmüştür.

Çalışmanın ikinci kısmında askeri standartlar açısından uygunluk denetimi yapılmış, sıcaklık ve elektromanyetik uyumluluk testleri tamamlanmıştır. Doğrudan şaseli bir cihaz hedeflenmediğinden mekanik uygunluk testlerine ihtiyaç duyulmamıştır. Askeri çevre koşulları testleri kapsamında standartların gerekliliği olarak sıcaklık testleri fırın ortamında -40°C ile +55°C arasında gerçekleştirilmiş olup ilk testlerde sınır sıcaklılara yakın değerlerde işlemcinin saat frekansında gözlemlenen bozulmalar harici osilatör kullanımı ile aşılmıştır. Bu testte moment dalgalanmasında bir artış görülse de en büyük değer %3’ün altında kalmıştır.

Elektromanyetik uyumluluk testlerinde standartlarda belirlenen test ortamları kurulmuştur. MIL-STD 461 CE101 (“İletilen Emisyonlar Ses Frekans Akımları, Güç Kabloları”) ve CE102 (“İletilen Emisyonlar Radyo Frekansı Potansiyelleri, Güç Kabloları”) testleri yapılmış olup cihazın çeşitli frekans aralıklarında ortama yaydığı gürültüler ölçümlenmiştir. CE101 testinde 10 kHz’e kadar olan frekans aralığı taranmış olup CE102 testinde 10 kHz ile 10 MHz arasındaki frekans bandı incelenmiştir. Kontrollü deney yapabilmek adına başlangıçta ortam gürültüsü ölçülmüştür ve ortama gürültü yayan başka bir cihaz olmadığının doğrulaması yapılmıştır. Motor sürücüler çalıştırıldıktan sonra yapılan ilk CE102 testinde başlangıçta gürültü kabul edilebilir seviyenin üzerinde kalsa da uygun filtre tasarımı ile devre testlerden başarı ile geçmiştir. Elektromanyetik uyumluluk testlerinde kabul edilebilir gürültü limitleri farklı olan hava, kara ve deniz platformlarının her biri için gözlemlemeler yapılmış ve hepsinde başarı sağlanmıştır. Ayrıca yapılan çalışma ile sonraki çalışmalar için malzeme seçimi konusunda da bir altyapı oluşturulmuştur.

Sonuç olarak, bu tez kapsamında askeri sıcaklık ve EMC standartlarına uygun, daimi mıknatıslı senkron motorun düşük moment titreşimli, yüksek hassasiyetli alan yönlendirmeli moment kontrolü gerçekleştirilmiştir. Tez çıktısı ile milli uygulamalarda yurt dışından temin edilerek kullanılan donanım ve yazılım ürünlerinin yerli muadilleri elde edilerek ülke ekonomisine katkı yapılmış olup bu alandaki dışa bağımlılık azaltılmıştır.

1. INTRODUCTION

Motors are one of the most important devices in the industry for years. Motors are started to use with the industrial revolution and internal combustion engines, which were invented at the end of the 18th century. Electric motor studies also started in the early 19th century. In 1832, William Sturgeon introduced the first commutator DC electric motor. In 1888, Nikola Tesla published a paper that would replace existing converters and motors, and it can be said that AC motor history started. Before the development of semiconductor components at power electronics, frequency operations, and varying frequency was difficult so constant speed applications were applied. Generally, cage induction motors were used, and a variable external resistance was connected to the rotor circuit. Thus, a considerable range of speed control was allowed. Although synchronous and asynchronous motors were developed daily, the biggest breakthrough was achieved with semiconductor technology in the late 20th century. AC motors are based on frequency technology, and transistors have a very important role for high switching applications. With the development of variable frequency drives, scalar and vector control techniques were invented. By scalar control, only the magnitude of supply voltage is controlled without position control. If a load is constant, this method can be preferred. Vector control allows magnitude and phase control so torque and speed control of the motor can be achieved sensitively. Constant speed control can be satisfied at varying torque loads, and constant torque can be satisfied at varying speed loads.

Motor drive technologies are developing, and their importance is increasing day by day. Motor driving is important for civil applications and energy systems such as washing machines, wind tribunes, electric generation, etc., and electric car technology is another important sector nowadays. Military applications are also a very important area for governments, and a variety of technologies are developing under the military's leadership. Motor driving is also used in military applications. Stabilization systems are one of the important military applications. Continuously and non-interruptible communication is a crucial thing, and these stabilization systems satisfy satellite communication. Servo motors and Permanent Magnet Synchronous Motors can be used for stabilization systems.

Military applications should satisfy some requirements, and generally, these applications do not accept any errors. This thesis was focusing high sensitive torque control of Permanent Magnet Synchronous Motor, which satisfies military standards.

1.1 Purpose of Thesis

Purpose of this thesis is achieving torque control of PMSM with national design drivers those are compatible with military temperature and EMC standards instead of using imported foreign made drivers. In this thesis, PMSM torque control was satisfied with high sensitivity. It was intended that this motor driver provided the military standards, and it was examined. The torque control algorithm was created with the base of field oriented control topology and this algorithm was tested within the scope of this thesis. Simulink platform and TMS320F28069M microprocessor from Texas Instruments (TI) were used. The main aim was to provide an algorithm for the motor driver. This algorithm was also implemented and tested in the real world. Performance analyses were done. These motor drivers would intended to use a lot of platforms like aircraft, submarines, ships, and land platforms.

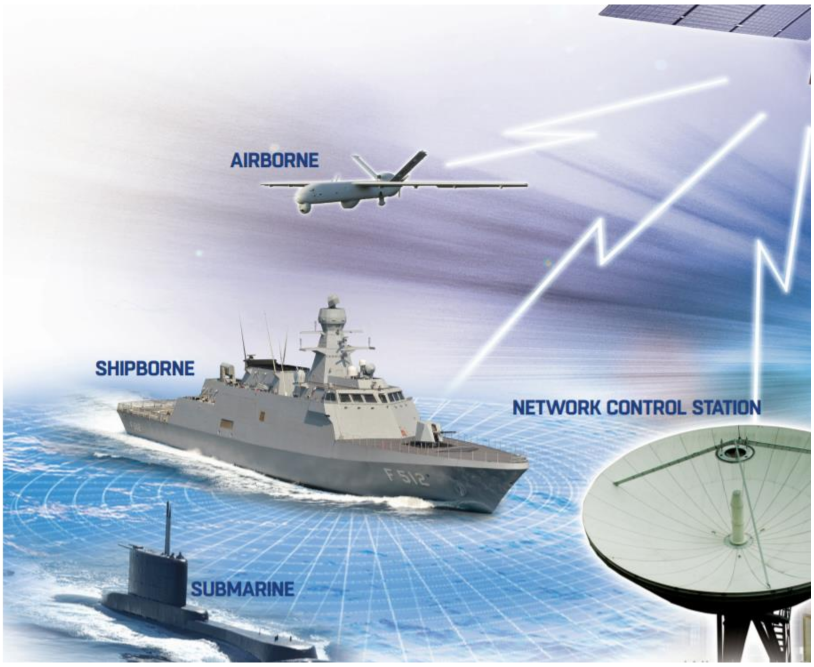

Figure 1.1 : Satcom on the move for aircraft, submarine and ship platforms [1].

Figure 1.2 : Satcom on the move for varying land platforms [1].

Some of application areas for motor drivers are shown in Figure 1.1, and Figure 1.2. The amount of power and torque for the motor drivers will be updated according to the application. Therefore, generic torque value was tested, and demo boards were used for control, inverter, and encoder cards that would be explained in the next parts.

1.2 Literature Review

Permanent Magnet Synchronous Motor driving studies gained speed with the development of using semiconductors at power electronics applications. Inıtially, the importance of PMSM and its invention was reviewed. Driving methods of PMSM were examined, and it was investigated whether there were studies for military applications or not.

Electric Motors are widely used in the industry, and invention of electric motors dates to the 19th century. With the necessity of high efficient motors and with the development of permanent magnets, Permanent Magnet Synchronous Motor technology has been developing day by day. D.P.M Cahill and B. Adkinds published "The permanent magnet synchronous motor" in 1962 [2]. Also, R. Krishman and A.J. Beutler published "Performance and design of an axial field permanent magnet synchronous motor servo drive" in 1985 [3]. E. Richter et al. published "The ferrite PM ac motor-A technical and economic assessment" in 1985 [4]. In this sources, the properties of PMSM and PMSM drives were explained. Brush maintenance, high power density, high efficiency properties were mentioned. These sources were important for developing PMSM usage. In 2008, M. Benhaddadi and G. Oliver experimented with high efficiency motors and drive penetration [5]. These motors were used from low speed to high speed applications. Do-Kwan Hong et al. and Zhang Fengge et al. mentioned high speed motor applications for aerospace, energy, medical treatment areas. [6, 7]. Actually, PMSM control systems developed with the advance of semiconductor and microprocessors in the early 1970s. Flux and current have to be controlled in most digital motor drive systems. Control theories for motor control were invented in 1970s. Capolino and G. Andre stated that field oriented control was introduced in the early 1970s in Germany, and it was very popular up to the end of the 1990s. Good transient performances were observed with this method. In addition, direct torque control was also introduced in both Germany and Japan from Depenbrock and Takahashi in the 1980s. It was stated that Mechanical sensors can be eliminated with this method [8, 9]. In 1986, a paper was published about microprocessor-based FOC of a current source inverter-fed induction motor drive [10]. In the following years, FOC has been developed and a very popular technique. Park transformation and d-q transformation were initially proposed by Robert H.Park in 1929 [8]. These theories showed the conversion from three phase systems into two phase systems. Thus, AC machine can be modeled as DC machine thanks to these theories. D.W. Novotny and P.L. Jansen mentioned the torque production, d-q axes, and maximum, minimum torque conditions in "Field oriented control of synchronous machines" [11]. Inverters could be controlled with several techniques. Smooth and sinusoidal waveform with less harmonic was intended with these techniques [12]. PWM was the most convenient strategy converters control. SVPWM was an advanced control method which was used to generate AC voltage to drive AC machines with variable speed [13]. It was stated that Total Harmonic Distortion (THD) minimization is satisfied with SVPWM [14]. M. Sulaimanl et al. reported that the three-phase voltage source inverter's upper three devices have a special switching sequence for space vector modulation. This special switching sequence results in three pseudo-sinusoidal currents in the stator phase [15]. SVPWM technique was used in this thesis. Speed and torque control can be satisfied sensorless at PMSM [16]. However, high-resolution rotor position feedback is required for a smooth and noiseless steady state behavior. Therefore, position information should be obtained with encoders or resolvers. Encoders are a form of analog to digital converters. Angle is converted to corresponding digital code with the electrical pulses or data bits. Data processing is satisfied with these digital codes. Optical encoders are used in sensitive drives such as numerically controlled machines, digital servo systems, radar antennas, and robots as position feedback indicator, as Qureshi stated [17]. Rotary encoders mainly include incremental encoders and absolute encoders [18]. Wekhande and Agarwal mentioned high resolution absolute position with absolute encoder for high performance PMSM servo drives. They stated that incremental encoders are prone to noise and fatal error may occur on power fail. Also, they said that, absolute encoders suffered from the inherent problem of quantization noise on account of the limited resolution they process [19]. However, the absolute position can be preferred, the resolution also can be increased, and noise can be reduced. Therefore, the absolute encoder is suitable for highly sensitive servo applications. Ioakimidis and Wexler mentioned stabilization systems for antennas (SATCOM on the move). They used incremental encoders [20]. Its cost is lower, and volume is smaller compared to the absolute encoder. However, the absolute encoder is more reliable to estimate exact position. In my thesis, an absolute encoder was preferred, military standards were also examined in terms of temperature and electromagnetic compatibility. Also, torque response characteristics are shown.

2. ELECTRIC MOTORS AND THEIR PROPERTIES

Electric motors are one of the most important device in industry. These motors and driving methods are developing dy by day. In this chapter, general properties and types of electric motors, their models and control methods, driving techinues, their hardware structures, communication protocols during the motor control and some military requirements will be identified.

2.1 Types of Electrical Motors

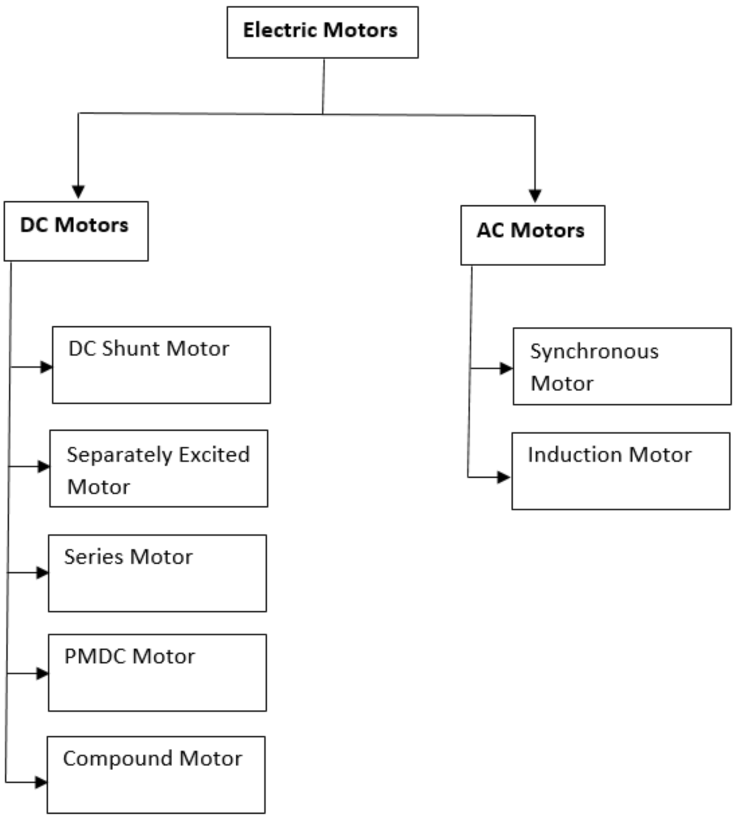

Figure 2.1 : Electric motor types.

2.1.1 DC motors and their properties

DC machines are characterized by their versatility. By means of various combinations of the shunt, series, and separately excited field windings, they can be designed to display a wide variety of volt-ampere or speed-torque characteristics for both dynamic and steady-state operation. Due to the ease of control, systems of dc machines have been frequently used in applications requiring a wide range of motor speeds or precise control of the motor output. In recent years, solid-state ac drive system technology has developed sufficiently that these systems are replacing dc machines in applications previously associated almost exclusively with dc machines. However, the versatility of dc machines in combination with the relative simplicity of their drive systems will ensure their continued use in a wide variety of applications [21].

DC motors are used to convert electrical energy to mechanical energy. These type of motors are preferred for high performance systems. DC motors operate on DC power–non-sinusoidal, unidirectional power. Their torque and their flux can be controlled independently; therefore, they are chosen commonly.

2.1.1.1 DC motor structure

DC motor contains;

- Rotor, is the part of the machine that rotates; also known as the “armature”
- Stator, which known as the field windings, or “stationary” part of the motor
- Commutator, which can be brushed or brushless, depending on the motor type, and it satisfies commutation, and it periodically changes the direction of the current between the rotor and external circuit.
- Field magnets, which provide the magnetic field that turns an axle connected to the rotor.

All DC machines mainly consist of two main parts. One is the stator, and the other is rotor [22].

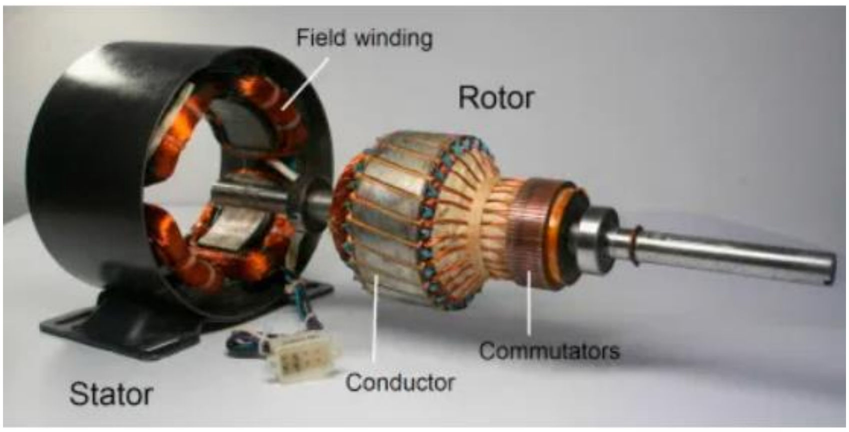

Figure 2.2 : Structure of motor [22].

Stator: The stator, which is a stationary part, includes yoke, pole, pole winding, and interpolates. The stator produces the magnetic flux.

Yoke: The yoke is the outer frame of a dc motor. It can be made up of cast steel or cast iron. Mechanical support and protection against mechanical damage are provided thanks to yoke. Also, the magnetic flux produced by poles can be transmitted in the yoke.

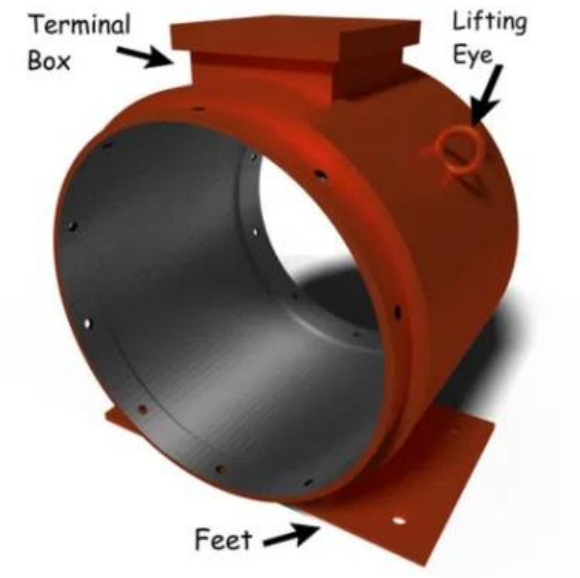

Figure 2.3 : Structure of yoke [22].

Pole: Pole includes pole core and pole shoes. Both of them are cast steel. Pole core is excited by the field winding, and it supports field winding which will be explained next part. Pole shoes are close to the armature. If the load changes during the application, armature current; hence magnetic flux also changes. This causes to eddy current. The laminated structure produces pole shoes in order to minimize the eddy current because the reluctance of the magnetic path can be reduced, and magnetic flux can be spread with a laminated structure.

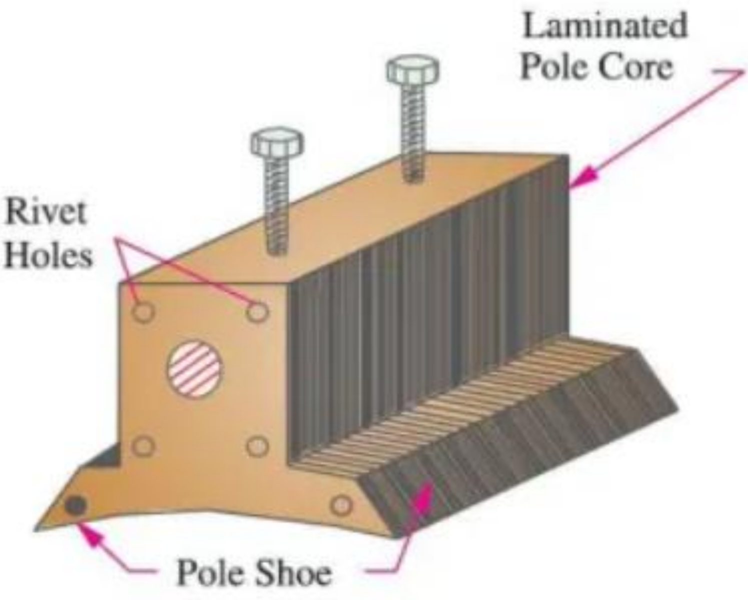

Figure 2.4 : Structure of pole [22].

Field winding: Field windings are made up of copper wire that is called coil around the pole core. When current is produced through these coils, magnetic flux is produced. This flux passes through the rotor and arrives at to armature. Finally, it produces rotating torque in the rotor.

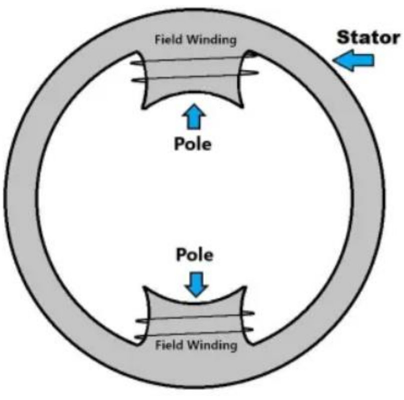

Figure 2.5 : The field winding on the core [22].

Rotor: Rotor is the rotational part of a DC machine. When the current flows, the rotor rotates in an external magnetic flux produced by the stator. The rotor in a DC machine consists of armature core, armature winding, commutator, and brushes.

Armature core: Armature is the rotating part of motors. It is made up of steel and it produced with laminated structure in order to reduce reluctance path hence reduce eddy current.

Figure 2.6 : Armature core [22].

Armature winding: Armature winding includes coils embedded in core slots. When the current is carried, EMF is produced in the machine due to relative motion between windings and the main field. Also, there is an isolation between each slot in order to prevent a short circuit.

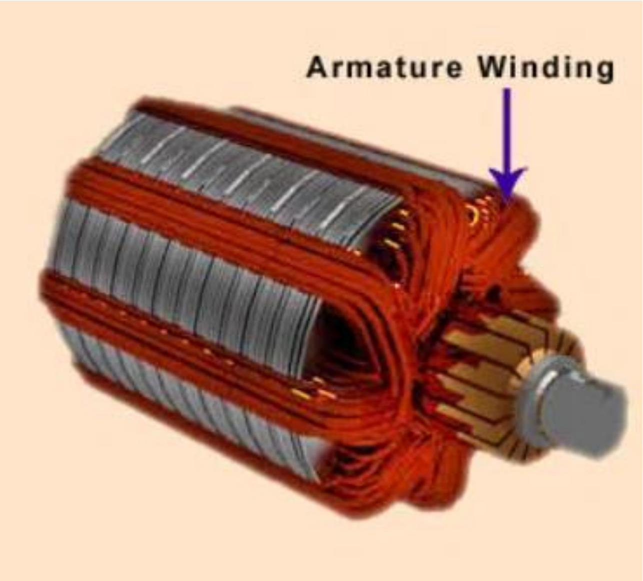

Figure 2.7 : Armature winding [22].

Commutator: The commutator contains copper segments, and there is insulation between each segment. A commutator periodically changes the direction of the current between the rotor and the external circuit. It ensures unidirectional torque in the dc motor. The commutator acts as a switch.

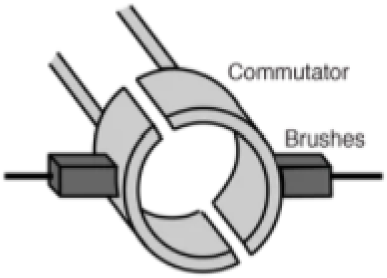

Figure 2.8 : Commutator ring [22].

Brushes: Generally, brushes are made up of carbon blocks in brush holders. It supplies the current from the external DC source to the commutator.

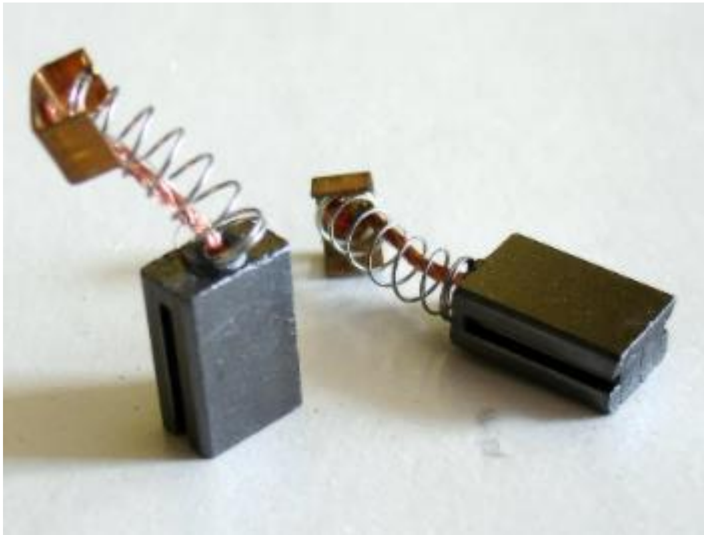

Figure 2.9 : A pair of carbon brushes [22].

2.1.1.2 DC Motor Working Principles

The working principle of a DC motor requires magnetic flux and a current-carrying conductor. For example, consider a coil carrying DC current through a commutator and brushes. These commutator segments rotate freely around their axis.

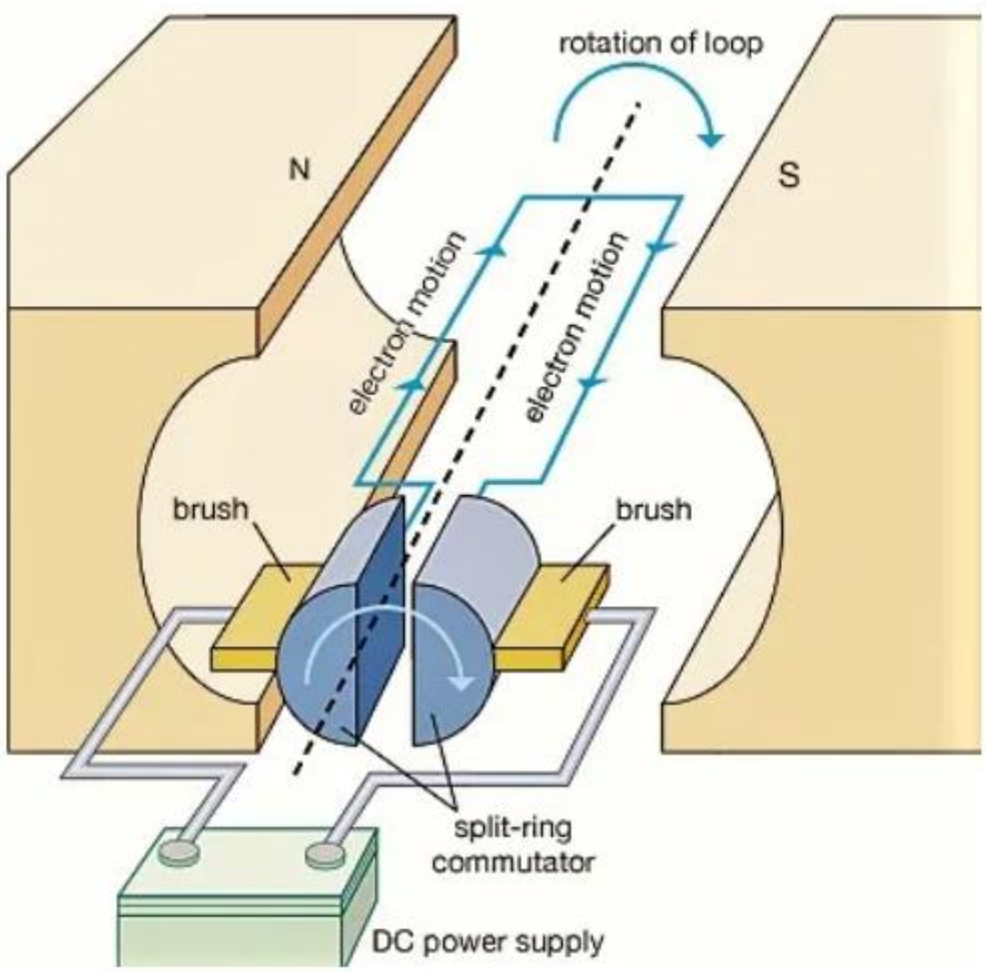

Figure 2.10 : DC motor working principles [22].

The commutator segment, which comes in contact with the left brush, gets positive polarity while the right one gets negative polarity. This situation leads to the flow of current in the coil.

By applying Fleming's Left-Hand Rule, the conductor on the left side always experiences a force upward while the conductor on the right side experiences a downward pressure. Hence, unidirectional torque is achieved in DC motors.

Maximum torque is obtained when the magnetic field of the stator and rotor are perpendicular to each other. Therefore, the commutator can play an essential role in supporting maximum torque.

Back EMF: The interaction of the current-carrying conductor with the changing magnetic field produced by the field winding induces an EMF in the conductor. This EMF acts in the opposite direction to the applied voltage. This induced EMF in the motor is known as BACK EMF.

Back EMF is vital for a DC motor because it provides regulation. Back EMF is proportional to motor speed. If a motor load is reduced suddenly, the required torque will be small compared to the current torque, so motor speed will increase and Back EMF will increase. As a result of increased back EMF, armature current will decrease. Therefore, the speed of the motor is regulated.

2.1.1.3 Mathematical model of DC motor

DC Motor can be modeled as shown in Figure 1.12.

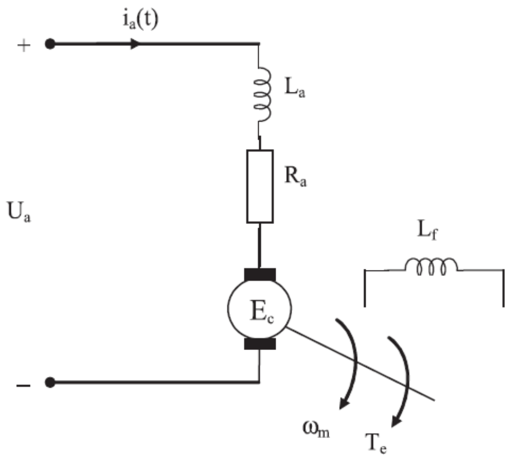

Figure 2.11 : Equivalent Circuit of DC motor [23].

Back EMF voltage of the motor is proportional with motor speed, and electrical torque is proportional with armature current as shown in (1.1) and (1.2) respectively. Also, the electrical circuit equation and mechanical equation of loaded DC motor are shown in (1.3) and (1.4) respectively.

$$E_C = K_b \omega_m \tag{1.1}$$

$$T_e = K_b I_a \tag{1.2}$$

$$E_C + R_a I_a(t) + L_a \frac{dI_a}{d_t} = U_a \tag{1.3}$$

$$B\omega_m + J\frac{d\omega_m}{d_t} = T_e - T_L = T_a \tag{1.4}$$

Where;

E_c = Back EMF voltage of the DC motor

K_b = Back EMF constant,

ω_m = Rotational Speed,

T_e = Electrical Torque,

I_a = Armature Current,

L_a = Armature Inductor,

R_a = Armature Resistance,

U_a = Terminal Voltage,

B = Viscous Friction coefficient

T_L = Load Torque

By putting (1.1) into (1.3), equation (1.5) is obtained.

$$K_b\omega_m + R_a I_a(t) + L_a \frac{dI_a}{d_t} = U_a \tag{1.5}$$

Also equation (1.6) is obtained by putting (1.2) into (1.4)

$$B\omega_m + J\frac{d\omega}{d_t} = K_b I_a(t) - T_L = T_a \tag{1.6}$$

Equations (1.5) and (1.6) can be written as matrix form as shown in (1.7).

$$\frac{d}{dt}\begin{bmatrix} i_a \\ \omega_m \end{bmatrix} = \begin{bmatrix} -\frac{R_a}{L_a} & -\frac{K_b}{L_a} \\ -\frac{K_b}{J} & -\frac{B}{J} \end{bmatrix} \begin{bmatrix} i_a(t) \\ \omega_m(t) \end{bmatrix} + \begin{bmatrix} \frac{1}{L_a} & 0 \\ 0 & -\frac{1}{J} \end{bmatrix} \begin{bmatrix} U_a \\ T_L \end{bmatrix} \tag{1.7}$$

Also, $\frac{dI_a}{d_t} = 0$ and $\frac{d\omega_m}{d_t} = 0$ in steady state so this equation can be simplified as (1.8).

$$\begin{bmatrix} R_a & K_b \\ K_b & -B \end{bmatrix} \begin{bmatrix} i_a \\ \omega_m \end{bmatrix} = \begin{bmatrix} U_a \\ T_L \end{bmatrix} \tag{1.8}$$

2.1.2 AC motor properties and advantages over DC motors

There are two types of AC motors. Synchronous and Asynchronous (Induction) motors. Synchronous motors are Brushless DC (BLDC) motors and Permanent Magnet Synchronous (PMSM) motors. AC motors are more efficient motors comparing to DC motors. Unlike DC motors, a mechanical commutator and brush are not necessary for AC motors, so maintenance cost is lower. Also, it requires lower startup demands, and it has higher torque to volume ratio, higher durability, and longevity, compact structure [24].

Besides these, AC motors offer better control opportunities over starting current levels and acceleration. Customizability can be satisfied for motor control applications. It also offers different configuration requirements and changing speed and torque requirements.

In this thesis, motor torque control for military applications was satisfied, and PMSM was used because high sensitivity and torque control for stabilization systems were intended. Furthermore, a variety of communication skills were applied, which would be explained in the following parts.

2.2 Permanent Magnet Synchronous Motor

Permanent Magnet Synchronous Motors (PMSM) are widely used in industry. They are used for civil and military applications. Currently, electric vehicles are the other target application for PMSMs. They have some desirable features that;

- PMSMs are high efficient motors,
- They have high torque to volume ratio, high torque to inertia ratio, high air gap flux density, high deceleration and acceleration rates, high power factor,

- They have compact structure,
- Maintenance cost is lower,
- There is a linear response in the effective input voltage,
- It has higher speed ranges, and torque can be controlled at zero speed,
- It has better speed-torque characteristics, so that customizable control applications can be made [25].

These properties make the PMSM indispensable for a lot of applications. It can be used in a broad power range from Watt to Megawatt. Stabilization systems are one of these applications.

2.2.1 Operational principles

Permanent magnet synchronous motors working principle depends on rotating magnetic field on the stator that generates electromotive force at synchronous speed. These motors have permanent magnets on the rotor, and it creates a constant magnetic flux. When the stator is excited with a three-phase supply, the rotating magnetic field is produced between the air gaps. Rotor field poles hold the rotating magnetic field at synchronous speed, and the rotor rotates continuously. Also, this magnetic field produces torque.

As a result of the rotation of the motor, back EMF (electromotive force) is observed, which is a voltage that opposes applied voltage according to Lenz's Law. It reduces the flowing current through the coils. In a PMSM, sinusoidal back EMF is observed. Combination of sinusoidal three-phase drive current and sinusoidal back EMF results in low torque ripple and high efficiency. In a synchronous motor, the average EMF induced per conductor can be calculated with;

$$E_{ph} = (4.44)\, f\, \phi_m T_{ph} \text{ Volts} \tag{2.2}$$

Where,

E_{ph} = Electromotive force (Volts) ,

f = frequency (Hertz) ,

$Ø_m$ = flux per pole (Weber),

T_{ph} = number of turn per phase

Cogging torque is the other important issue for Permanent Magnet Synchronous Motors. It causes by the interaction between the permanents magnets of the rotor and the stator slots of a Permanent magnet machine. It is an undesirable torque. It is especially shown at lower speeds. Actually, it is known as no current torque. Position, number of magnetic poles, number of teeth at stator, and speed affect this cogging torque characteristic. Some techniques are applied in order to reduce cogging torque. Optimization of magnet pole arc or width is a method. Also, stator stack or magnets are skewed, and fractional slots are used per pole in order to reduce cogging torque [26, 27].

The other one of the most crucial issues is torque ripple. Steady-state torque ripple and short response time are the most important things for stability and reliable operations. Torque is related to rotor current, and ripple should be as low as possible, especially for sensitive applications like position control. In addition, response time against the varying torque is aimed to be quiet at PMSM control applications.

2.2.2 Mathematical model

The mathematical model of the PMSM should be well known in order to control the motor properly. There are some assumptions and transformations for motor modeling. The three-phase motor model is converted to a two-phase model in order to make PMSM look like a DC motor, so the complexity is also reduced. The two-phase d-q axis is modeled as a separately excited DC motor. In this model, produced torque is controlled with q axis current, and d axis current is used for field weakening operations. In field-oriented vector control, the d axis can be zero. As a summary, the two-phase motor model can be modeled as Figure 2.12 with these assumptions:

- Saturation is neglected, although it can be taken into account by parameter changes,
- The back EMF is sinusoidal,
- Eddy current and hysteresis losses are negligible [28, 29]

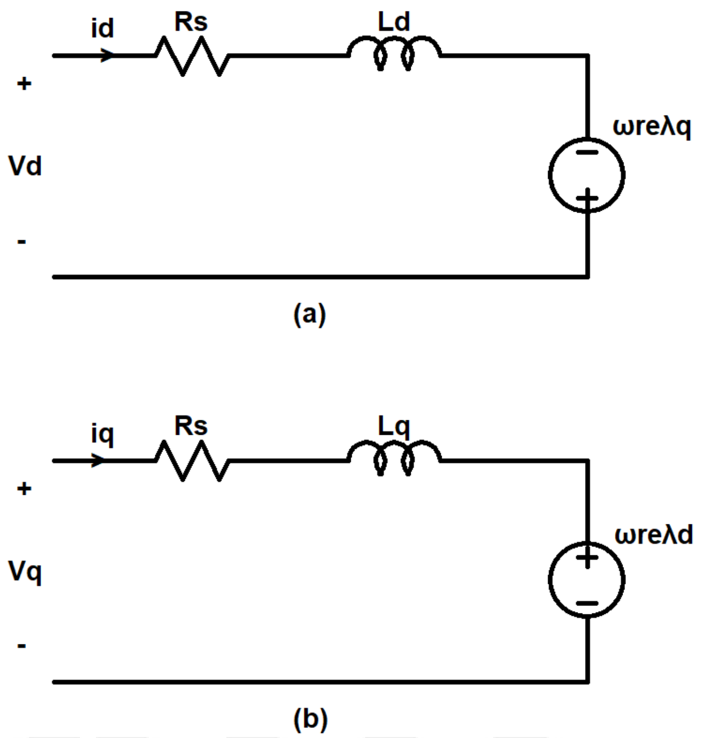

Figure 2.12 : Dynamic equivalent circuit of PMSM with d-q axis.

From Figure 2.12(a),

$$Vd = R_s i_d + L_d \frac{di_d}{dt} - \omega_{re} \lambda_q \tag{2.2}$$

From Figure 2.12(b),

$$Vq = R_s i_q + L_q \frac{di_q}{dt} + \omega_{re} \lambda_d \tag{2.3}$$

It is known that (2.4), and (2.5)

$$\lambda_d = L_d i_d + \lambda_m \tag{2.4}$$

$$\lambda_q = L_q i_q \tag{2.5}$$

Equation (2.6) can be obtained by putting (2.4) into (2.3)

$$Vq = R_s i_q + L_q \frac{di_q}{dt} + \omega_{re} L_d i_d + \omega_{re} \lambda_m \tag{2.6}$$

As a summary (2.7) is obtained

$$\begin{bmatrix} V_d \\ V_q \end{bmatrix} = \begin{bmatrix} R_s & -\omega_{re} L_q \\ \omega_{re} L_d & R_s \end{bmatrix} . \begin{bmatrix} i_d \\ i_q \end{bmatrix} + \begin{bmatrix} L_d & 0 \\ 0 & L_q \end{bmatrix} . \frac{d}{d_t} \begin{bmatrix} i_d \\ i_q \end{bmatrix} + \omega_{re} \lambda_d \begin{bmatrix} 0 \\ 1 \end{bmatrix} \tag{2.7}$$

2.2.3 Power and torque calculation

Torque equation is shown in (2.8)

$$T_e = \frac{3}{2} P \lambda_m i_q + \frac{3}{2} P.(L_d - L_q) i_d i_q \tag{2.8}$$

If $I_d = 0$,

$$T_e = \frac{3}{2} P \lambda_m i_q \tag{2.9}$$

$$T_e = J \frac{d_{\omega_{re}}}{d_t} + B\omega_{re} + T_L \tag{2.10}$$

$$\frac{d_{\omega_{re}}}{d_t} = \frac{T_e - B\omega_{re} - T_L}{J} \tag{2.11}$$

$$\frac{d_{\theta_r}}{d_t} = \omega_{re} \tag{2.12}$$

Clarke Transform

$$\begin{bmatrix} i_\alpha \\ i_\beta \\ i_0 \end{bmatrix} = \sqrt{\frac{2}{3}} \begin{bmatrix} 1 & -1/2 & -1/2 \\ 0 & \sqrt{3}/2 & -\sqrt{3}/2 \\ 1 & 1 & 1 \end{bmatrix} \begin{bmatrix} i_a \\ i_b \\ i_c \end{bmatrix} \tag{2.13}$$

Park Transform

$$\begin{bmatrix} V_q \\ V_d \\ V_0 \end{bmatrix} = \frac{2}{3} \begin{bmatrix} \cos(\theta) & \cos(\theta - \frac{2\pi}{3}) & \cos(\theta + \frac{2\pi}{3}) \\ sin\ (\theta) & \sin(\theta - \frac{2\pi}{3}) & \sin(\theta + \frac{2\pi}{3}) \\ 1/2 & 1/2 & 1/2 \end{bmatrix} \begin{bmatrix} V_a \\ V_b \\ V_c \end{bmatrix} \tag{2.14}$$

Inverse Park Transformation

$$\begin{bmatrix} V_a \\ V_b \\ V_c \end{bmatrix} = \frac{2}{3} \begin{bmatrix} \cos(\theta) & \sin(\theta) & 1 \\ \cos(\theta - \frac{2\pi}{3}) & \sin(\theta - \frac{2\pi}{3}) & 1 \\ \cos(\theta + \frac{2\pi}{3}) & \sin(\theta + \frac{2\pi}{3}) & 1/2 \end{bmatrix} \begin{bmatrix} V_q \\ V_d \\ V_0 \end{bmatrix} \tag{2.15}$$

$$Power = V_a i_a + V_b i_b + V_c i_c \tag{2.16}$$

$$Power = 3(V_d i_d + V_q i_q) / 2 \tag{2.17}$$

2.3 Control of Permanent Magnet Synchronous Motor

Permanent Magnet Synchronous motor is used commonly in industry, servo applications, electric vehicles, etc. PMSM is a big rival for induction motors. Efficient and varying control techniques play an important role in choosing the PMSM. It can be run at different speeds by using Variable Frequency Drive (VFD). Control methods are separated into two categories as Scalar and Vector control.

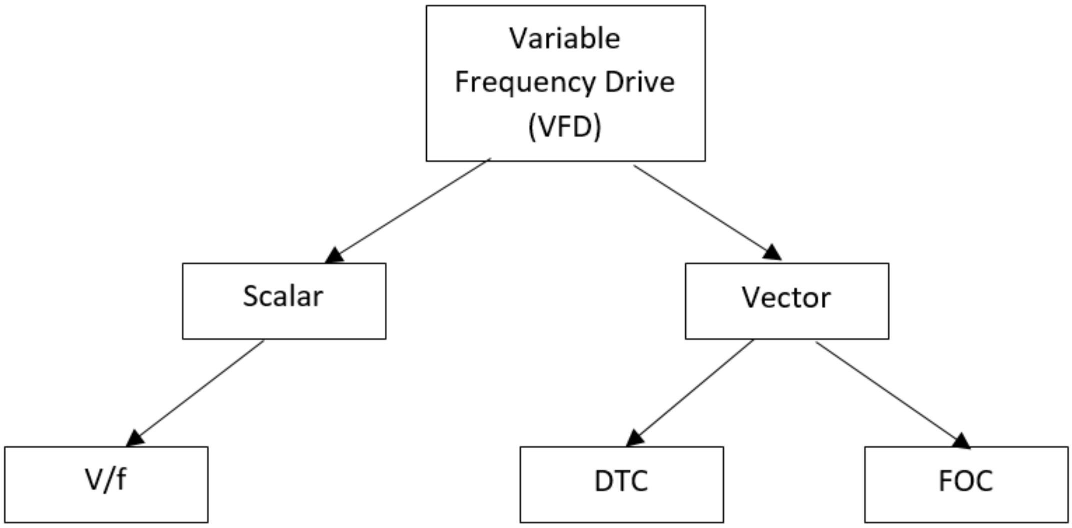

Figure 2.13 : PMSM control strategies.

2.3.1 Scalar control

Scalar control is the simplest method to control PMSM. Magnitude is the only issue for this control method. Angle is not taken into account. Frequency, voltage, and current ratio are target points for this control technique. Synchronous speed is set with frequency, and voltage/frequency ratio is kept constant. There is not any position feedback; that is, open-loop control is realized [30]. Therefore, implementation is easy, and there is a low demand for computational power. However, some negative conditions are observed in this technique. One of them is that if a certain applied frequency is exceeded, instability of the dive system may occur. The rotor has to be constructed with damper windings to assure synchronization of the rotor to the electrical frequency to overcome this problem [31]. This situation restricts the number of design choices for the rotor. For example, the magnets of the PMSM have to be located on the inside of damper bars. However, most PMSMs are constructed without damper windings, and they are not suitable for traditional scalar control. The other disadvantage is that feedback of position is insufficient in scalar control, which causes low dynamic performance, which limits the use of control methods for PMSM drives [30]. Vector control is preferred for complex control applications.

2.3.2 Vector control

Vector control is the other technique to control PMSM. Both magnitude and angle are crucial issues in this type of control method. Also, closed-loop feedback is applied. Vector control is used to achieve higher dynamic response and is used for more complicated control applications. Vector control can be divided into two types of strategies that are field-oriented control and direct torque control.

2.3.2.1 Field oriented control

Field-oriented control (FOC) represents a method that has a reference frame for rotor, stator and air gap fluxes, and the other quantities are a product of this reference frame. Flux and current are decoupled in order to simplify the three-phase motor model into DC motor, which are direct and quadrature axis. The goal of FOC is to control the direct and quadrature axis to achieve the intended torque. Direct and quadrature currents directly affect torque value, and these currents are controlled separately to achieve maximum torque. In this condition, these currents are perpendicular. Direct current Id has no effect on torque production if there is no saliency, so direct current should be zero for maximum torque. On the other hand, Quadrature current Iq affects the torque production directly, as shown in (2.9). Therefore, this current is controlled by the FOC algorithm. The other important issue is that position information should be known for the FOC. Incremental, absolute, quadrature encoders or resolver can be used in order to obtain position data. Also, sensorless position data can be estimated from flux or back EMF vectors.

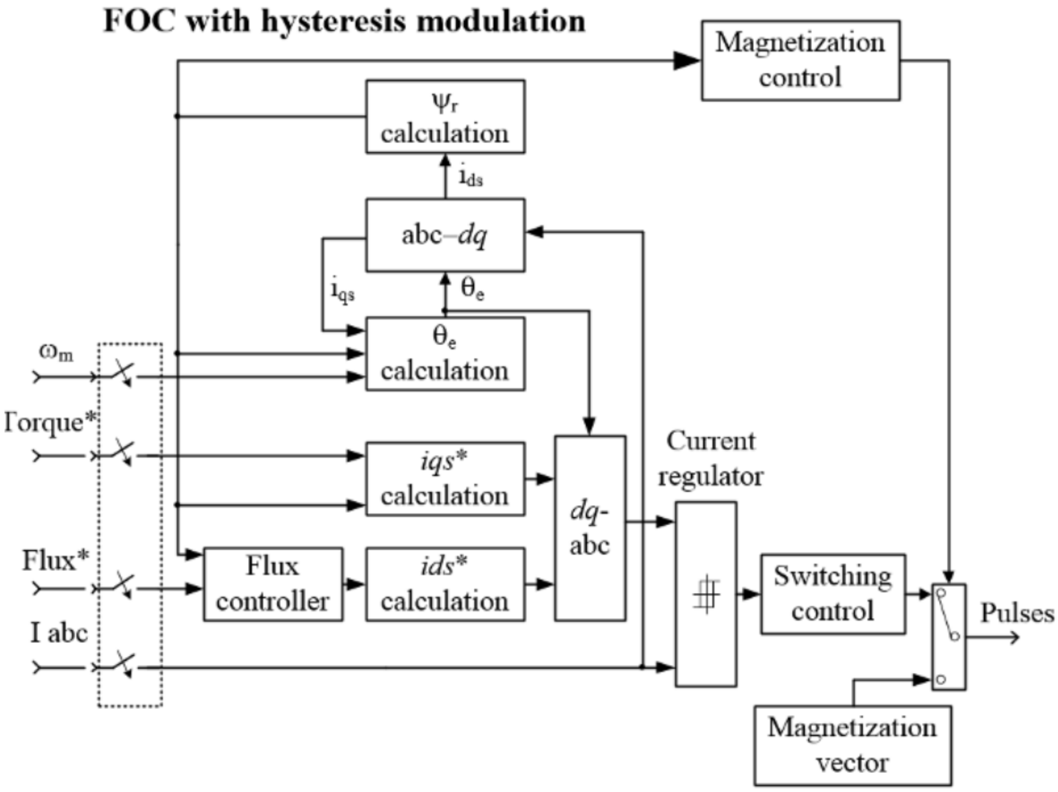

Figure 2.14 : FOC with hysteresis modulation [32].

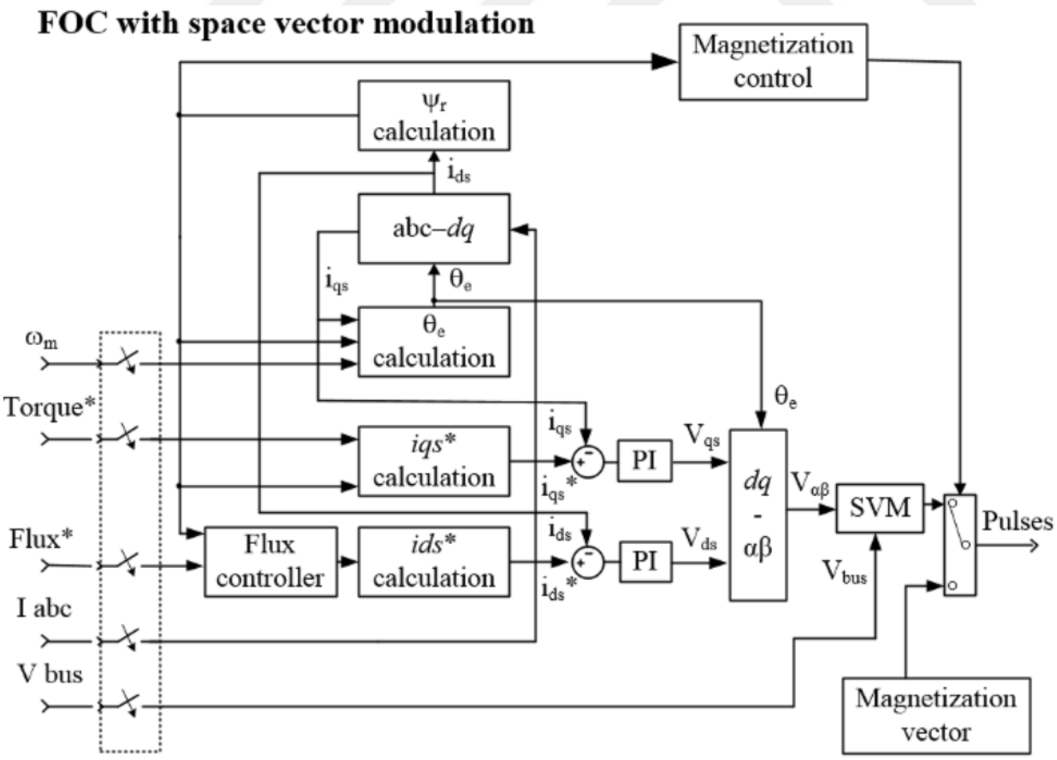

Figure 2.15 : FOC with space vector modulation [32].

2.3.2.2 Direct torque control

Direct Torque Control (DTC)'s working principle is that voltage vectors are selected. After that, actual and intended torque are compared with flux. These errors between torque and flux are processed in the hysteresis comparator. DTC has a less complex structure compared to FOC because the position is not measured with an external sensor to find the rotor position. Rotor position is required only for the motor start-up. In addition, transformations are not necessary; the stationary frame is used instead of the rotating frame. Also, a PWM generator is not required. Instead, one of the six Voltage Source Inverter is used during the sampling period. Furthermore, there is low computational power for implementation. However, there are some disadvantages. Although DTC has a good dynamic response and short settling time, steady-state response is not so good. Stator current ripple, torque, and flux linkage are high. Especially, torque control is difficult at low speed. Higher torque ripple, current ripple, higher noise are observed at low speed. The other difficulty is varying the switching frequency to torque control [33, 34, 35].

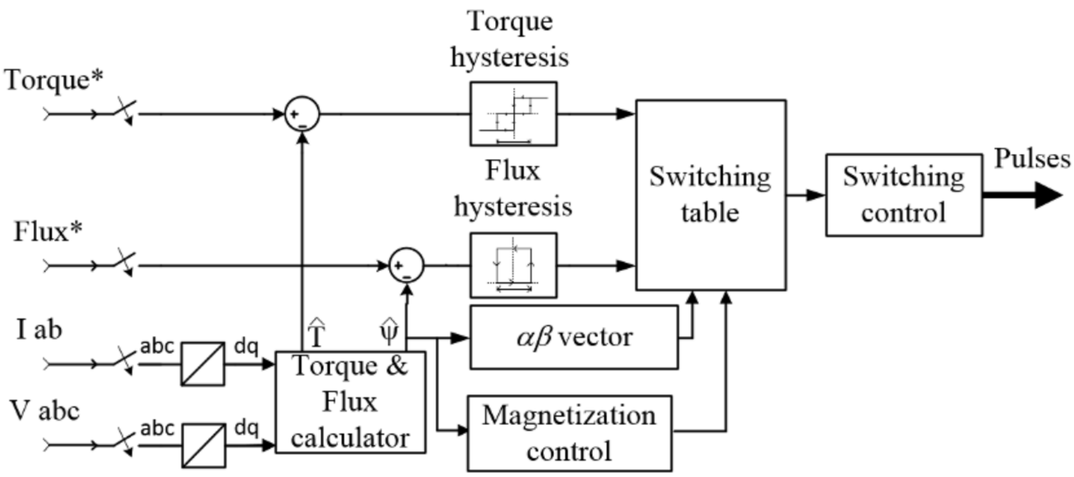

Figure 2.16 : DTC with hysteresis modulation [36].

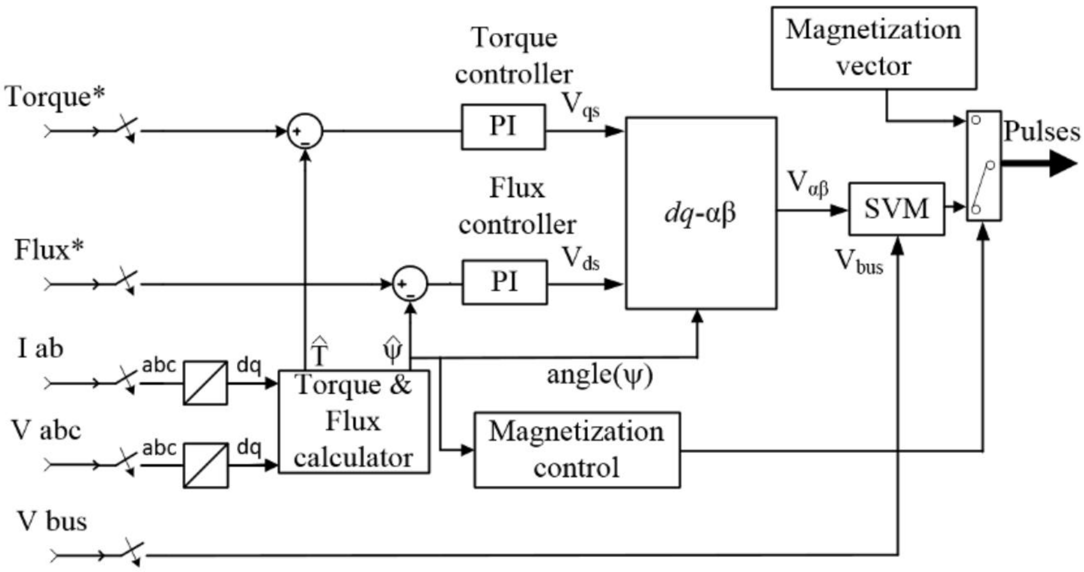

Figure 2.17 : DTC with space vector modulation [36].

2.4 Hardware structure

In this thesis PMSM was controlled with field oriented control topology and at this topology, PMSM motor control applications basically include an inverter, microprocessor, and position sensor (also, sensorless control is possible). The microprocessor is one of the most important components for PMSM control. Current information is read by the ADCs of the microprocessor. This current is compared with the intended current with PI tools. Also, three-phase to two-phase transformation is satisfied with Clarke transform, and rotational reference is achieved with Park transform. Position information is necessary during these transformations. This position information can be supplied with encoders, resolvers or it can be supplied with sensorless estimations. All of these operations can be satisfied thanks to microprocessors. Also, some driving techniques are applied. SVPWM, SVM, etc. are some of the techniques. By these driving techniques, voltage source inverter gates are switched with a determined sequence, and three-phase current waveforms are obtained in order to drive Permanent Magnet Synchronous Motor.

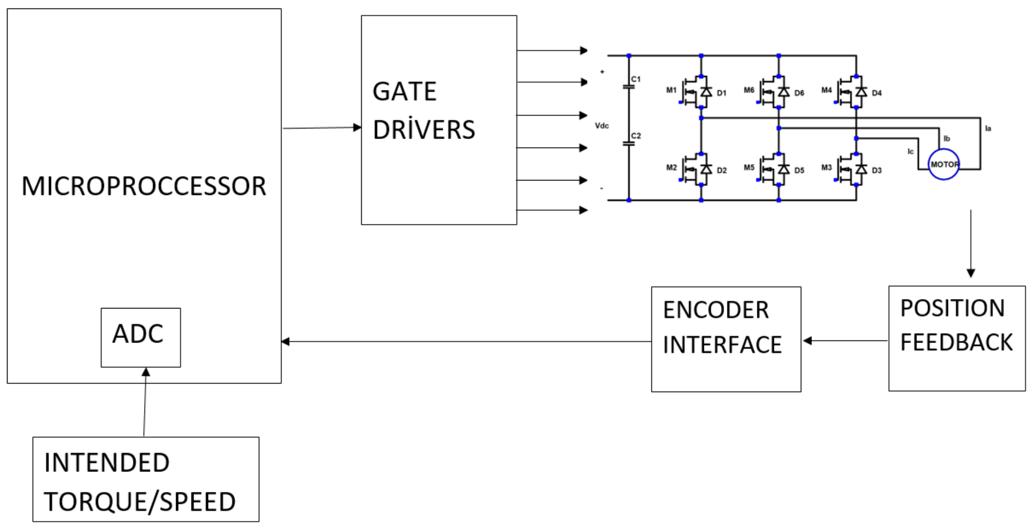

Figure 2.18 : Basically PMSM control hardware structure.

During the PMSM control, the microprocessor can communicate with the encoder and inverter. Also, intended torque, speed values, and output waveforms can be observed with transmission and communication methods. Some communication protocols are used for them.

2.4.1 Communication protocols between intelligent units

There are a lot of communication protocols for data transferring at PMSM control applications. Ethernet, USB, I2C, RS232, RS485, CAN, 1-Wire communications are some of them. Some of the commonly used protocols are mentioned.

2.4.1.1 SPI protocol

Serial Peripheral Interface (SPI) is a synchronous communication protocol that allows several SPI microcontrollers to be connected together. There are different wires for data and clock lines in SPI. Also, the clock is not included in the data stream; it should be a separate signal. SPI can be master or slave, and it has four main signals, which are MISO (Master Input/Slave Output), MOSI (Master Output/Slave Input), SCLK (Clock), SS/CS (Slave select/Chip select). These signals are part of data communication. Also Vcc and Ground are necessary to supply power. That is, six wires are needed in order to receive and send data from slave or master. There are unlimited slaves at SPI communication. It supports up to 10Mbps (megabit per second), and it is ideal for high-speed data communication.

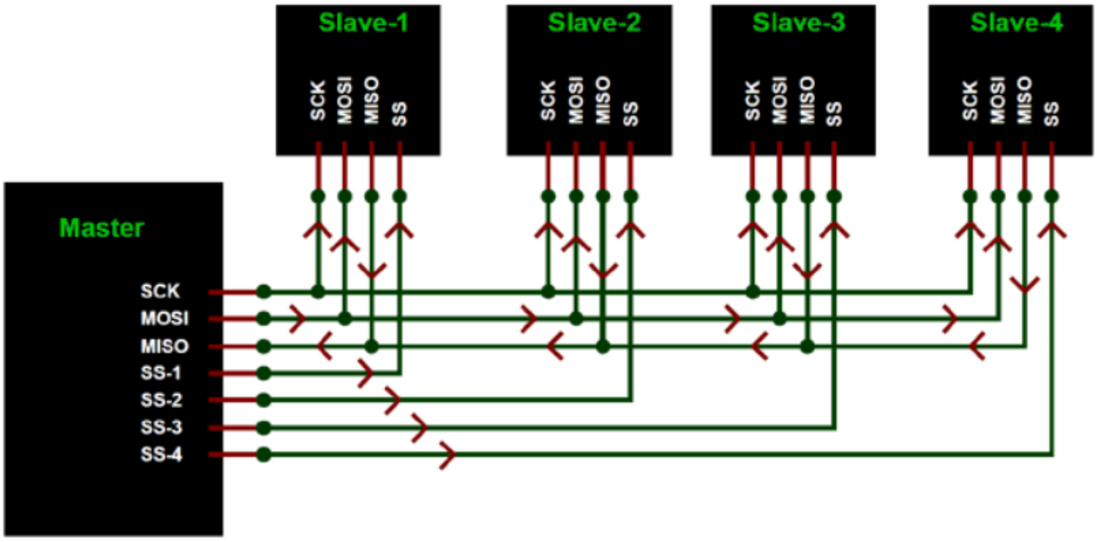

Figure 2.19 : SPI protocol [37].

2.4.1.2 I2C protocol

Inter-Integrated Circuit (I2C) has lines which are SDA (data) and SCL (clock). Setup is easy because there are only two wires. Both wires should be connected to a positive power supply with a pull-up resistor. I2C can deliver up to 400 kbps (kilobit per second), and it can be connected to up to 1024 devices.

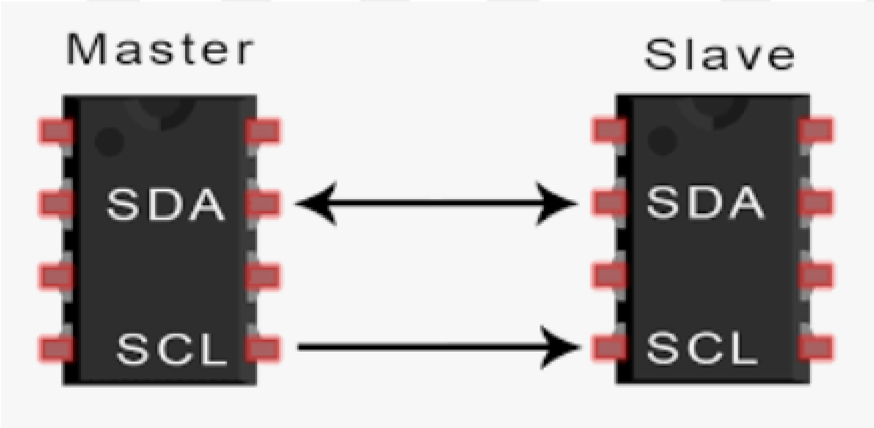

Figure 2.20 : I2C protocol [37].

2.4.1.3 RS232 protocol

Different peripherals can be connected in this communication protocol, such as monitors, CNCs, etc. There are male and female connectors, and these connectors are tied to each other. RS232 contains nine pinouts. Information is transferred as "0" and "1" in this protocol. It is commonly used at a point to point connections and applications. Baud rate is the other important issue. It describes the transferred data between transmitter and receiver in the form of bits per second. 9600 bps is popular. Also, generally, the baud rate is set up to 115200 bps. Both communicated devices should have the same baud rate.

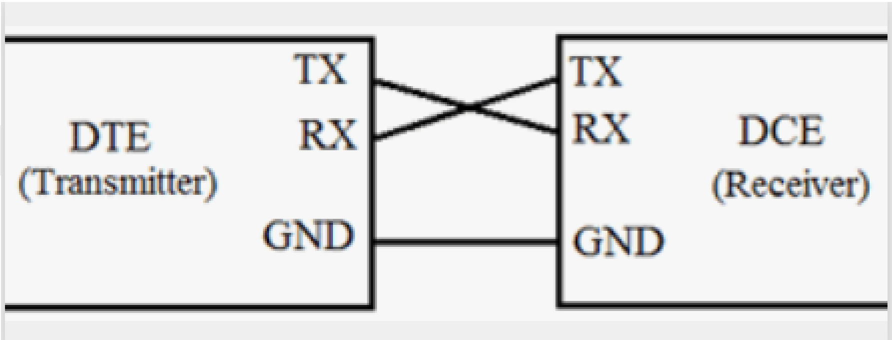

Figure 2.21 : RS232 protocol [37].

2.4.1.4 CAN protocol

The Controller Area Network (CAN) is one of the most popular communication protocols in the automotive and military sectors. It is a robust, low-cost, fast communication method. For example, it can be used between engine control units and sensors for automotive. CAN messages are prioritized with message IDs, and the highest priority can be determined, and it can be done non-interrupted. CAN bus systems can provide 1 Mbps (Megabit per second).

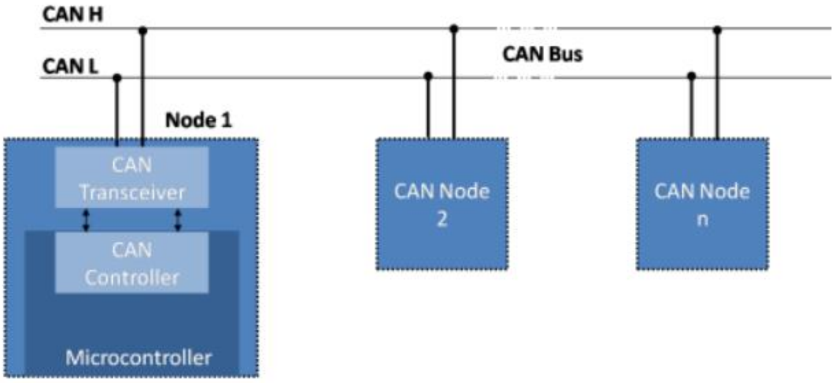

Figure 2.22 : CAN protocol [37].

2.5 Military Standards at PMSM Control

There are some military standards for devices used in this area. Electromagnetic compatibility is one of the most important standards. MIL-STD-461 is a United States Military Standard that describes how the test equipment in order to satisfy electromagnetic compatibility.

MIL-STD-461 is a military standard that establishes electromagnetic interference (EMI) limits and test procedures for military equipment. Currently, this standard is valid for military applications. EMI consists of any undesired signals, that is, "noise" generated by electronic equipment. It can cause interference with other equipment and be detected by the enemy. Some noise limits depend on the application (e.g., ground, air, ship, submarine, etc.). Keeping EMI under control is critical for military applications. It should be checked whether the noise is under the acceptable limits.

In addition, devices should satisfy some temperature requirements in the military area. These temperature limits can be changed for applications. Devices are tested at intended temperatures to ensure temperature durability.

3. IMPLEMENTATION OF FIELD ORIENTED CONTROL OF PMSM

Field-oriented control (FOC) has the decoupled torque and flux channels with feedback. The rotor position of the motor must be known for the feedback algorithm. This information can be obtained by using a mechanical encoder or resolver. Also, sensorless position feedback with estimation is possible. Furthermore, speed is calculated from rotor position, and motor speed is compared with reference speed. After error speed is obtained, it is used as PI controller input whose output will be proportional with torque producing component of stator current Iqref. This current is compared with the q-axis component of stator current (Iq), and error is fed to another PI controller to find the q-axis reference voltage component Vqref. The d-axis component of stator reference current, which is the flux producing component (Idref), is taken equal to zero to satisfy maximum torque per ampere condition. This current is compared with the motor d-axis current component, and the error is fed to the PI controller to find Vdref. This feedback diagram is shown in Figure 3.6 [38].

3.1 d-q Reference Coordinate System and Transformations

The three-phase coordinate system is converted to two-phase orthogonal system in order to reduce complexity. It can be done with Clarke transformation, as shown in (3.1). In this conversion, the α-β two-phase system is created instead of a-b-c three-phase system. Both of these systems are static coordinate systems [39].

Clarke Transformation:

$$\begin{bmatrix} i_\alpha \\ i_\beta \\ i_0 \end{bmatrix} = \sqrt{\frac{2}{3}} \begin{bmatrix} 1 & -1/2 & -1/2 \\ 0 & \sqrt{3}/2 & -\sqrt{3}/2 \\ 1 & 1 & 1 \end{bmatrix} \begin{bmatrix} i_a \\ i_b \\ i_c \end{bmatrix} \tag{3.1}$$

This static α-β coordinate system is also converted to a rotating reference frame which is d-q coordinate system with Park transformation as shown in (3.2).

$$\begin{bmatrix} i_d \\ i_q \end{bmatrix} = \begin{bmatrix} \cos(\theta) & \sin(\theta) \\ -\sin(\theta) & \cos(\theta) \end{bmatrix} \begin{bmatrix} i_\alpha \\ i_\beta \end{bmatrix} \tag{3.2}$$

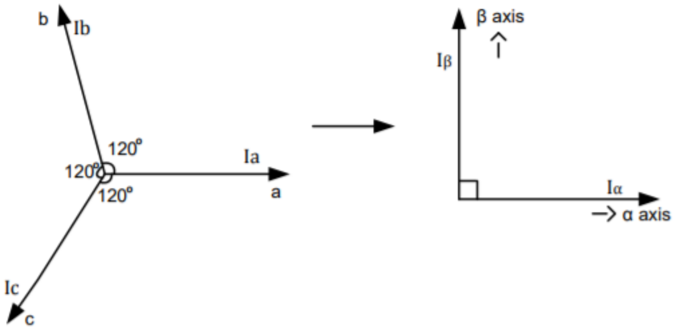

Figure 3.1 : Clarke transformation logic [40].

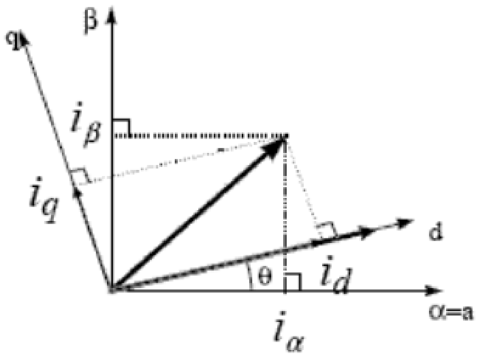

Figure 3.2 : Park transformation logic [41].

3.2 SVPWM Production

Space vector pulse width modulation (SVPWM) technology is used in order to control the voltage source inverter switch. In this topology, the stator three-phase motor is tracking the rotating magnetic field. The utilization rate of the DC power supply voltage can be improved. Besides, sample calculation and reducing the switching losses also can be satisfied thanks to the SVPWM method. This provides that harmonic loss of motor and torque ripple are reduced in this control strategy.

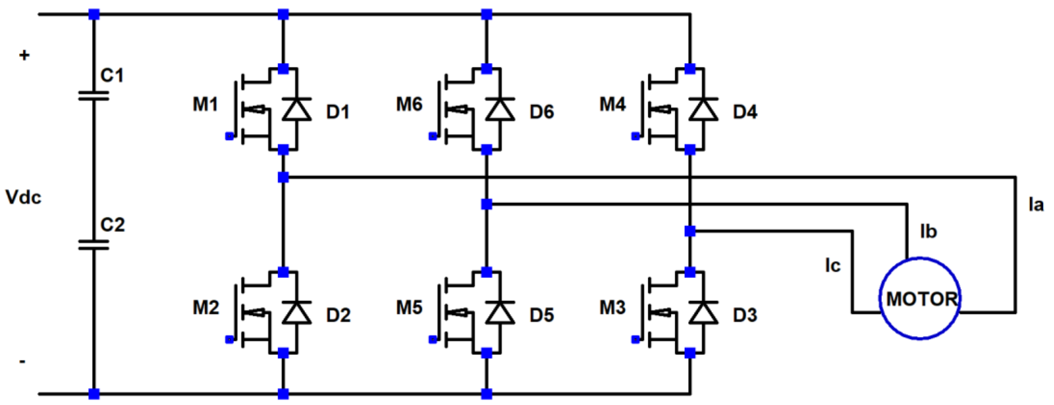

Figure 3.3 : Voltage source inverter diagram.

Space vector pulse width modulation strategy is based on a special switching sequence at voltage source inverter. That is, the upper three MOSFETs and their complements are switched with a special logic. As a result, three sinusoidal currents are produced for three-phase systems [13]. These three sinusoidal currents are sent to the stator for PMSM.

The three-phase voltages can be controlled according to the rotation of a space vector Vs and three-phase systems can be controlled by converting these two coordinates systems. To do this, the alpha-beta transform is applied with this matrix (3.3).

$$\begin{bmatrix} V_\alpha \\ V_\beta \end{bmatrix} = \sqrt{\frac{2}{3}} \begin{bmatrix} 1 & -\frac{1}{2} & -\frac{1}{2} \\ 0 & \frac{\sqrt{3}}{2} & -\frac{\sqrt{3}}{2} \end{bmatrix} \begin{bmatrix} V_a \\ V_b \\ V_c \end{bmatrix} \tag{3.3}$$

Space vector Vs can also be expressed as;

$$V_s = \sqrt{{V_\alpha}^2 + {V_\beta}^2} \tag{3.4}$$

$$V_s = \arctan(\frac{V_\beta}{V_\alpha}) \tag{3.5}$$

Eight possible commutation sequences are due to voltage source inverter (V0, V1, V2 …V7). Six are active vectors (V1, V2, V3, V4, V5, V6), and V0 and V7 are zero voltage vectors. These vectors divide the modulation plane into six sectors with π/3 phase angle difference.

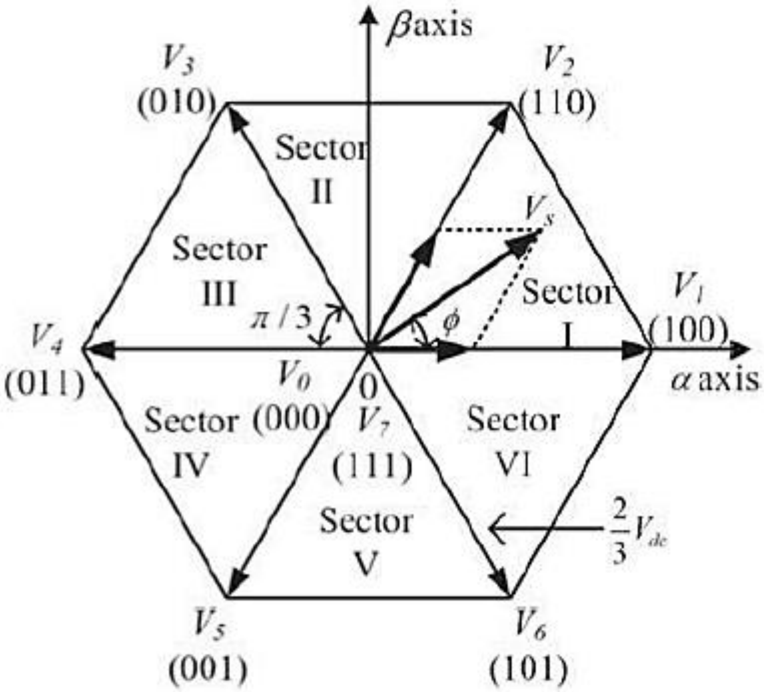

Figure 3.4 : Basic voltage vectors, reference vector and modulation plane[13].

Space vector Vs caused from the k^{th} sector can be expressed with two adjacent vectors and their application times as (3.6).

$$\int_{nT}^{(n+1)T} V_s dt = T_k * V_k + T_{k+1} * V_{k+1} + T_0 * V_0 \tag{3.5}$$

V_k = k^{th} active vector,

T_k = time period duration that applied V_k vector,

T_{k+1} = time period duration that applied V_{k+1} vector,

T_s = time period of PWM switching which corresponds to T_0+T_k+T_{k+1},

T_0 = time period duration that applied zero voltage vector,

V_k and V_{k+1} are two adjacent vectors during the application times T_k and T_{k+1}. Actually, T_k + T_{k+1} is smaller than 1, and the rest of the time, zero voltage vectors are applied (V_0 or V_7).

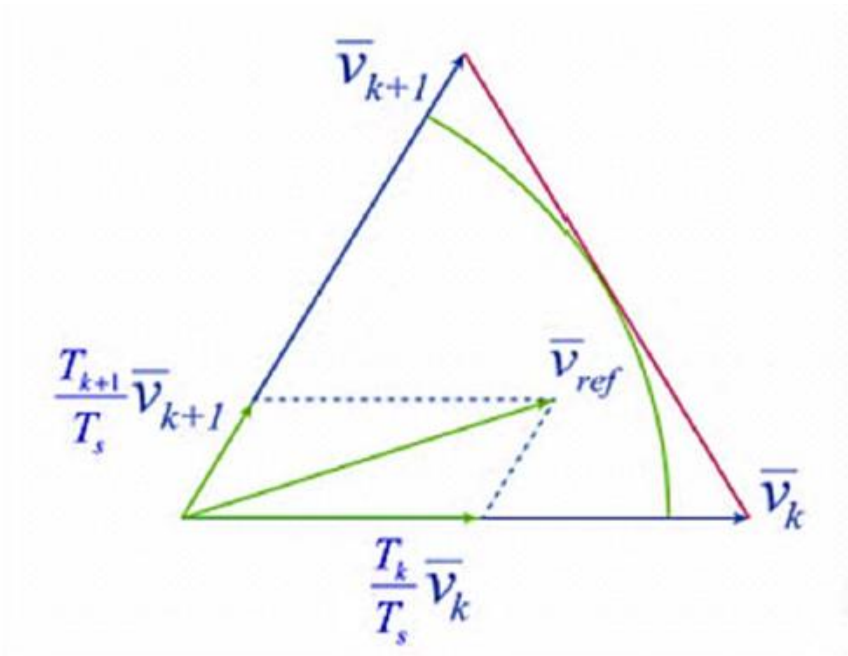

Figure 3.5 : Two adjacent vectors and resulting reference vector V_{ref} which is associated with space vector V_s [13].

Any voltage vector with varying magnitude and direction can be obtained for every PWM period by controlling the switching sequence and ON time duration of pulses. The SVPWM aims that switching sequences that correspond to every PWM period are generated to obtain a continuously rotating space vector. Thus, less harmonic distortion can be satisfied. Also, this method has advantages for unbalanced load operations.

In summary, the space vector pulse with modulation technique produces a reference voltage vector to generate an appropriate gate signal for the voltage source inverter every PWM period, and a constant rotating space vector is aimed.

3.3 Torque Control with Field Oriented Control System

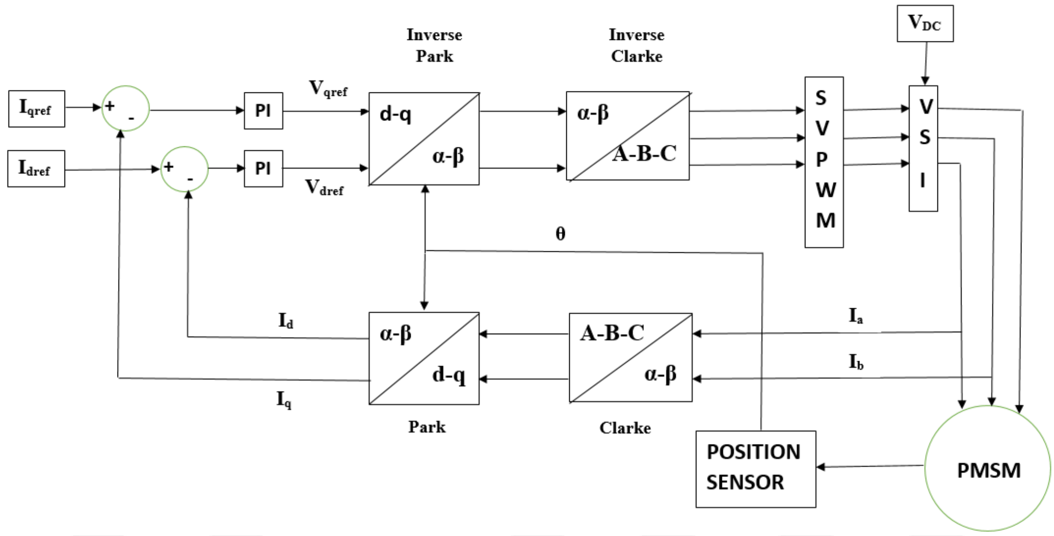

Figure 3.6 : Torque control block diagram with FOC.

In this control system, phase currents Ia and Ib are obtained from the inverter with sense resistor and these values are read by the microprocessor's ADC. Also, Ic can be calculated from (Ic=-(Ia+Ib)). These currents are converted from three-phase frame to α-β and d-q coordinate systems with Clarke and Park transformations, respectively, and Id and Iq currents are obtained. Iq current is directly related to torque production, and Id is related to flux which is taken as zero for maximum torque production. In the torque control algorithm, desired torque is determined, and it is filtered in order to obtain the Iqref current. That is, the intended Iqref current is compared with Iq current, which was obtained with Park transformation. After Iqref and Iq comparison, the error value feeds to the PI controller in order to obtain Vqref. If the stator voltage vector Vqref, Vdref, and its sector number are known, voltage space vector PWM technique can be used, and PWM signal can be produced to control the inverter and closed-loop control of PMSM can be achieved. Therefore, the d-q coordinate system is converted to α-β and a-b-c coordinate systems with inverse Park and inverse Clarke transformations, respectively [42].

In this thesis, PMSM torque control was satisfied with high sensitivity for Military applications. The torque control algorithm was verified at Simulink. EMC and temperature tests were observed for military acceptance. Field Oriented Control was preferred due to its steady state reliability. TMS320F28069M microprocessor was used from Texas Instruments. This microprocessor is very suitable for Simulink platform because toolbox support is pretty successful. Furthermore, an incremental encoder was selected for PMSM drive applications generally because its volume is small and it is cheap; however, an absolute encoder was preferred in this study because sensitivity is crucial for military applications. In other words, this experiment focused on high sensitive applications, and an absolute encoder was used in order to ensure exact position with high accuracy.

In this experiment, a variety of communication methods were tested and applied. RS232 communication, CAN communication, SPI communication, Simulink external mode skills were some of them. Finally, CAN communication was selected because external mode can fault if there is a lot of receiving and sending data. SPI communication was also selected to integrate the absolute encoder with the motor control algorithm in Simulink.

A motor drive development setup was constituted, which includes two Permanent Magnet Synchronous Motors whose type numbers are M-2310P-LN-04K, two absolute encoders with INC-3-075-181001-SSI1-AFL4-5-AN type number and a torque meter DR-2477. Motors were tied with shaft and torque meter. One side motor was tested motor; the other side motor was controlled motor. In other words, one side motor was driven with a constant speed which was a controlled motor, and the other side motor was used for torque control test. Always, a constant speed was saved, and torque value was changed, so torque control algorithm reliability was satisfied.

3.4 Control Cards, Demo boards and MATLAB Programming

In this part, properties of control cards, demo boards, the motor that used in this thesis, and programming process at MATLAB will be clarified.

3.4.1 MATLAB properties and application

MATLAB is a computer program that is used for positive science and engineering calculations. MATLAB, which was developed by MathWorks firm, is also a programming language. MATLAB actually consists of "Matrix Laboratory" words and its working principle base upon matrices. MATLAB is used for Linear algebra, optimization, and numerical analysis. Besides that, it is used for 2D and 3D drawing, graphics, and calculations.

Algorithm development, data analysis, control applications, mathematical calculations, scientific and mathematical graphs, real-time programming, modeling, simulations, etc., can be ensured via MATLAB. In addition, a lot of toolboxes can be added, so MATLAB and SIMULINK can be privatized for the intended application. In this thesis, TMS320F28069M microprocessor from Texas Instruments is used, and SIMULINK is preferred because SIMULINK is suitable for Texas Instrument's microprocessors Embedded Coder Toolbox in Simulink. Furthermore, Simscape Power Electronic tools are the other crucial factor because of their useful interface, and suitable development environment. SIMULINK also supply real-time observation opportunity thanks to "External Mode" and "CAN communication" support.

3.4.2 Model based simulations

System simulations can be simulated in a computer environment without a real microprocessor, so many observations can be estimated. However, the motor drive setup has a complex structure that includes an absolute encoder, PMSM motor, torque meter, and these tools cannot be simulated exactly. Even so, Inverter, PMSM, Park-Clarke transformations can be modeled easily, and general characteristics can be observed.

3.4.3 Hardware in the loop and embedded coder support package

PMSM driving algorithm can be built and embedded to TMS320F28069M microprocessor. "Embedded Coder Support Package for Texas Instruments C2000 Processor" toolbox is used in order to embed the code. This toolbox is produced with Texas Instruments and MATLAB cooperation. ADC blocks that satisfy to measure voltage or current, EPWM blocks that satisfy switching, Park-Clarke transformation blocks, SVPWM blocks, GPIO's (General Purpose Input Output) CAN blocks, SPI blocks, etc. are used from this toolbox, and the microprocessor identifies this toolbox.

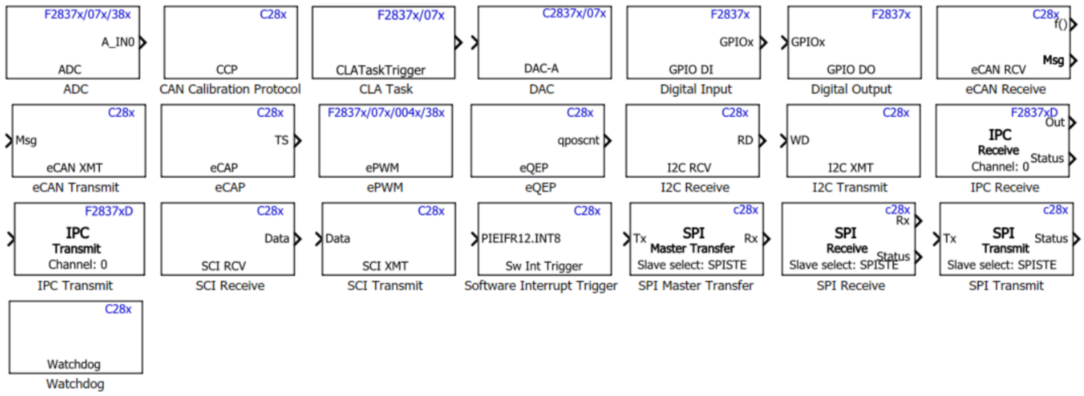

Figure 3.7 : C2000 toolbox.

After the code is embedded into the microprocessor, data transferring can be satisfied in real-time. External mode is a method for real-time communication and tuning. SCI (serial communication interface) is used for external mode. Receiving and transmitting pins have a role in this communication protocol. Serial communication is satisfied with microprocessor and computer via USB interface. Measurement can be observed simultaneously, and tuning can be done in order to examine the differences. Improvements and tries can be applied in real-time. Rx (receive) and Tx (transmitting) GPIO's are selected from "Configuration settings" and related COM port, which can be shown in the computer "Device Manager" is assigned. Also, the baud rate can be selected.

The other real-time communication method is "CAN communication". SIMULINK has CAN communication ability. There are CAN transmit and receive blocks. Data are packed and transmitting via CAN communication. After that, this data is unpacked at the desired place. The intended data can be sent to the microprocessor; after that, processing-related data is sent to the computer again. Also, PCAN emulator from PEAK-System firm is used in this thesis for CAN communication. There is "Network Vehicle Toolbox" in Simulink, and PCAN can be selected thanks to "Network Vehicle Toolbox". Addresses are identified so CAN communication can be satisfied. Real-time data can be observed at the virtual scope and display block in SIMULINK. PID tunes can be done fast and intended reference torque can be changed in real-time so response characteristics can be examined easily. Measurement time can be reduced quietly. It is one of the most important opportunities satisfied from MATLAB.

3.4.4 Microprocessor, inverter and position manager (encoder) demo board's properties

In this application, C2000 series microprocessor TMS320F28069M was used. LAUNCHXL-F28069M demo board which includes TMS320F28069M was preferred because it was cheap, easily achievable, and suitable for development studies. It had input and output pins, so output characteristics could be observed easily. Current calculations from ADC, EPWM processes, etc., could be managed by using these pins easily.

Features for LAUNCHXL-F28069M:

This board has;

- USB connected isolated XDS100v2 JTAG debug probe for real-time debug and flash programming
- 4x 20-pin headers/connectors
- Programmable buttons and LEDs
- TMS320F28069M: 90 MHz C28x CPU, 256 KB Flash, InstaSPIN-FOC and InstaSPIN-MOTION enabled, 12-bit ADC, CAN, 2x encoder interface (eQEP), UART, SPI, and more
- Supports two BoosterPacks
- Two encoder interface connectors
- Isolated CAN transceiver connector

In addition, BoostXL-DRV8301 inverter demo board was used. It was 10A, 3-phase brushless DC drive stage based on the DRV8301 pre-driver and CSD18533Q5A power MOSFET. The module has three low-side current sense amps (2 internal to DRV8301, 1 external). The module also had a 1.5A step-down buck converter, was fully protected with short circuit, thermal, and shoot-through protection, and was easily configured via an SPI interface. First, DC voltage was sent to the inverter. After that, control processing, switching frequency, and PMSM properties were set via microprocessor over Simulink project. Current values were read with ADC. After the control loop, EPMW data was produced and sent to MOSFETs, and three-phase output was connected to PMSM. TMS320F28069M and BoostXL-DRV8301 were pin-compatible, so phase current, phase voltage data, etc. could be transmitted to each other easily.

Features for BOOSTXL-DRV8301:

- 6 to 24V supply input
- Supports up to 14A peak, 10A continuous current output
- Supports voltage and current feedback for InstaSPIN-FOC sensorless control solution
- 3x low side current sense amps, 6x Power FETs (< 6.5mΩ) & 1.5A step down buck converter
- The drive stage is fully protected, including short circuit, thermal, shoot-through, and under voltage protection.

The other board used in this experiment was BOOSTXL-POSMGR. The Position Manager BoosterPack was a flexible low voltage platform intended for evaluating interfaces to absolute encoders and analog sensors like resolvers and SinCos transducers. This low-cost evaluation module becomes a powerful tool for interfacings many popular position encoders types such as EnDat, BiSS, SSI and T-format with C2000 Real-Time Control devices. This thesis used to interpret position data achieved from an absolute encoder that type number is INC-3-075-181001-SSI1-AFL4-5-AN from Zettlex firm. This board was connected with a microprocessor board and PMSM by setting suitable hardware connection. Position data was taken with SPI communication protocol and interpreted in Simulink. This position information was used in control loop.

Features for BOOSTXL-POSMGR:

- 2x channels of RS-485 line interface supporting up to 100m distances
- 1x SinCos analog interface
- 2x 20-pin headers/connectors to LaunchPad
- Capable of supporting 2x absolute encoders simultaneously
- Works with C2000 MCUs

3.4.5 Motor properties

In this thesis, a permanent magnet synchronous motor whose type number M-2310P-LN-04K was used. It had these properties:

- 60 V maximum ınput voltage
- 0.72 Ω phase to phase resistance

- 0.40 mH phase to phase inductance
- 4.64 Vpeak/kRPM back EMF
- 0.28 Nm rated torque
- 4000 RPM rated speed
- 8 pole
- 7A maximum continuous current

3.5 Simulink Model

PMSM torque control algorithm was realized at Simulink platform. In this study, TMS320F28069M microprocessor from Texas Instruments' C2000 series was used. In this algorithm, phase currents Ia and Ib were read with the microprocessor's ADC, as shown in Figure 3.8. These values are transformed to Vd and Vq with Clarke and Park transformations, as shown in Figure 3.9. Also, desired torque was sent with CAN communication as Iq current, and it was compared with Vq as shown in Figure 3.10. Id current was zero (Id=0) for maximum torque production. CAN communication blocks were used to achieve real-time observations, as shown in Figure 3.11.

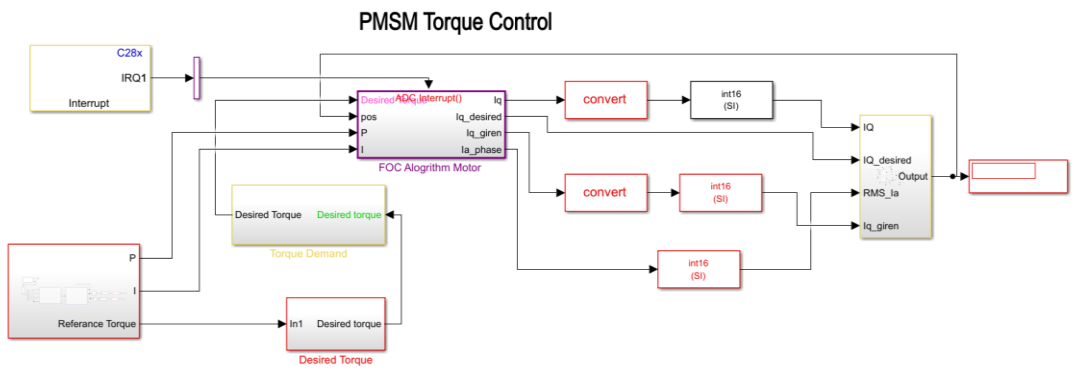

Figure 3.8 : Torque control blocks at SIMULINK.

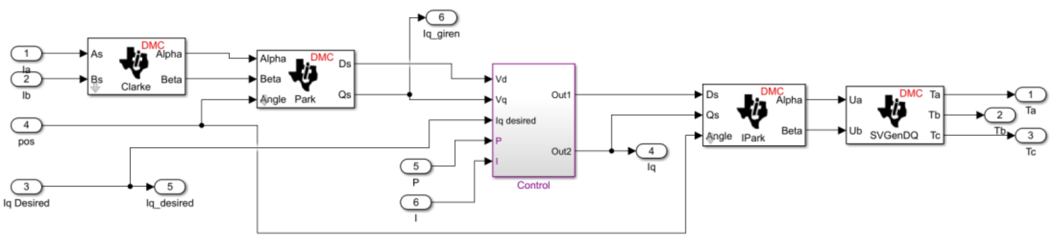

Figure 3.9 : Clarke, park, control, SWPWM structure.

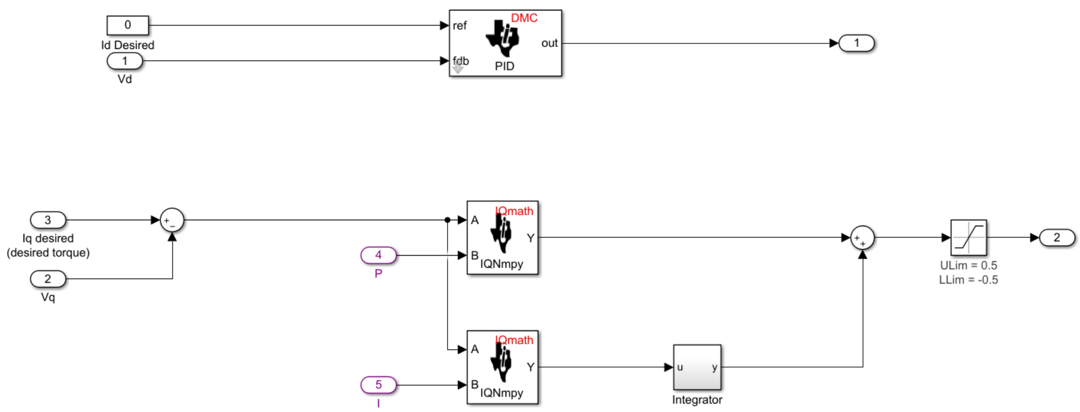

Figure 3.10 : Control PI blocks for Id and Iq.

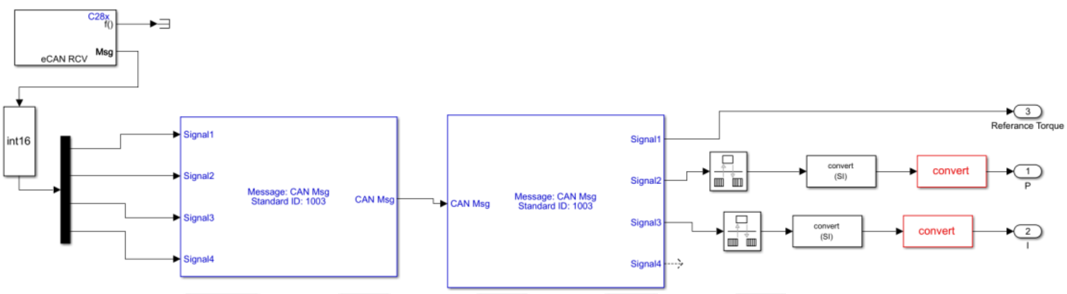

Figure 3.11 : CAN message blocks.

Differences of Fixed and Floating Point Number Units

Digital signal processors (DSPs) are essential for the real-time processing of real-world digitized data, performing the high-speed numeric calculations necessary to enable a broad range of applications. In addition, DSPs enable designers to build innovative features, differentiate value into their products, and get these products to market quickly and cost-effectively.

There are many considerations that system developers weigh when selecting digital signal processors for their applications. Among the key factors to consider are the computational capabilities required for the application, processor and system costs, performance attributes, and ease of development. Balancing these factors together, designers can identify the DSP that is best suited for an application.

Fixed and floating-point numbers are commonly used in digital control applications. Data lengths are the same for both types of applications and identified with bits. However, the dynamic value range is wider at the floating point compared to the fixed point for the same word length. Numbers should be scaled at fixed number systems due to overflow and quantization errors, so floating point systems can be implemented easier for real-time applications and digital filters because scaling is not required for floating-point systems as the numeric display range is wide. Number units are shown with IQ format in fixed-point systems, and resolution of the numbers are the same independent of the piece of numbers; whereas, the resolution of number varies according to piece of numbers in floating-point units. After all, almost all microprocessors and controllers are designed in fixed-point number units. The reasons for this can be listed as follows.

The logic circuit design of fixed-point number units is easier than floating-point units in terms of size and power pulses. That is, the area occupied by fixed-point number units and the power pulse is less than the floating-point unit.

In terms of memory usage and speed, fixed-point number unit calculators are capable of processing faster by taking less space than the floating-point unit.

Fixed-point units are cheaper when economy and cost requirements are taken into account.

The range of values of the units that we will use in our application is selected between -1 and 1. The voltage value read from the output is normalized in high precision fixed-point format, taking 24 bits for the decimal point, Q24 format, to signal that can vary between -1 and 1. The maximum value is 1, and the minimum value is -1. The product of any two numbers between -1 and 1 will again be between -1 and 1. That is, the format of the same number unit is preserved as a result of multiplication. In this way, the processor is used more efficiently by not using complex number conversion blocks. In addition, the algorithm can be easily moved from one platform to another, making it understandable for engineering units. TMS320F28069M microprocessor, which can operate with a fixed point number unit, was preferred to be used within the scope of this thesis since the fixed point number unit has the advantage of fixed resolution along with the features mentioned above.

All of the ADC, EPWM outputs, P,I (proportional and integral gain coefficient) parameters, Park-Clarke transformations, SPWM blocks, and all other parameters were scaled with fixed-point number units.

4. PROGRAMMING, TEST AND EXPERIMENTS

In this chapter, experimental works, results, and analyses were explained and interpreted.

4.1 Design and Practical Implementations

4.1.1 Motor driver block schematic

In this thesis, torque control of PMSM was satisfied and a test setup was constructed. Block diagram of intended motor driver was shown in Figure 4.1. Motor driver mainly included microprocessor, VSI (Voltage Source Inverter), DC-DC converters to supply feeding voltages, position manager card to obtain position feedback, CAN buffer and programming interface. Roles of these components would be explained at the next parts.

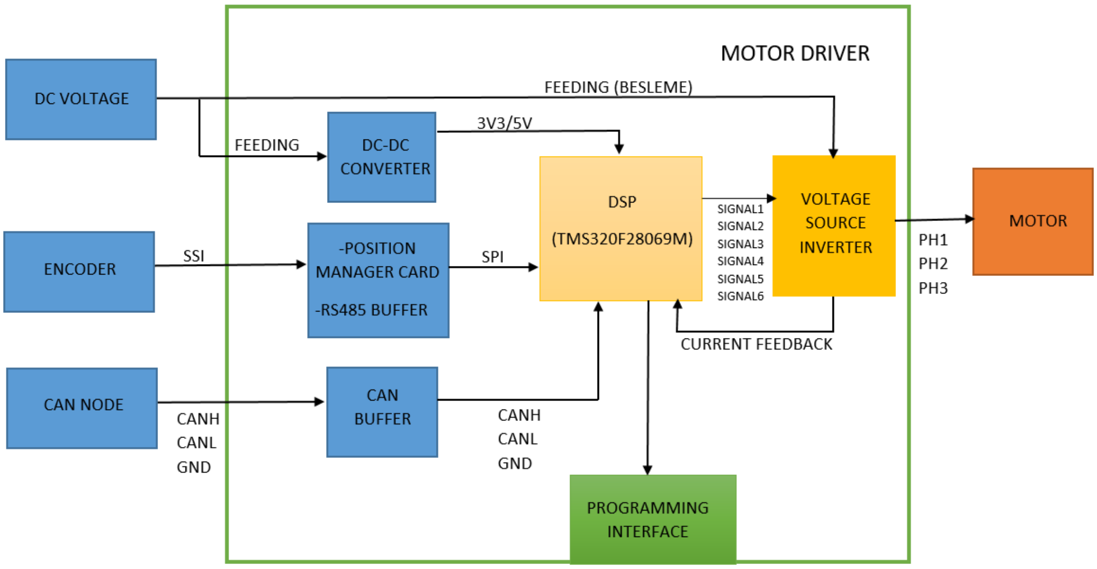

Figure 4.1 : Intended motor driver schematic.

Furthermore, motor driver implementation, tests and performance analyses were satisfied at real world with a test setup.

4.1.2 Test setup system and block schematic

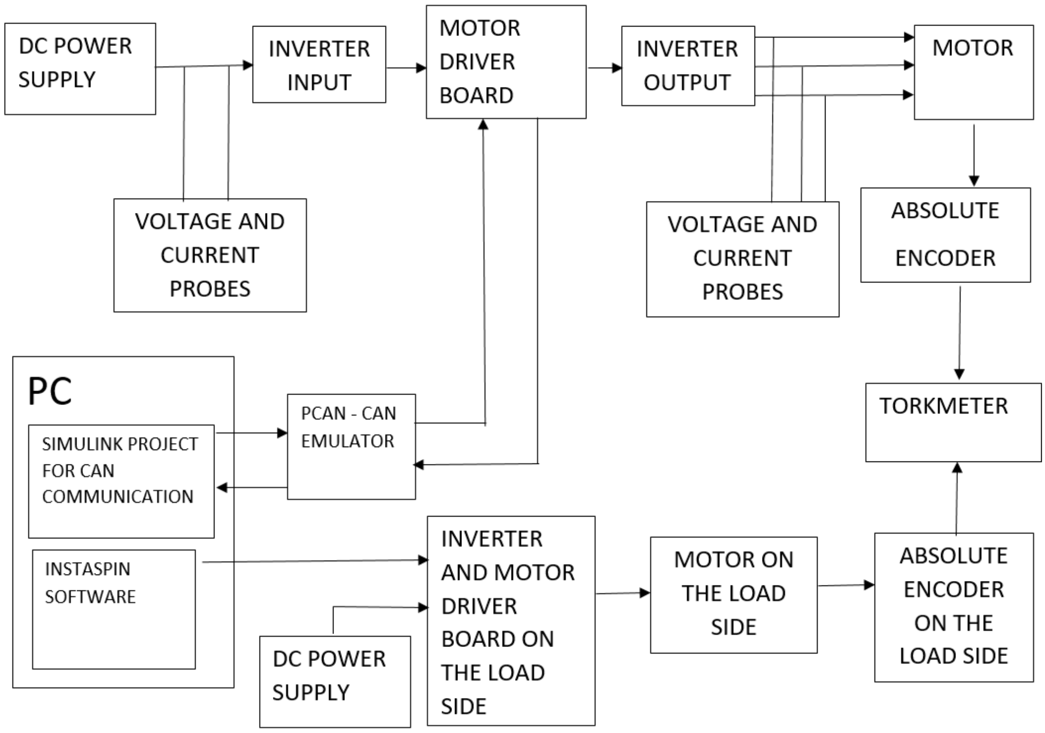

Figure 4.2 : Motor driver test setup block schematic.

Test block schematic and test setup were shown in Figure 4.2 and Figure 4.3. LaunchpadXL-F28069M and BoostXL-DRV8301 demo boards were used for microprocessor and inverter hardware. In addition, SIMULINK code constitution, absolute encoder integration, SPI communication, CAN communication, torque meter integration were satisfied.

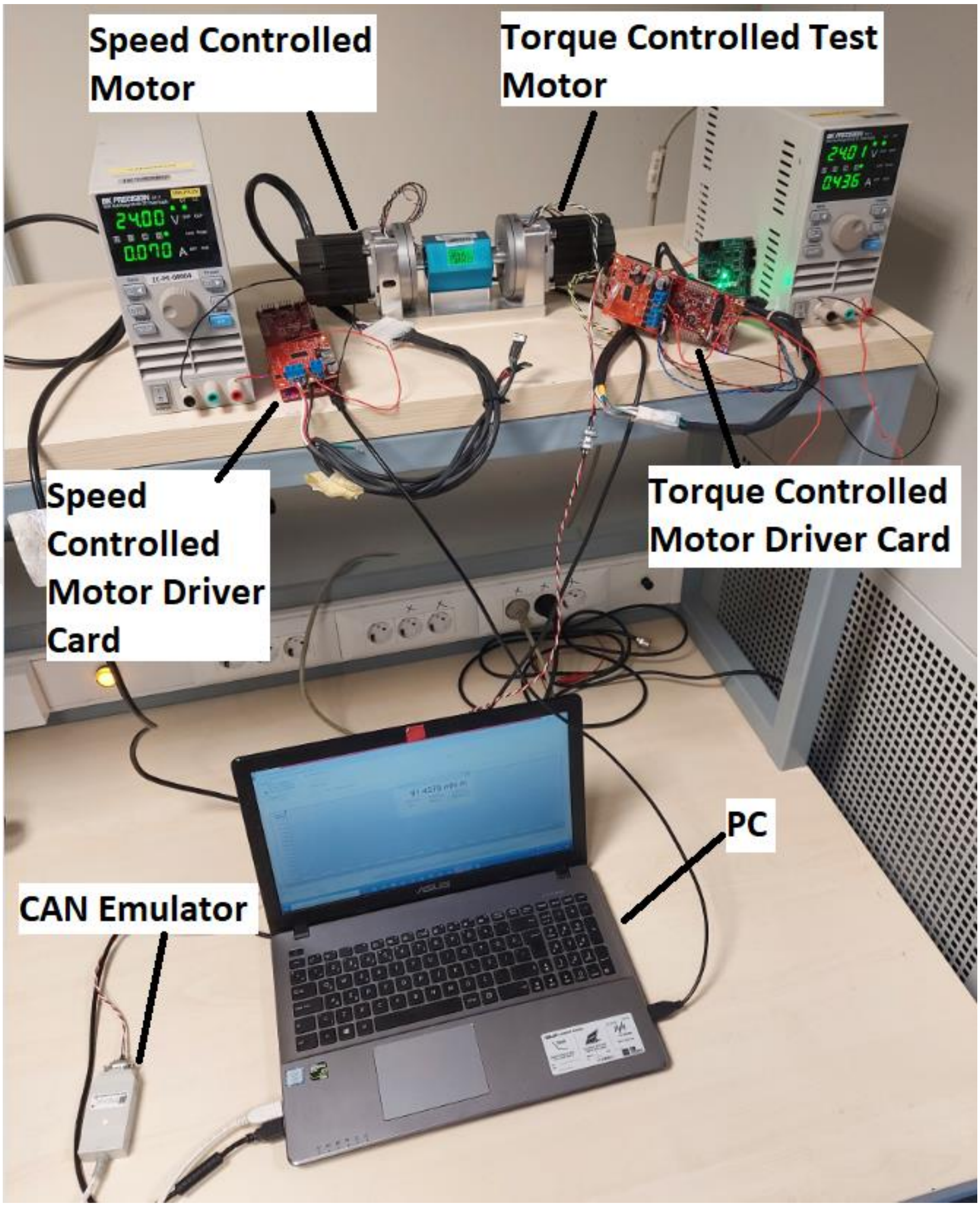

Figure 4.3 : Motor driver test setup.

The motor driver development setup included two motors, two encoders, and a torque meter, as shown in Figure 4.4. One side motor was used for constant torque control; the other side was used for constant speed control. Constant speed control was applied from one side in order to test the torque control algorithm from the other side. That is, a constant speed was satisfied for both motors, and varying torque values were applied from one side motor. Intended torque values in constant speed were observed from the torque meter.

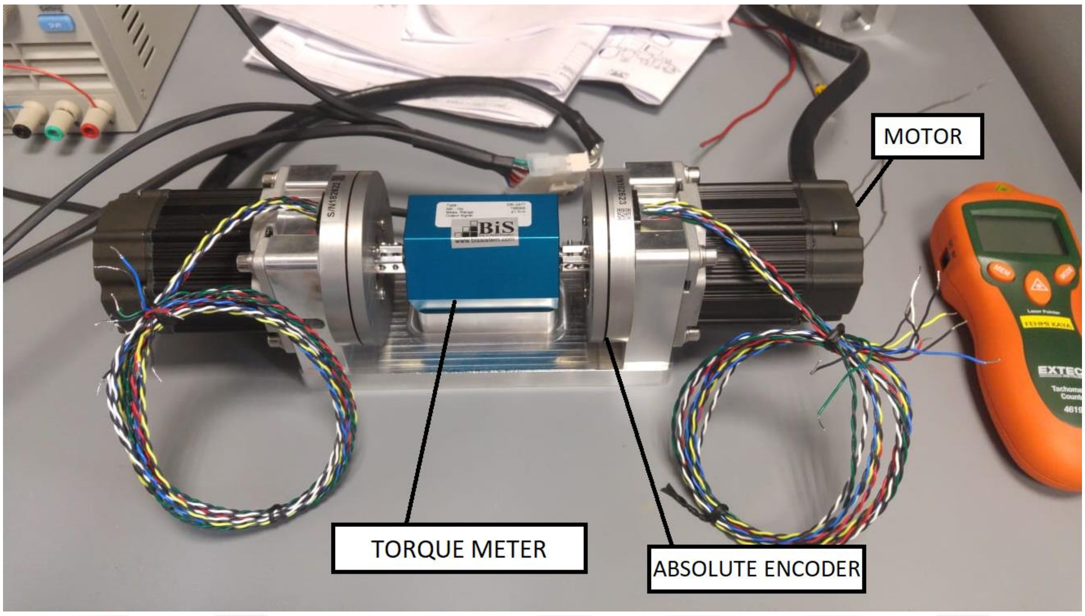

Figure 4.4 : Motor, encoder and torque meter.

4.1.3 Absolute encoder integration

Position information was obtained by using the absolute encoder, and this data was used in Clarke and Park transformations and control loops. The absolute encoder was useful for sensitive position control; hence, it was useful for torque control because position data was given as exactly. In contrast, incremental encoders were generally preferred for PMSM control because of their low cost and low volume. However, position data required reference points, and position information is not exact at incremental encoders. Therefore, incremental encoders were not selected in this thesis. The optical absolute encoder structure was shown in Figure 4.5. Position data is saved as binary, so the exact position can be determined. Also, position information is saved even if power is interrupted.

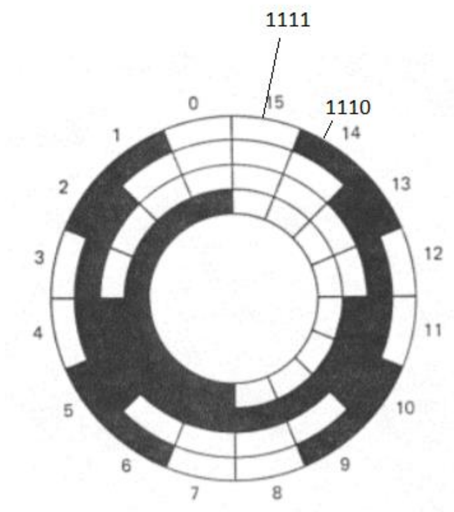

Figure 4.5 : Absolute encoder logic.

In this study, the absolute encoder was preferred because sensitive torque control was intended. BOOSTXL-POSMGR board was used in order to process encoder data. SPI communication was satisfied at Simulink. Position data were integrated into the control loop after required data type transformations. All of the applications were verified at Simulink.

Output of the absolute encoder includes “Data+”, “Data-“, “Clk+”, “Clk-“, “Power” and “Gnd” lines. These lines were arrived to position manager card with SSI (Synchronous Serial Interface) protocol. There were RS485 buffers in this position manager card and Data can be converted to single line instead of Data+ and Data- lines thanks to these buffers. Also, Clock can be managed from single line. In this experiment, the communication between the position manager card output and microprocessor was satisfied with SPI communication protocol. Microprocessor was selected as master, and the position card was slave (SIMO – Slave Input, Master Output). This can be set at Simulink’s Configuration Parameters. The communication protocol between the absolute encoder and the microprocessor was shown in Figure 4.6.

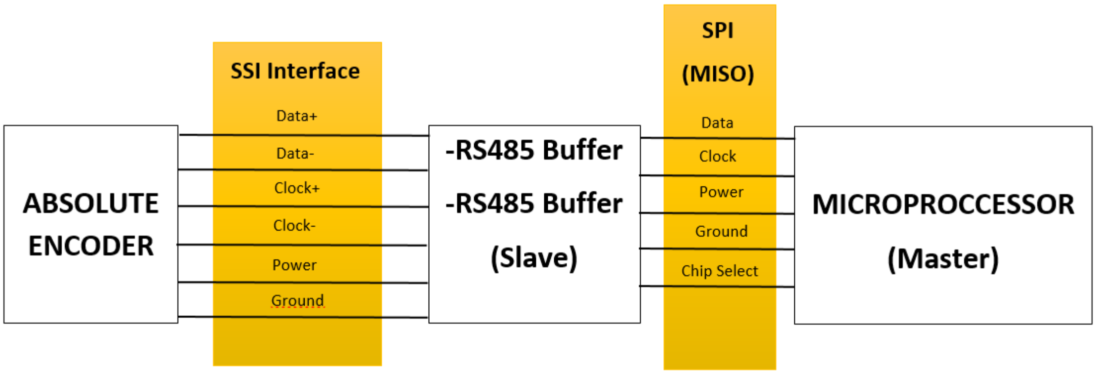

Figure 4.6 : Absolute encoder and microproccessor connection.

The encoder card was connected to the microprocessor. After the control loop, motor behavior was managed. Connections were shown in Figure 4.7.

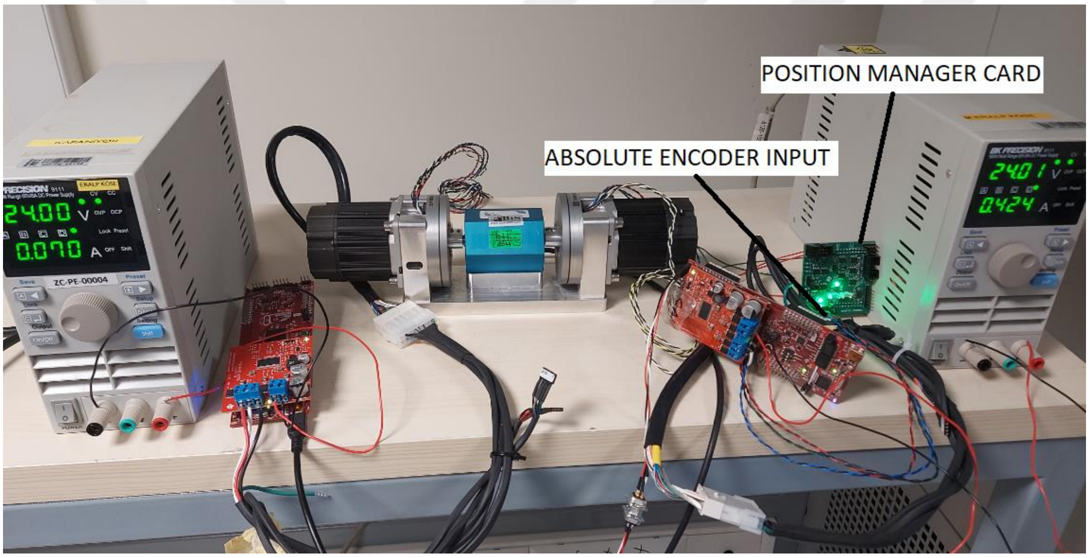

Figure 4.7 : Encoder, inverter, PMSM connections.

4.1.4 Motor torque constant verification

In this thesis, Permanent Magnet Synchronous Motor was used, which type number was M-2310P-LN-04K. Its torque constant value was not indicated in the motor's datasheet. Initially, the motor torque constant was verified experimentally for reliability. To do this, intended torque values were sent. After that, RMS current and torque meter output values were compared. Results were shown in Table 4.1.

Table 4.1 : Torque values and corresponding RMS currents

Torque Meter Output (mNm)	Phase RMS Current (mA)
8.5	232
17	383
25.5	551
34	723
42.5	898
51	1075
59.5	1252
68	1428
76.5	1605
85	1783

Torque value can be obtained as multiplication of RMS current and torque constant. If the torque constant was 0.047 Nm/Amps; that is, if the RMS current is multiplied with 0.047, the graph can obtained as follows (Figure 4.8).

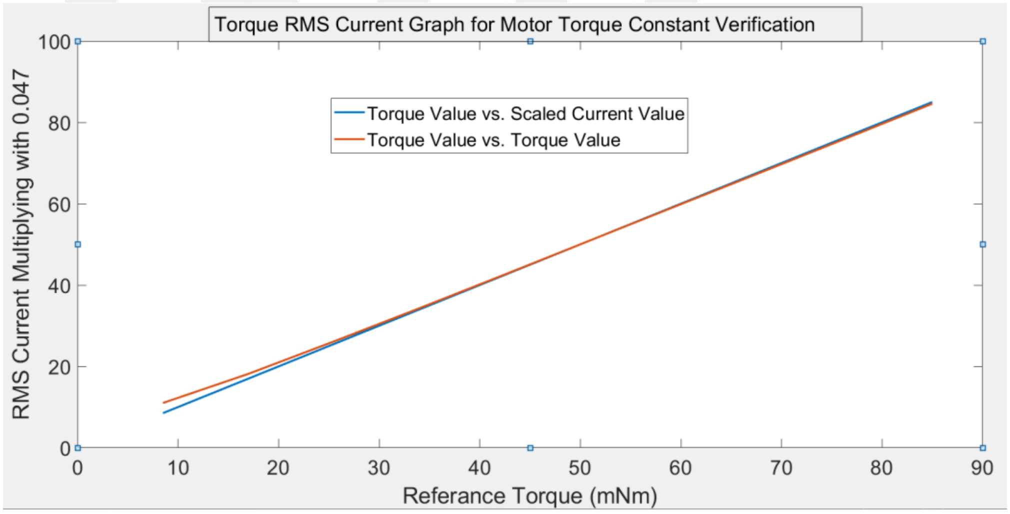

Figure 4.8 : Torque vs RMS current graph.

The blue line in Figure 4.8 indicated the torque vs. RMS current characteristic. And the red line was the linear Torque vs. Torque line. If motor toque constant was accepted as 0.047 Nm/Amps, Red and Blue lines could overlap, so the motor torque constant was about 0.047 Nm/Amps experimentally.

4.1.5 CAN communication basis and performance analysis

My torque control algorithm was tested for a variety of MOSFET switching frequencies. PMSM was driven with intended torque values at a constant speed which was 300 rpm. After that, step response and RMS current ripple were examined. These observations were applied at different MOSFET switching frequencies, which were 10 kHz, 15 kHz, 20 kHz, and 25 kHz. A new Simulink project which was different from the torque control algorithm project, was used for CAN communication. Intended torque values were transmitted, and Iq current ripple was observed in real-time via CAN communication at Simulink. To do this, PCAN from PAEK System firm was used, which was a hardware for CAN communication. Network Vehicle Toolbox in Simulink was used, and the PCAN device was selected to ensure communication. Fast and correct measurement was satisfied thanks to this method. Also, PI tuning could be done easily. It was not necessary to build the code to the processor constantly with real-time observation. That is, the control algorithm was built firstly; after that, the torque reference or PI values changing, etc., could be satisfied in real-time with a useful interface as shown in Figure 4.10. It was a very fast and efficient method.

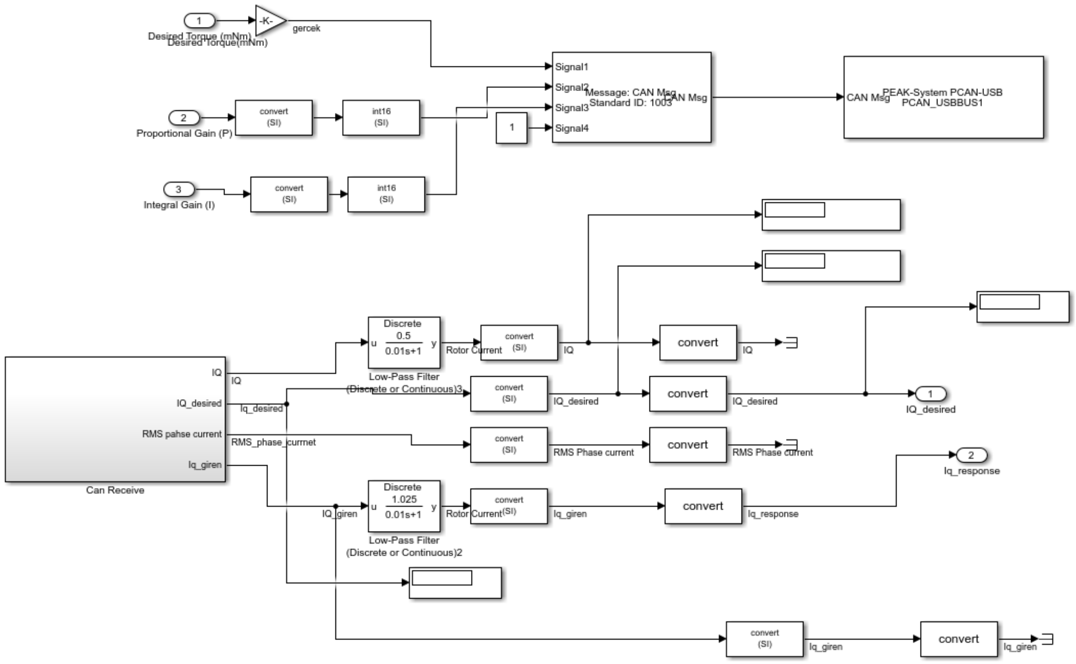

Figure 4.9 : Simulink project which satisfies receiving and transmitting via CAN communication.

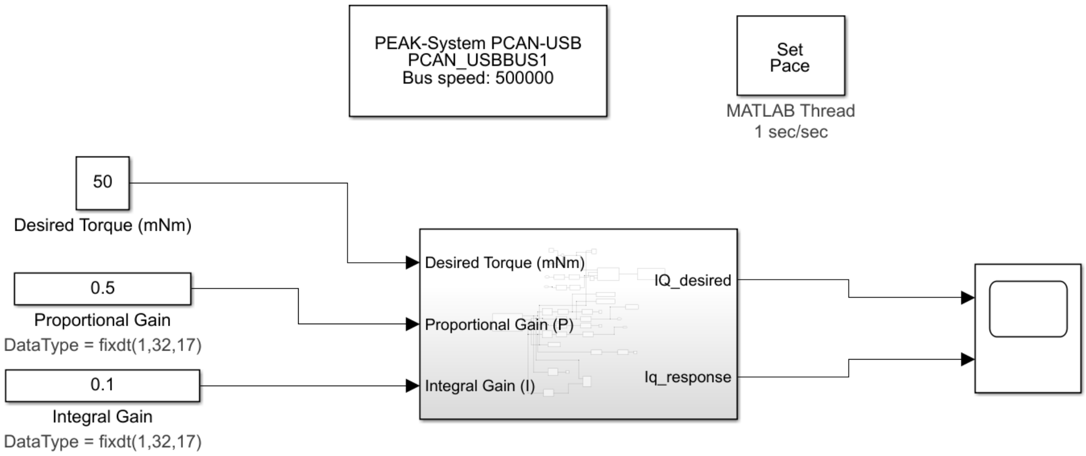

Figure 4.10 : Intended torque, proportional and internal gain coefficient blocks.

Intended torque reference value and proportional, integral gains were transmitted to the control algorithm in real-time via CAN communication. Step response time was examined with Iq (quadrature axis) current response; actually, the electrical response was obtained for step torque characteristics. To do this, Iq current data was received from the control algorithm with CAN communication. Also, the mechanical response could be observed with torque meter output. In addition, RMS current ripple was observed at SIMULINK.

4.2 Motor Driver Performance Tests

In this application, 70 mNm torque value was sent initially as a step operation. This torque was increased to 90 mNm after 10 seconds. The rated torque values of PMSMs used in this study were 280 mNm, and the 90 mNm torque value was selected randomly during the tests. These operations were repeated for different MOSFETs switching frequencies which were 10 kHz, 15 kHz, 20 kHz, and 25 kHz.

The Torque meter had a mechanical response. Torque ripple could be observed thanks to the torque meter, so reliability analysis could be ensured. Torque meter tolerance was 0.25%.

Initially, switching frequency was set to 10 kHz, and torque values were observed with torque meter as shown in Figure 4.11. Also, torque ripple was observed, as shown in Figure 4.12.

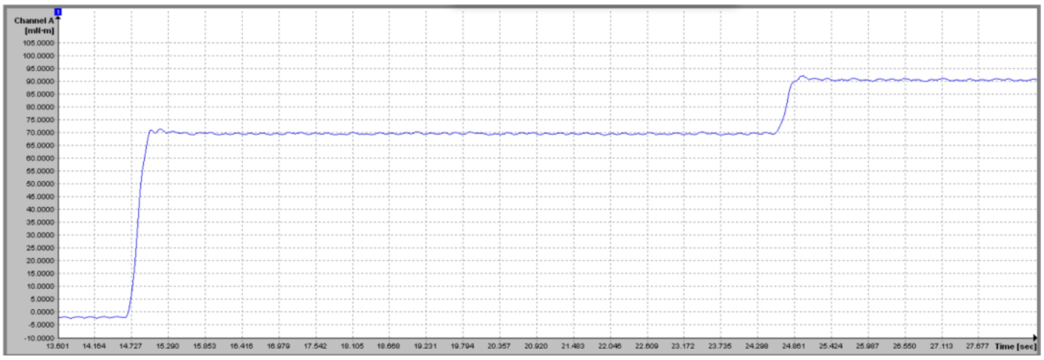

Figure 4.11 : Torque value observation at 10 kHz switching frequency.

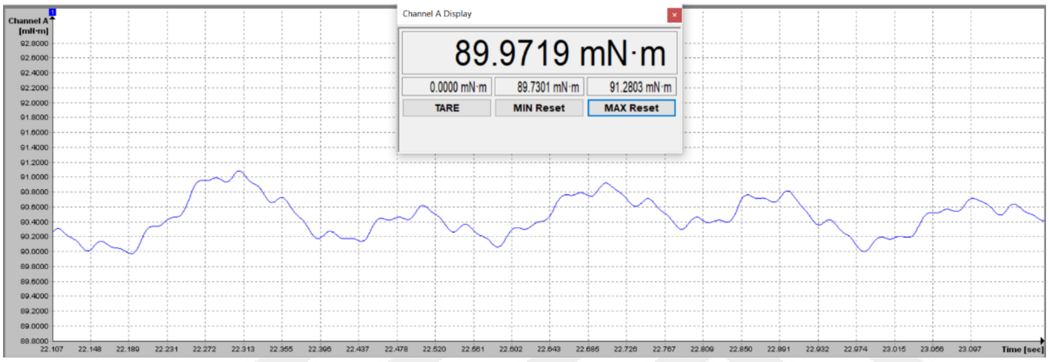

Figure 4.12 : Torque ripple at 10 kHz switching frequency.

Torque ripple was 1.72%, as shown in Figure 4.12. In addition, Iq current response, which proportional to torque, was observed at Simulink. Electrical response and settling time can be examined thanks to Iq current. CAN communication and virtual scope in Simulink were used in order to observe Iq current.

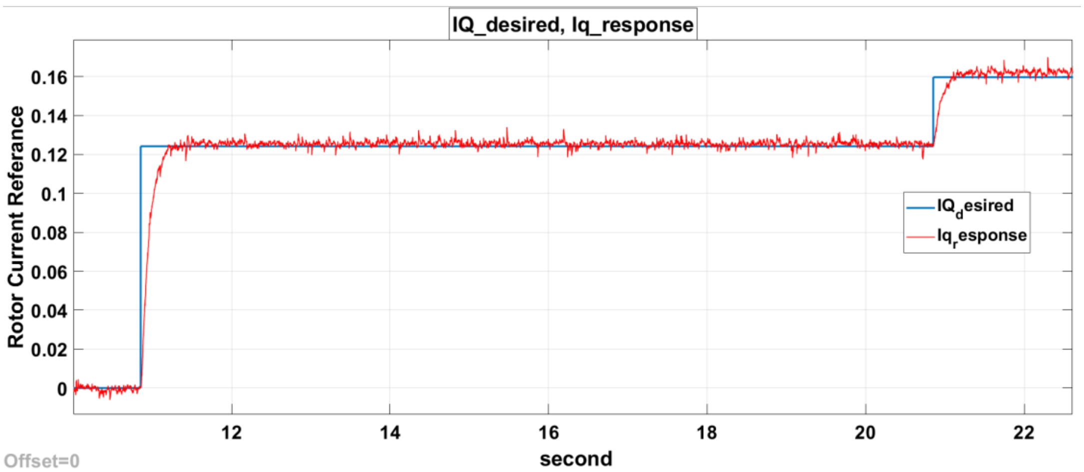

Figure 4.13 : Iq current characteristic at 10 kHz switching frequency.

Settling time at 10 kHz switching frequency was about 300 milliseconds, as shown in Figure 4.13.

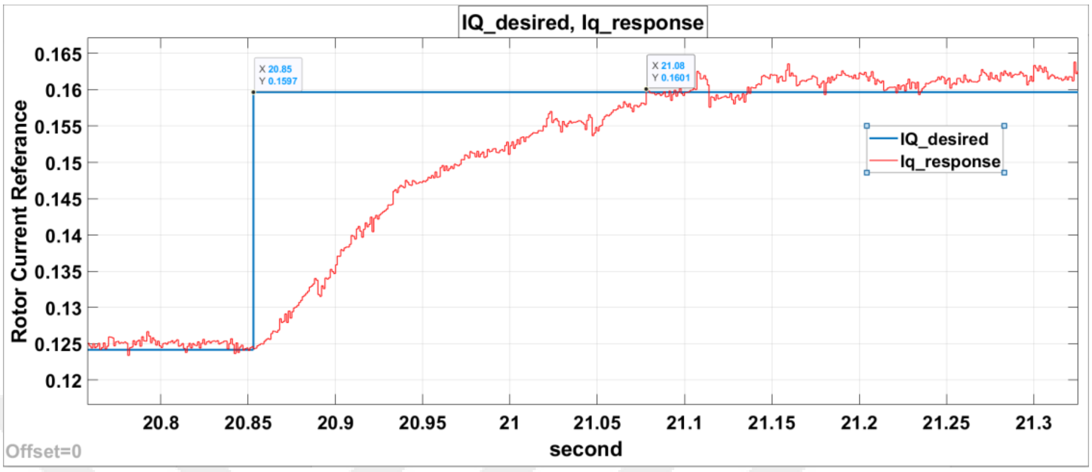

Figure 4.14 : Step response settling time at 10 kHz switching frequency.

Secondly, the switching frequency was set to 15 kHz, and the same torque values were sent that were 70 mNm and additive 20 mNm steps, respectively. Torque ripple was measured about 1.57% at this condition, as shown in Figure 4.16.

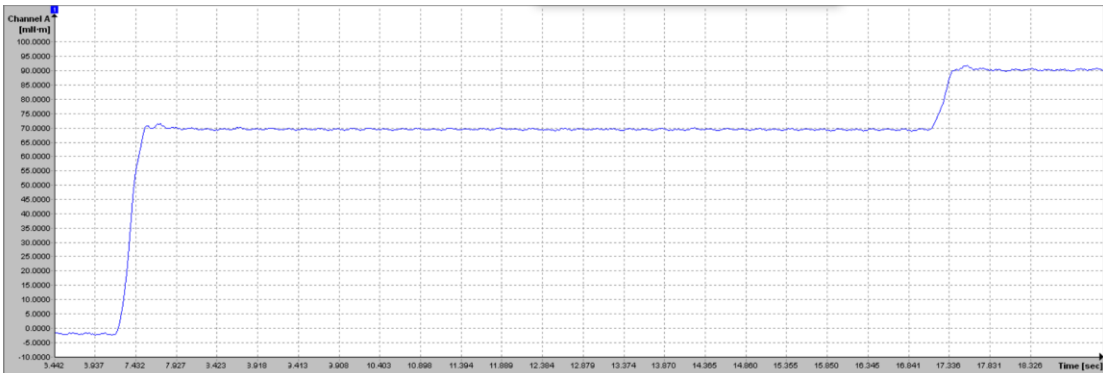

Figure 4.15 : Torque value observation at 15 kHz switching frequency.

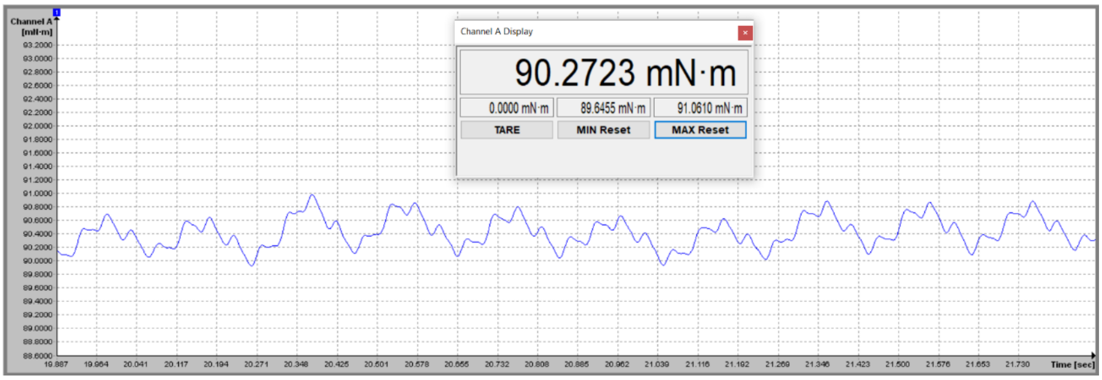

Figure 4.16 : Torque ripple at 15 kHz switching frequency.

Settling time was observed from SIMULINK, and its value was about 300 milliseconds, similar to 10 kHz switching frequency condition. This graph was shown in Figure 4.18.

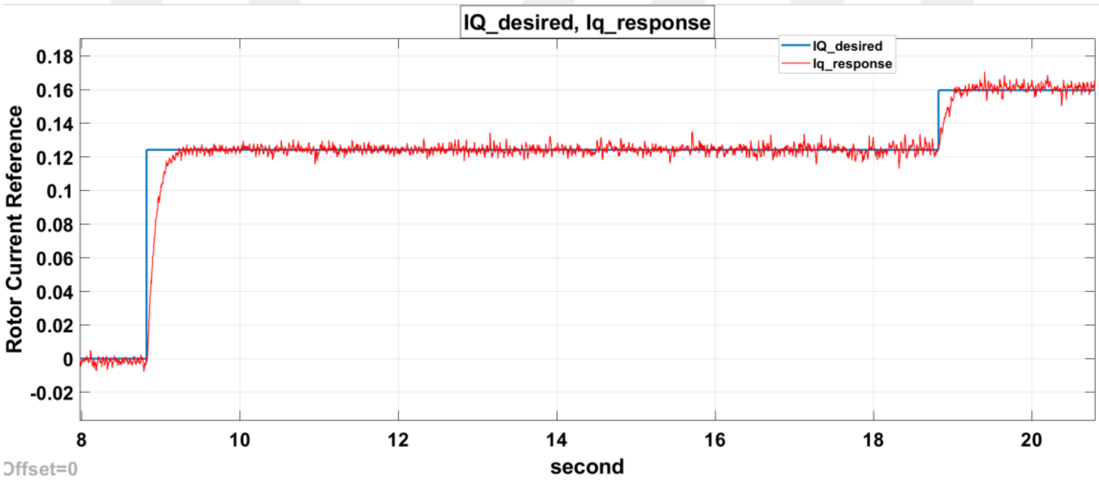

Figure 4.17 : Iq current characteristic at 15 kHz switching frequency.

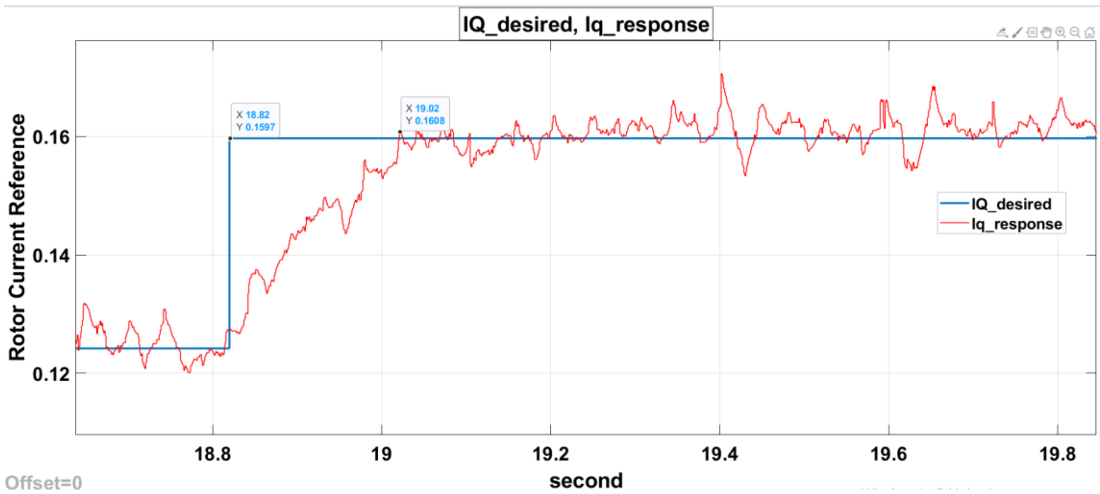

Figure 4.18 : Step response settling time at 15 kHz switching frequency.

After that, the same operation was repeated for 20 kHz switching frequency, and the torque ripple was measured about 1.3%, and settling time was about 300 millisecond, as shown in Figure 4.20 and Figure 4.22, respectively.

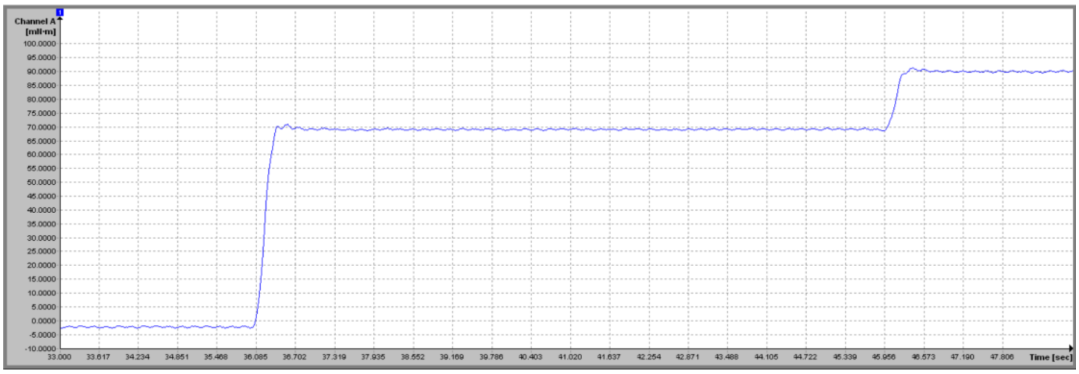

Figure 4.19 : Torque value observation at 20 kHz switching frequency.

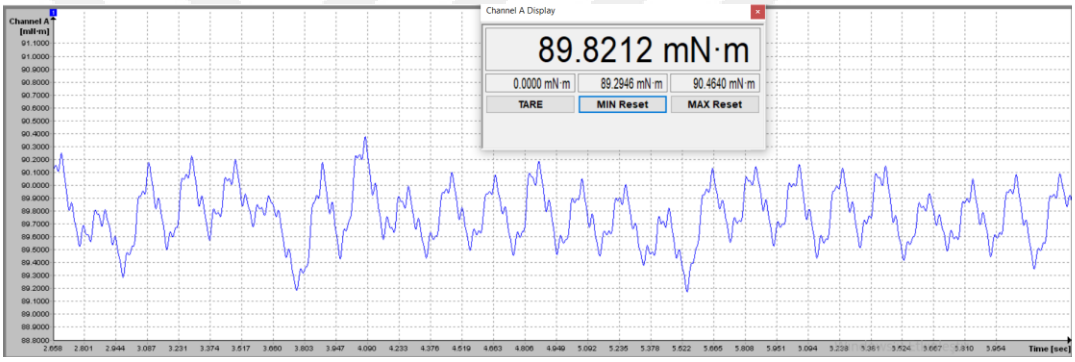

Figure 4.20 : Torque ripple at 20 kHz switching frequency.

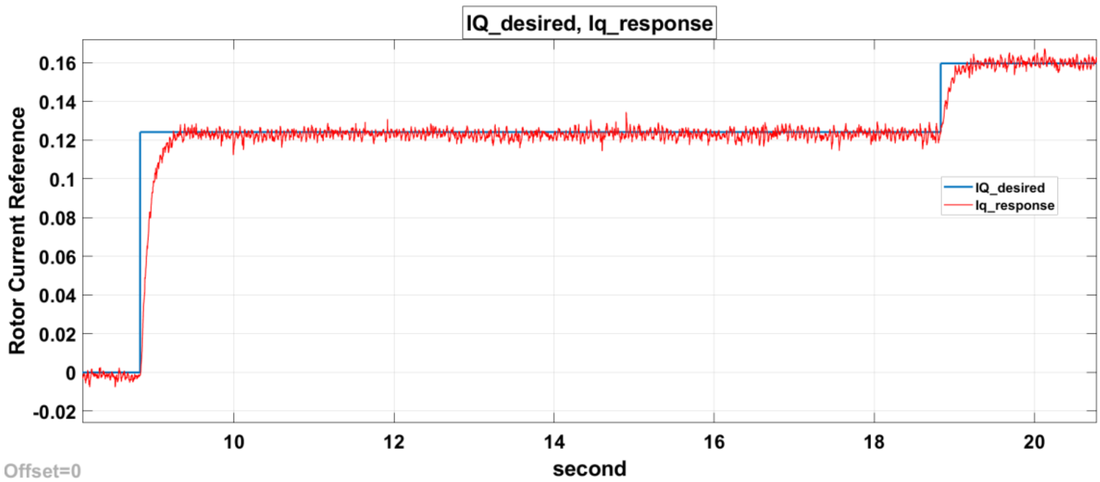

Figure 4.21 : Iq current characteristic at 20 kHz switching frequency.

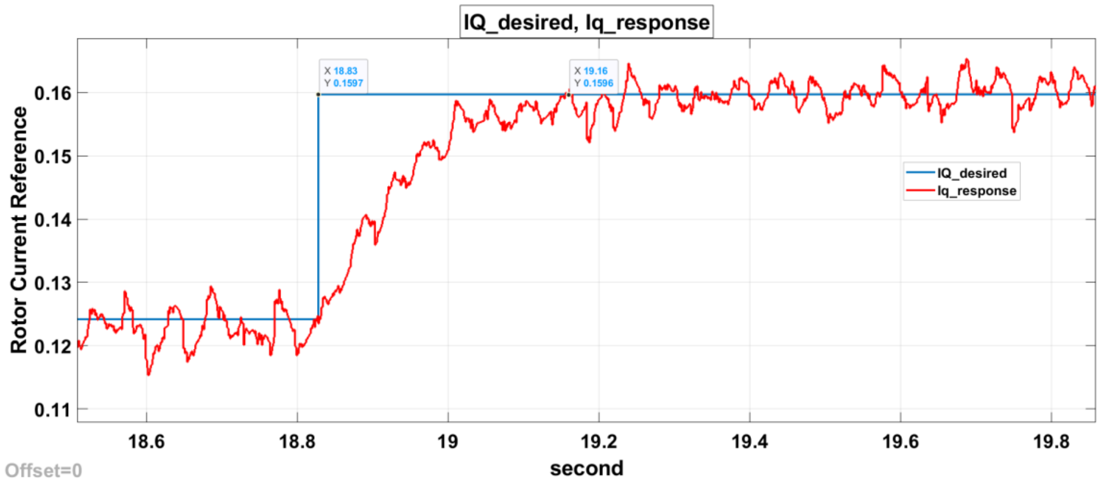

Figure 4.22 : Step response settling time at 20 kHz switching frequency.

Lastly, the switching frequency was set to 25 kHz. Torque ripple was about 1.41%, as shown in Figure 4.24, and settling time was about 300 milliseconds, as shown in Figure 4.26.

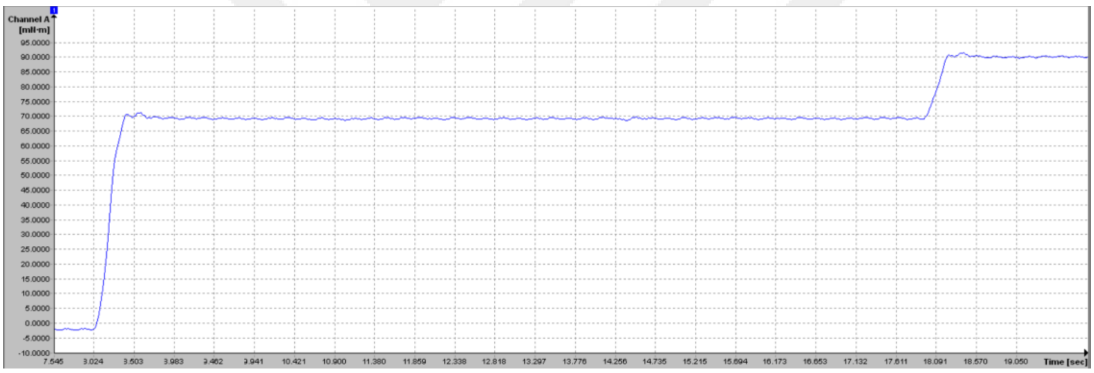

Figure 4.23 : Torque value observation at 25 kHz switching frequency.

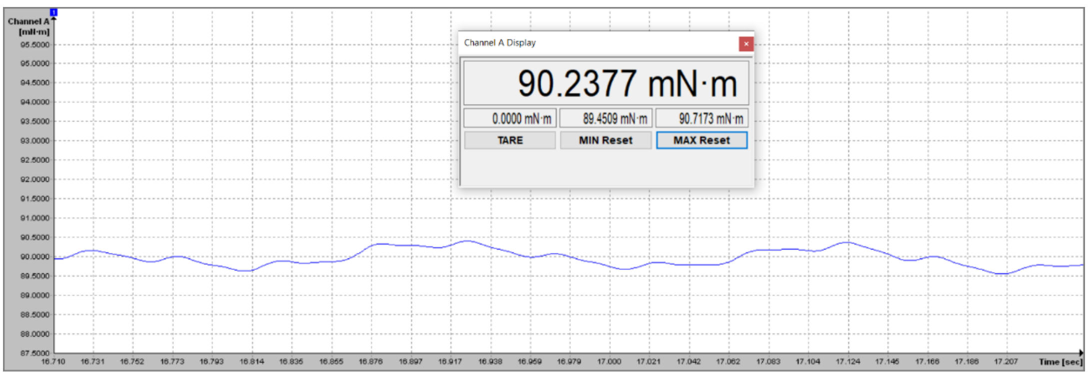

Figure 4.24 : Torque ripple at 25 kHz switching frequency.

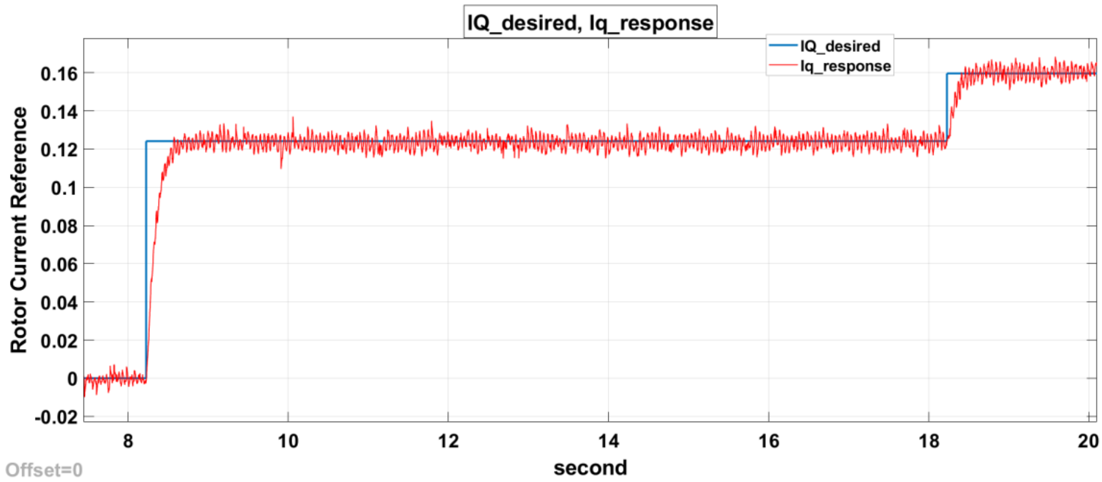

Figure 4.25 : Iq current characteristic at 25 kHz switching frequency.

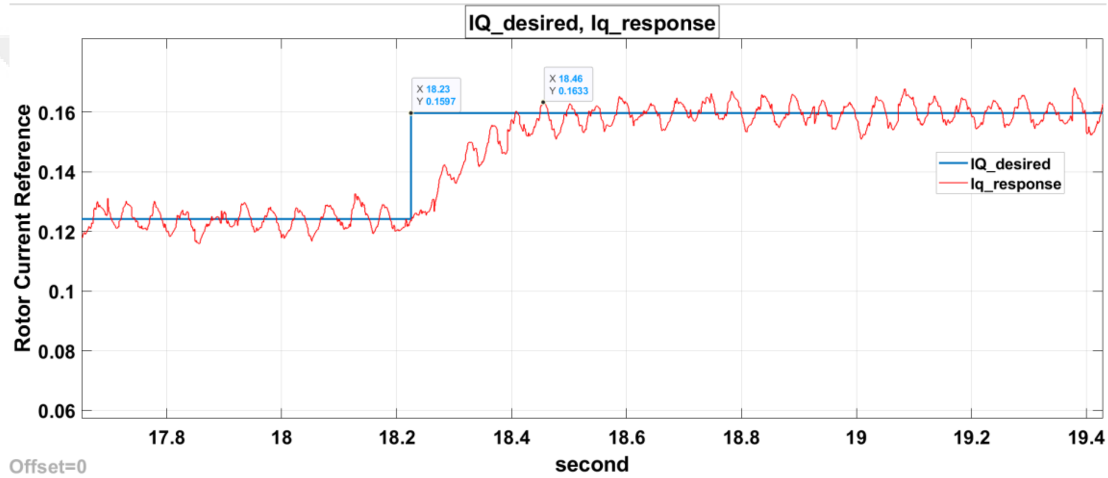

Figure 4.26 : Step response settling time at 25 kHz switching frequency.

In summary, settling time was about 300 milliseconds for all of the trying switching frequencies, and torque ripples were observed as Table 4.2. 20 kHz switching frequency was the ideal one for torque ripple. Therefore, 20 kHz switching frequency was selected.

Table 4.2 : Torque ripple according to corresponding switching frequency

Switching Frequency	Torque Ripple
10 kHz	1.72%
15 kHz	1.57%
20 kHz	1.30%
25 kHz	1.41%

In our stabilization systems, it was aimed that torque ripple should be less than %5, and currently used motor driver torque ripple, which is imported from abroad, was %5. However, torque ripple was less than 2% in our algorithm. Therefore, Torque ripple, which was tested with our algorithm, satisfies our specifications.

In addition, motor drivers should satisfy Military standards. MIL-STD CE102 Electromagnetic compatibility test, which was conducted emission test, and temperature test were observed at next part. -40 degree and +55 degree ambient temperature characteristics were observed. These tests could be applied at the electronic card stage. Vibration, drop tests, etc., could be applied to devices. In this thesis, there was not produced device. An electronic circuit board was used, and the torque algorithm, which was produced from us, was tried. Therefore, MIL-STD CE101, CE102 Electromagnetic compatibility tests, and temperature tests were sufficient at this stage. The other environment conditions tests and radiated tests could not be implemented on electronic circuit boards. In addition, other tests were not only related to our electronic card, but also, they were related to mechanical sufficiency, chassis quality, etc. These mechanical issues were not related to this thesis.

4.3 Temperature Tests For Motor Driver Card

Figure 4.27 : Temperature test setup at the oven.

Environmental conditions were one of the most crucial things for Military applications. Devices were intended to work between -40°C and +55°C. In this thesis, temperature tests were observed. It was important to ensure microprocessor, driver, MOSFETs, and encoder board preferences.

The motor driver board was placed in the oven as shown in Figure 4.28 and Figure 4.29.

Figure 4.28 : The oven test.

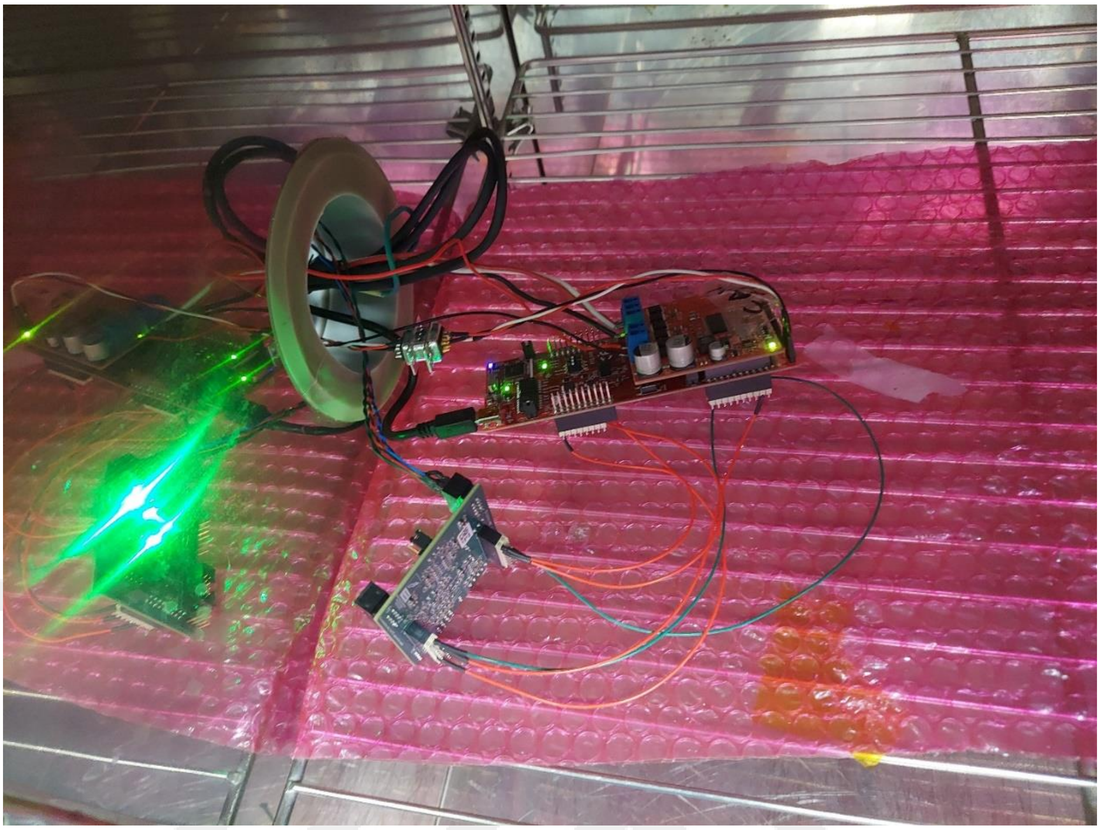

Figure 4.29 : Motor driver card in the oven.

Performance analysis was done for -40°C initially. Also, a thermistor was used to measure the circuit card's and the microprocessor's temperatures, as shown in Figure 4.30 and Figure 4.31.

Figure 4.30 : The temperature of the oven.

Figure 4.31 : Temperature measurement with the thermistor.

These observations were done with 20 kHz switching frequency which was the most ideal one as observed previous part. Step characteristic was the same with the previous part. Initially, 70 mNm torque value was sent as step operation. After that, 20 mNm additive torque value was sent. Initially, the motor driver worked successfully but CAN communication was not satisfied. It caused that, clock signal didn't work correctly. Normally, the microprocessor's internal clock was used. However, an external oscillator was added to solve this problem, so the clock signal worked properly, and CAN communication was achieved successfully. Torque characteristic, torque ripple, Iq current characteristic, and settling time at -40°C can be seen in Figure 4.32, Figure 4.33, Figure 4.34, and Figure 4.35, respectively.

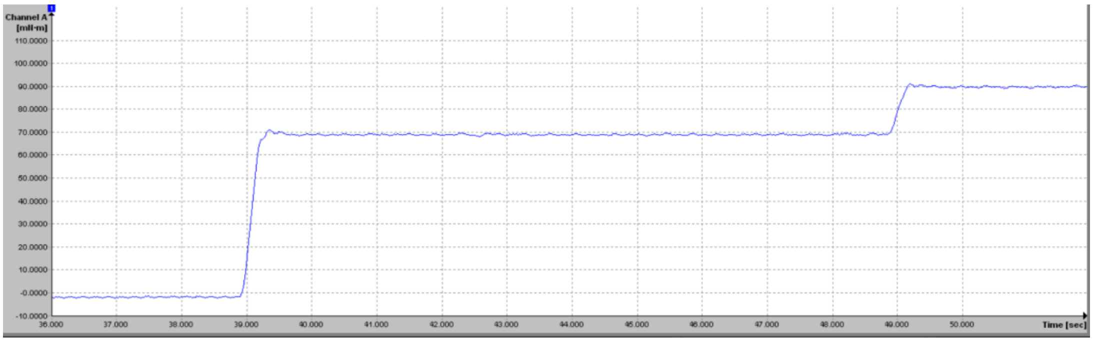

Figure 4.32 : Torque characteristic at (-40) degree.

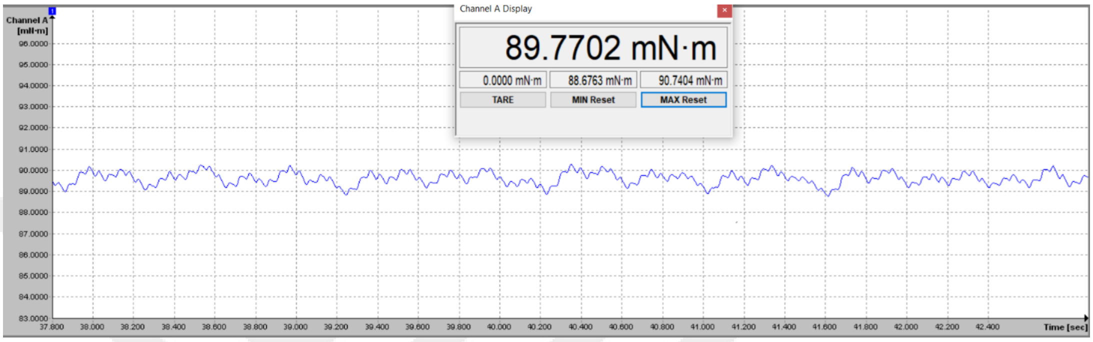

Figure 4.33 : Torque ripple at (-40) degree.

Figure 4.34 : Iq current characteristic at (-40) degree.

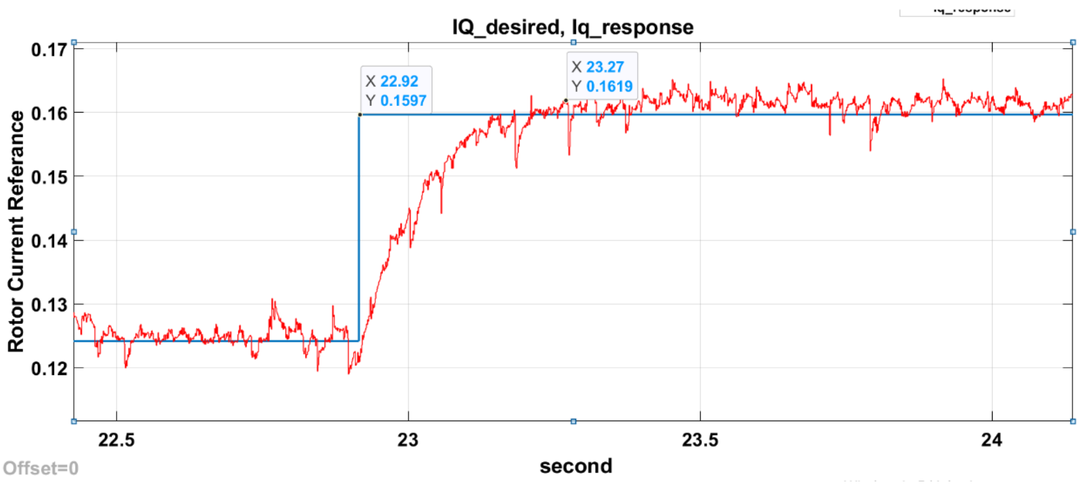

Figure 4.35 : Settling time at (-40) degree.

Torque ripple was 2.3%, and settling time was about 350 milliseconds, as shown in Figure 4.33 and Figure 4.35, respectively. It was observed that the performance of the motor driver was not significantly affected from -40°C. These performances were acceptable for Military standards.

These temperature tests were also repeated at +55°C. Torque characteristic, torque ripple, Iq current characteristic and settling time at -40°C cn be seen in Figure 4.36, Figure 4.37, Figure 4.38, and Figure 4.39, respectively.

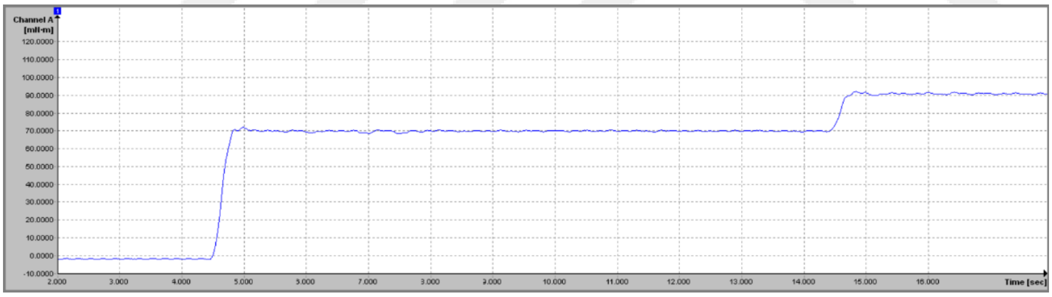

Figure 4.36 : Torque characteristic at 55 degree.

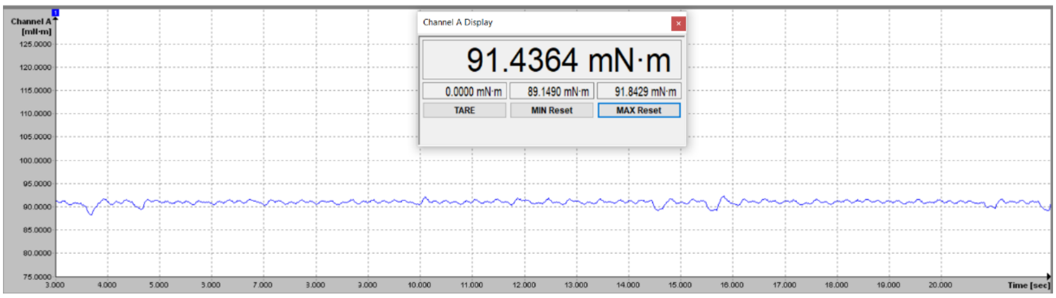

Figure 4.37 : Torque ripple at 55 degree.

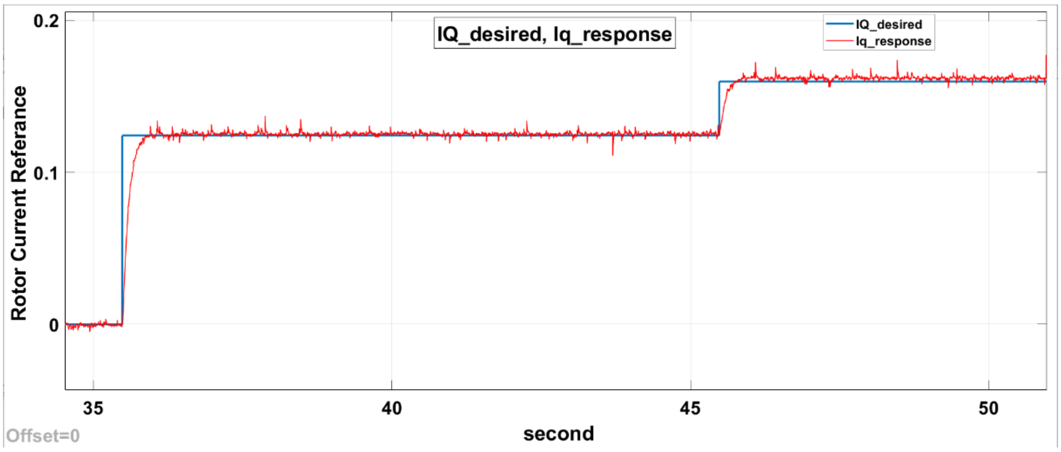

Figure 4.38 : Iq current characteristic at 55 degree.

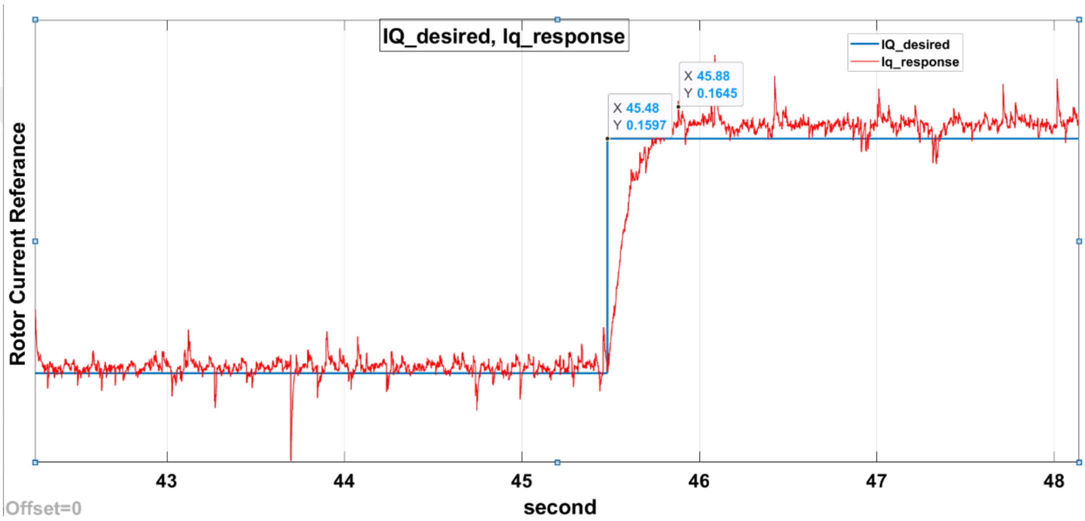

Figure 4.39 : Settling time at 55 degree.

Torque ripple was 3%, and settling time was about 400 milliseconds, as shown in Figure 4.37 and Figure 4.39, respectively. The performance of the motor driver was affected by temperature a bit. However, it was acceptable. The extreme differences were not observed, and it can be said that the motor driver that used in this study satisfied the Military standards in terms of temperature durability.

Electromagnetic acceptance was the other crucial thing for Military standards, and this card was also examined for EMC criteria in the next part.

4.4 Electromagnetic Compatibility Tests

In this thesis, electromagnetic compatibility was examined, and our motor driver card was tested whether it satisfied the MIL-STD-461 standards or not. Thus, CE101 and CE102 tests were applied, and the noise was tried to reduce acceptable limits.

4.4.1 MIL-STD-461 CE102 and CE101 tests

CE101 and CE102 tests were applied in this part and discussed whether it was acceptable or not according to MIL-STD-461 revision "G", the current version. The test title for CE101, "Conducted Emission Audio Frequency Currents, Power Leads" and CE102, "Conducted Emissions Radio Frequency Potentials, Power Leads" provided insight into the test frequency range and methods of measurement. 0-10 kHz frequency band was observed at CE101 test, and 10 kHz-10 MHz frequency band was examined gradually at CE102 test. These tests quantify undesired signals being placed onto the power lines from the equipment under test (EUT). If these tests were not applied or they failed, these signals would conduct via the power distribution to other equipment or radiate into the air for reception by other equipment and may cause harmful interference from either coupling method.

4.4.2 CE 102 Setup

In this setup, spectrum analyzer, metal conductor, and the LISN (Line Impedance Stabilization Network), shown in Figure 4.40 were used for CE102 tests. The LC filter was also formed at the input to reduce the noise, which would be explained in the next parts.

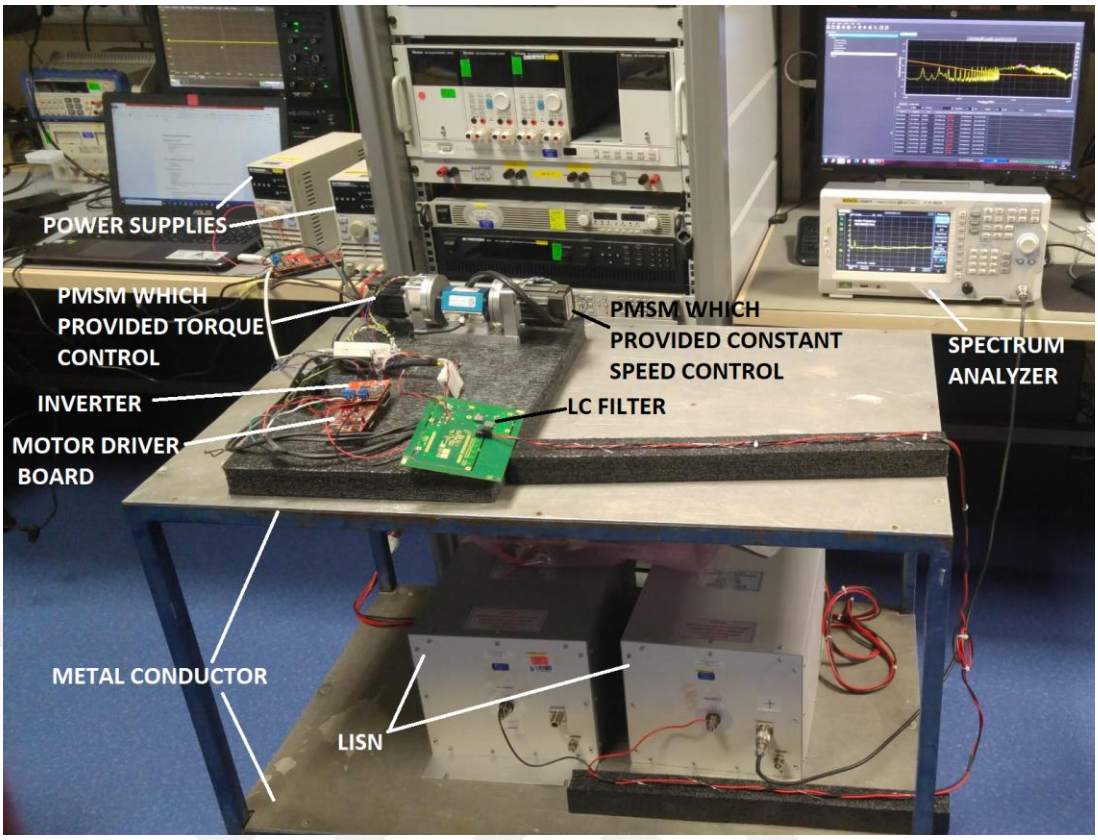

Figure 4.40 : CE 102 setup.

Initially, the CE102 test in MIL-STD-461 military standard was applied in order to check and satisfy electromagnetic compatibility. The current waveform of the power supply was examined in this test while the system was working, and the noise from equipment under test (EUT) to ambient was observed during current conduction.

A spectrum analyzer was used in this test, and the broadcasting noise was followed at different frequency bands. Firstly, 10 kHz - 150 kHz frequency band was scanned with 1 kHz bandwidth, and 150 kHz – 10 MHz frequency band was scanned with 10 kHz bandwidth according to standard. There was a limit line for ground, ship, submarine, and air applications. The noise unit was selected as dBµV (decibel microvolts).

In this test, a Spectrum analyzer from Rigol firm was used and this spectrum analyzer was connected to PC. Rigol's PC software was used, and the limit line is drawn. After that, the setup shown in Figure 4.40 was used, and our device's broadcast was observed whether it was acceptable.

4.4.2.1 Motor driver noise and improvement studies

10 kHz – 10 MHz frequency band was scanned before the motor driver is worked in order to measure ambient noise. It was a control test. Ambient noise should be under

the limit line to test motor driver noise. The graph which was shown in Figure 4.41 was obtained. Ambient noise was under the limit as expected.

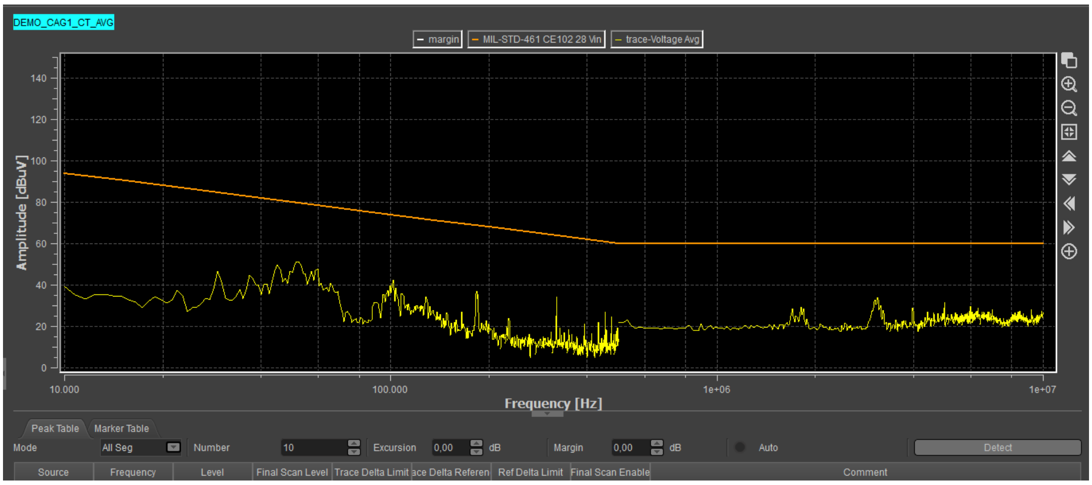

Figure 4.41 : Ambient noise.

After that, the test was repeated when the motor driver was working. 10 kHz – 10 MHz frequency band was observed, as shown in Figure 4.42.

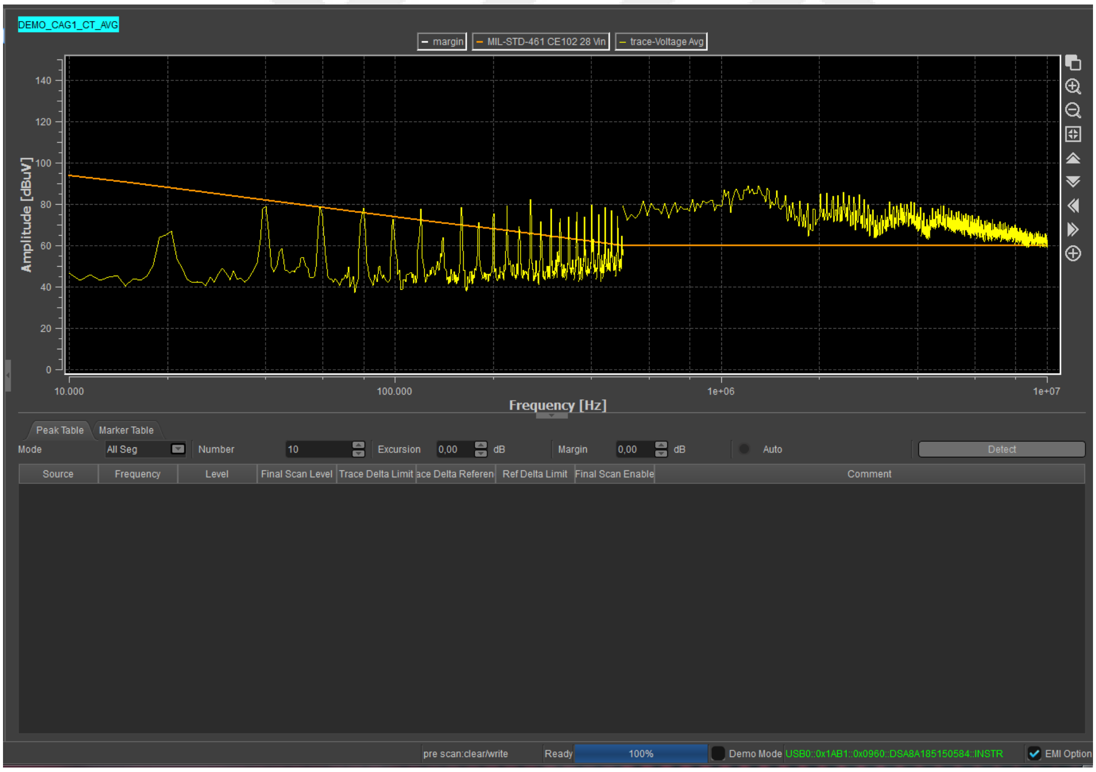

Figure 4.42 : Motor driver noise.

It was not acceptable because the limit line was exceeded for some frequency regions. LC filter was designed in order to reduce the noise from the motor driver to the ambient, as shown in Figure 4.43. Noise above the 10 kHz frequency can be suppressed significantly with this LC filter, as shown in Figure 4.44.

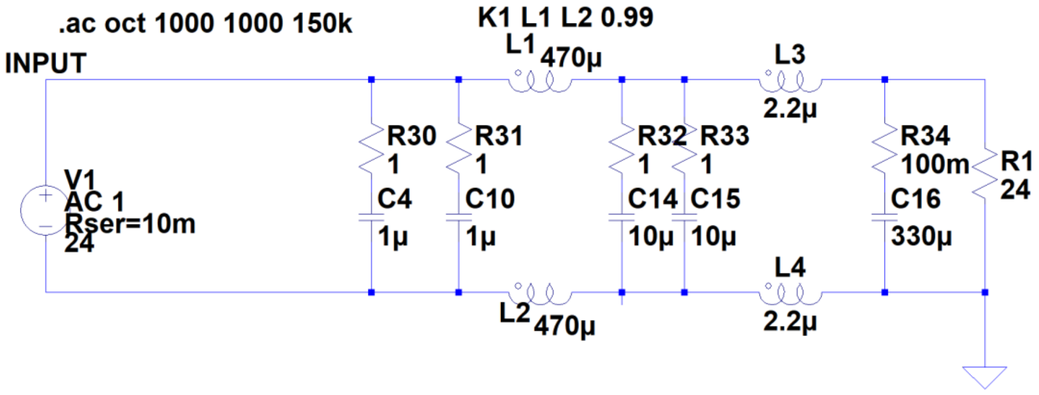

Figure 4.43 : LC filter.

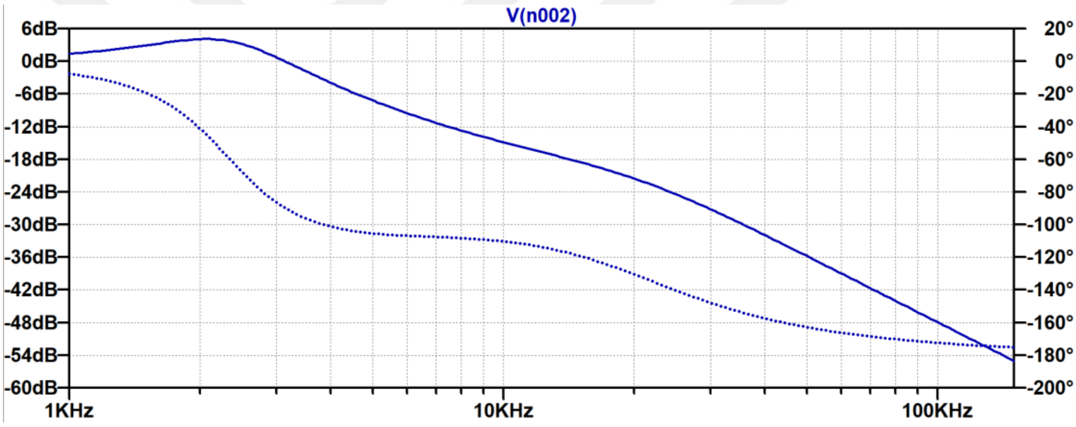

Figure 4.44 : Suppression curve for 100 Hz to 100 kHz.

LC filter that was shown in Figure 4.43 was used at the input of the motor driver. Acceptable noise levels could be satisfied with this filter, as shown in Figure 4.45.

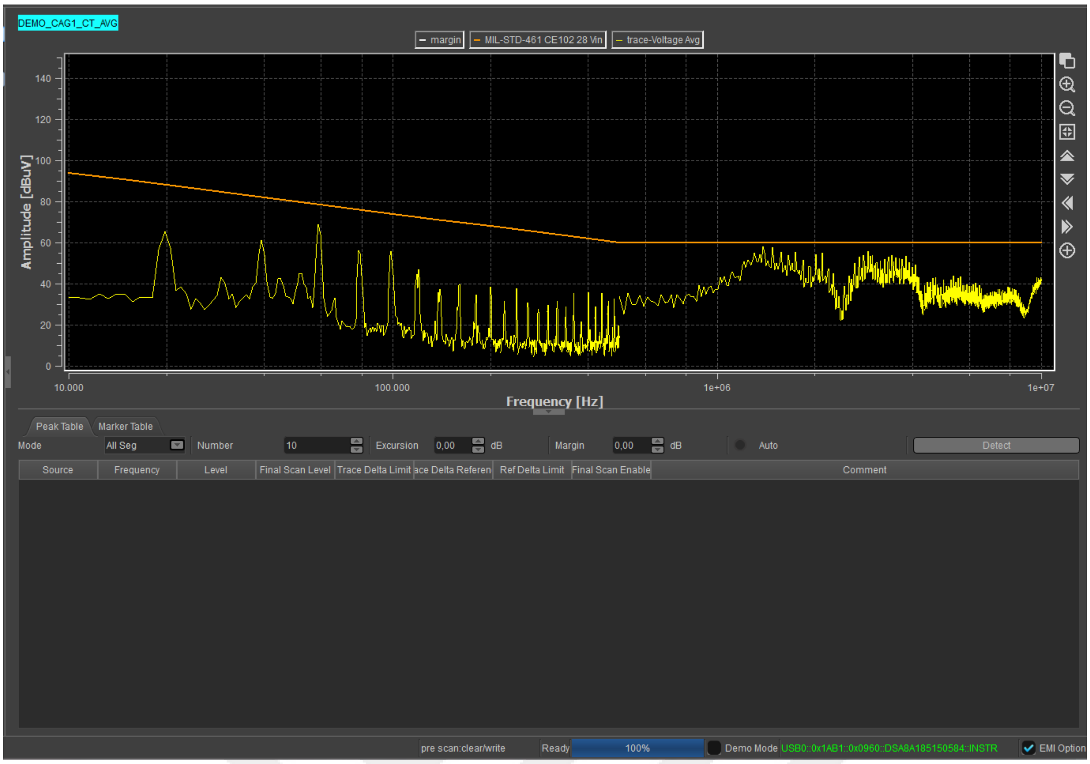

Figure 4.45 : Motor driver noise with LC filter.

4.4.3 MIL-STD-461 CE101 test

MIL-STD-461 CE101 test was the other electromagnetic compatibility test. 0-10 kHz frequency band was scanned, and conducted emission was observed in this test. To do this, the input current waveform was examined with a current probe. There were two limit lines that were for aircraft and submarine-ship platforms. It was intended that conducted emission should be less than limit lines which were determined MIL-STD-461 military standard.

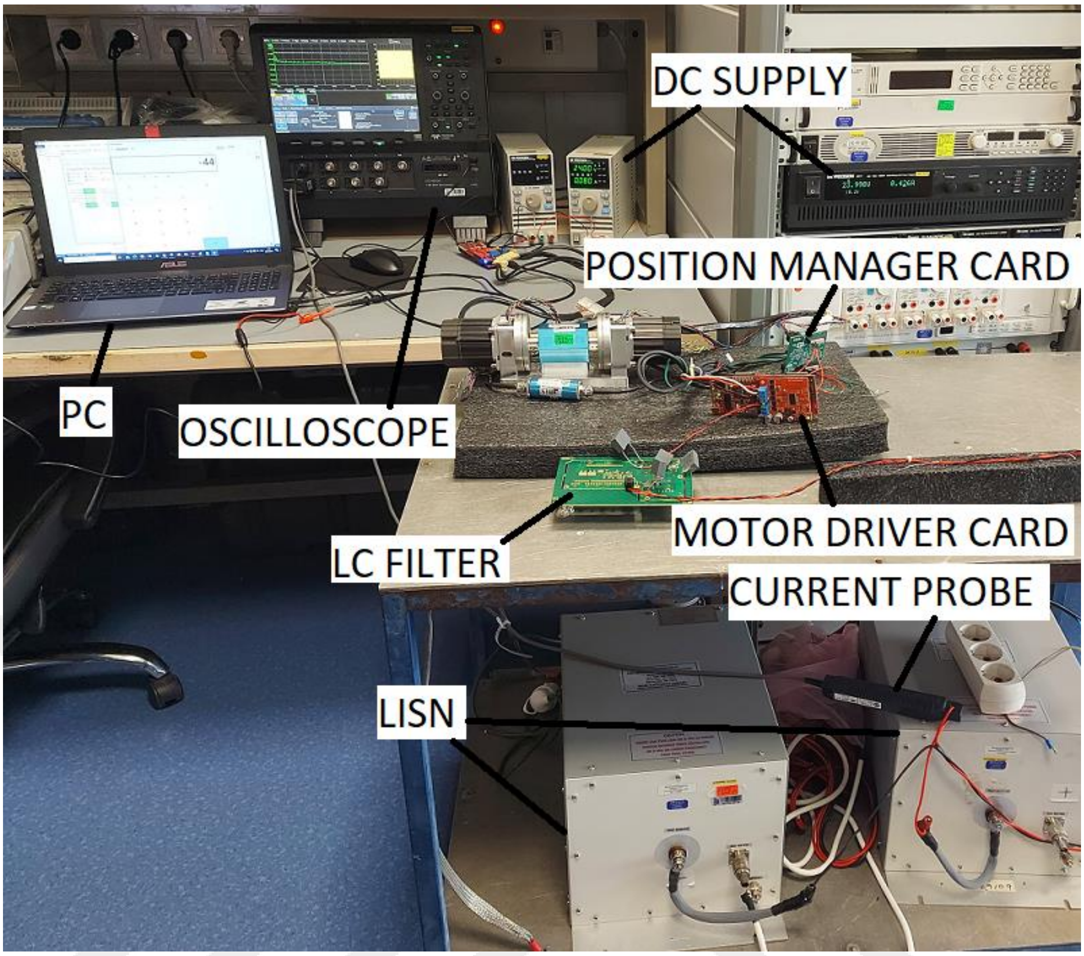

Figure 4.46 : Setup for CE101 test.

Military device's emission should be less than -20 bBA (decibel Ampere) between 0 and 1 kHz frequency band for aircraft platforms, and if it is less than -40 bBA between 1 kHz and 10 kHz frequency band acceptability is guaranteed. (Note: Conversion from dBμA to dBA can be done subtract 120 because $20\log10^{-6} = -120$)

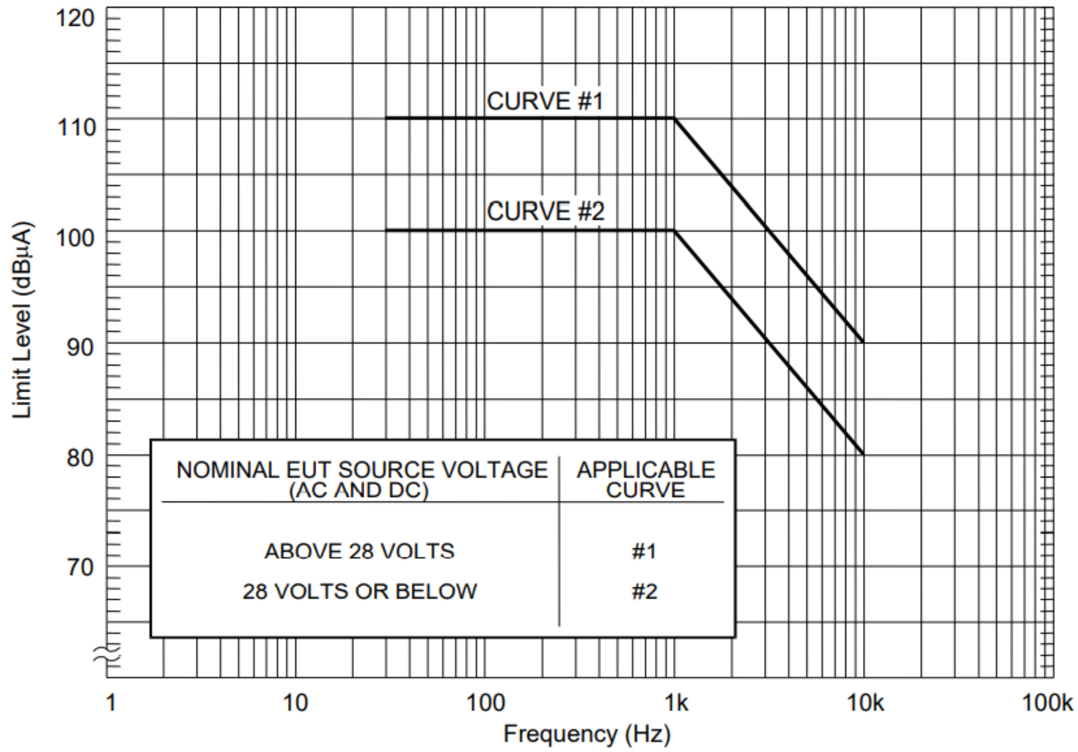

Figure 4.47 : CE101 limit for aircraft applications.

At this part, the CE101 test was applied without the LC filter firstly. After that, the LC filter was attached, and the tests were repeated.

Initially, this test was applied for the aircraft platforms. The Limit line of aircraft platforms was higher than that of submarine platforms. That is, if the test failed for aircraft systems, it would certainly fail for submarine and ship systems. Conducted emission was observed for 0-1 kHz and 1-10 kHz, as shown in Figure 4.48 and Figure 4.49, respectively. The dashed line was the limit line, and the emission of the motor driver card was below the limit line. Therefore, the CE101 test at the aircraft platform is successful for our motor driver card.

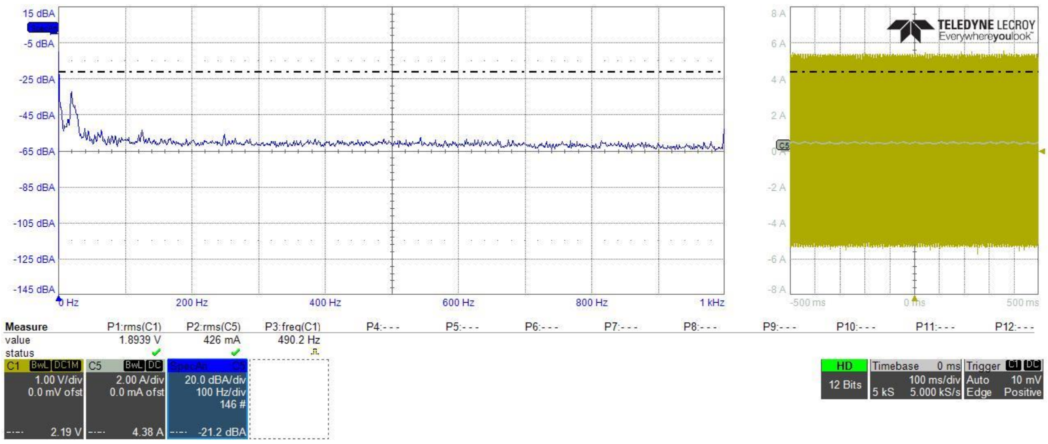

Figure 4.48 : 0-1 kHz frequency noise for aircraft platform.

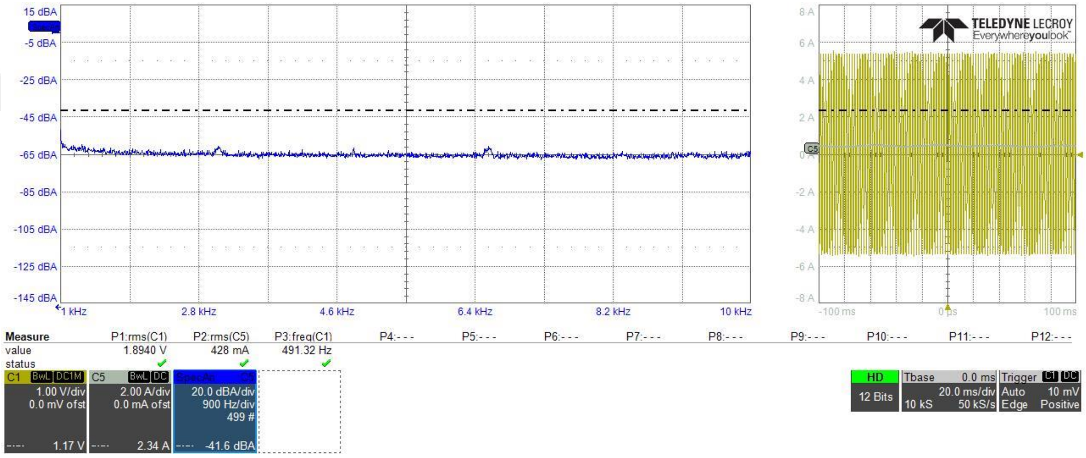

Figure 4.49 : 1-10 kHz frequency noise for aircraft platform.

Limit line changes for surface ship and submarine and ship applications. Limits of submarine and ship platforms are about 5 dBA less than that of aircraft. Emitted noise should be less than -25 dBA (decibel Ampere) between 0 and 2.6 kHz frequency band, and it should be less than -44 dBA between 2.6 kHz and 10 kHz frequency band for surface ship and submarine applications in order to guarantee CE101 acceptability. These standards were attached to appendices.

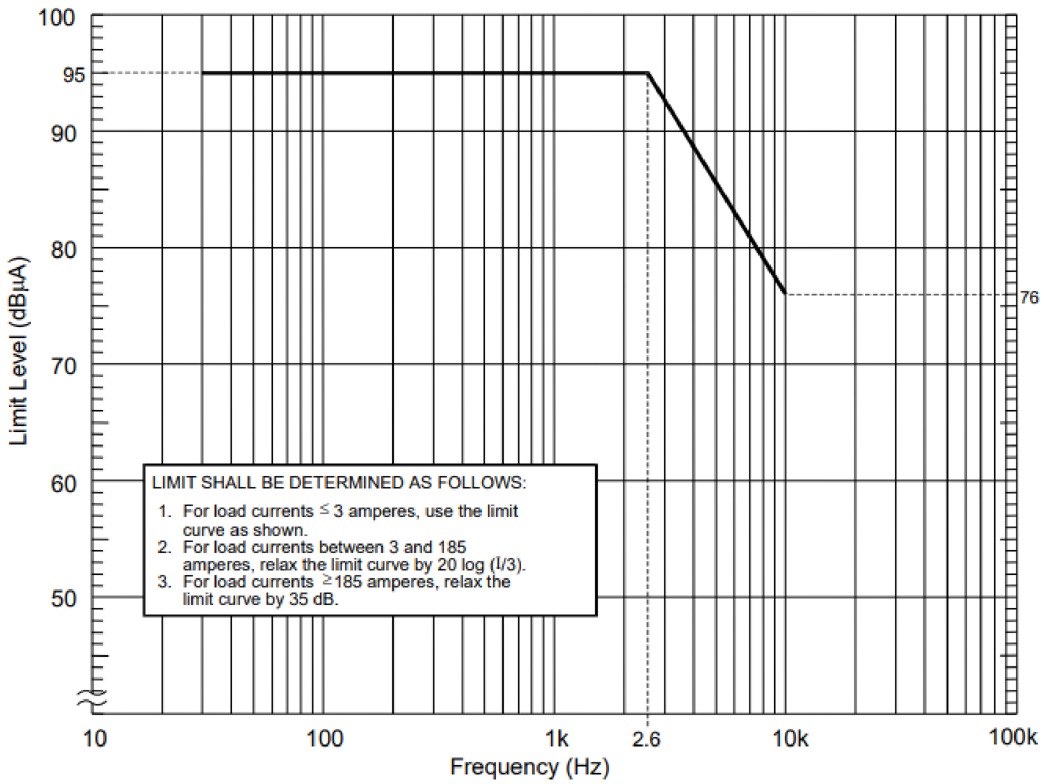

Figure 4.50 : CE101 limit for surface ships and submarine applications.

The conducted emission noise was observed in Figure 4.51 and Figure 4.52 for 0-2.6 kHz and 2.6-10 kHz frequency span, respectively. It was shown that noise was below the limit line; therefore, the CE101 test was also successful for submarine and ship platforms.

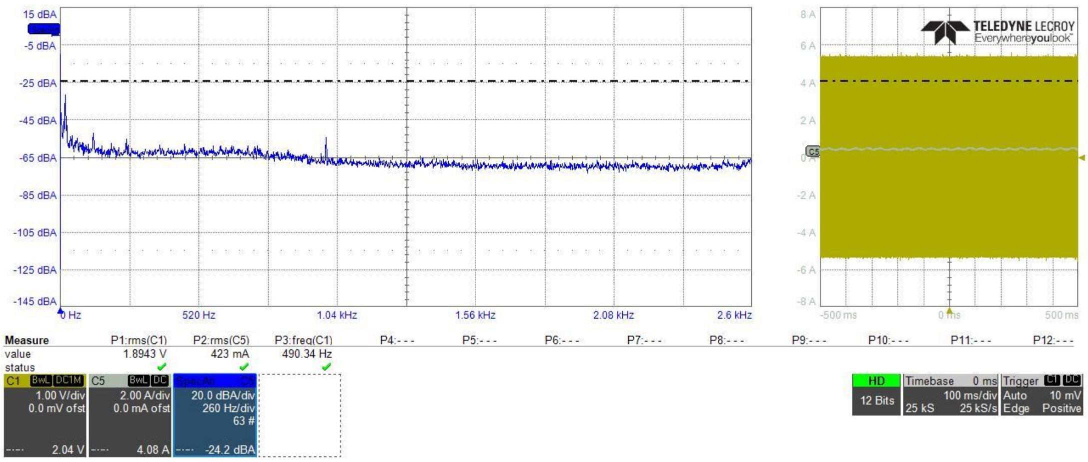

Figure 4.51 : 0-2.6 kHz frequency noise for submarine and ship platforms.

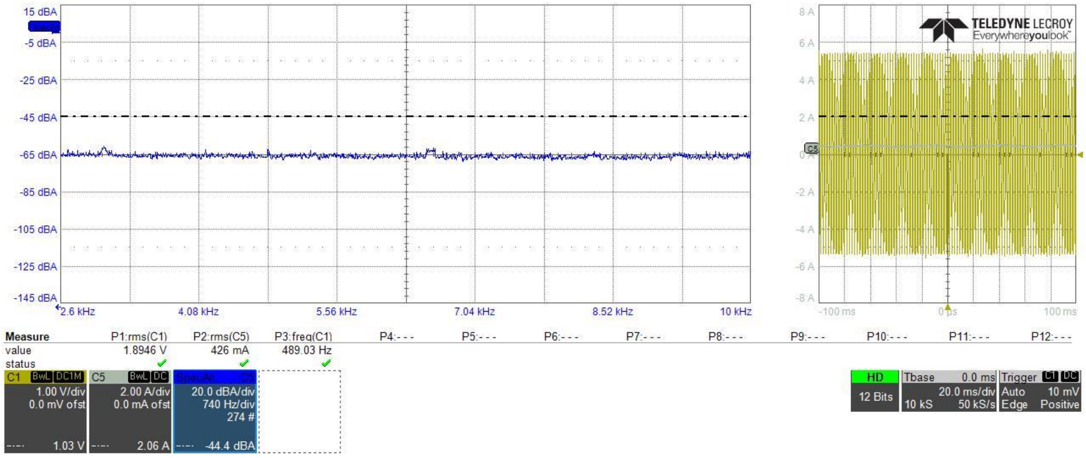

Figure 4.52 : 2.6-10 kHz frequency noise for submarine and ship platforms.

These CE101 tests were repeated after the LC filter was attached to the input of the inverter. Test results were shown for aircraft and submarine–ship platforms as shown in Figure 4.53, Figure 4.54, Figure 4.55, and Figure 4.56. Input filter did not suppress the noise significantly because this filter was designed for the frequency above 10 kHz, as explained CE102 test part. It was an expected result.

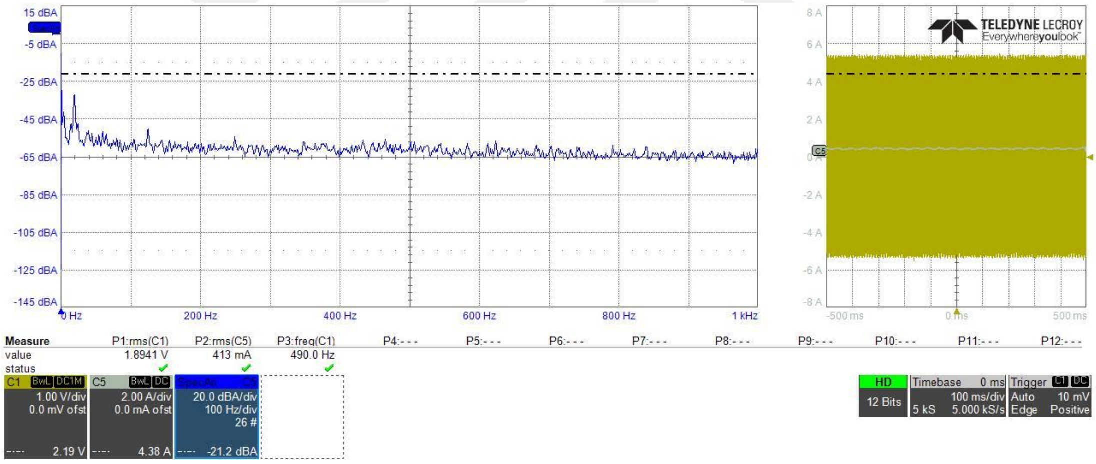

Figure 4.53 : 0-1 kHz frequency noise with LC filter for aircraft platform.

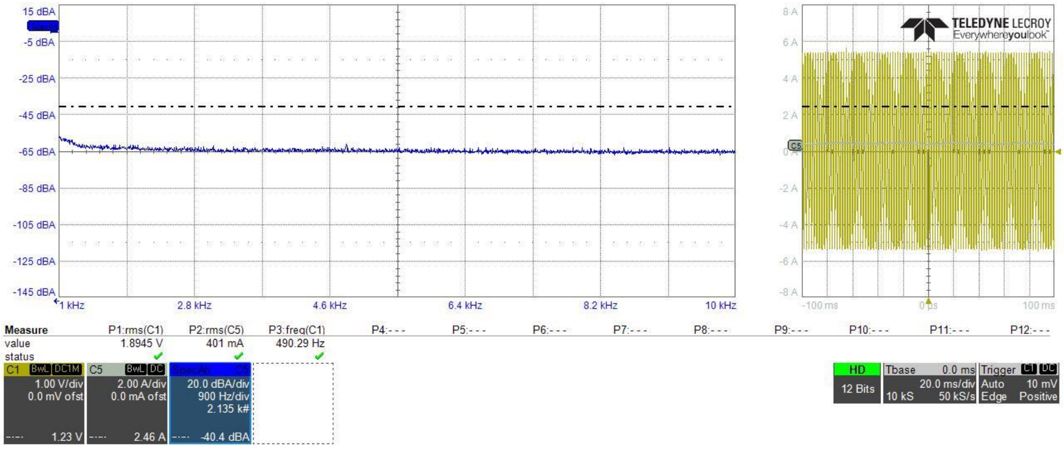

Figure 4.54 : 1-10 kHz frequency noise with LC filter for aircraft platform.

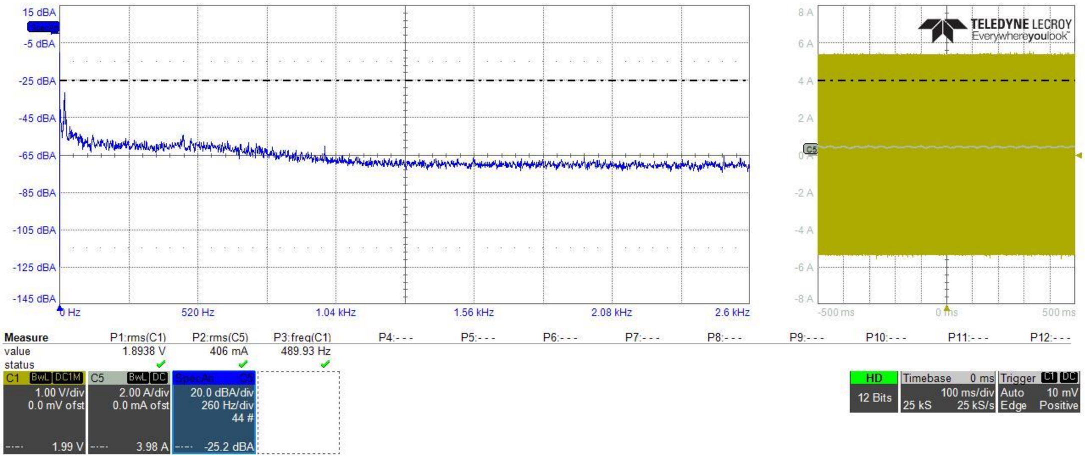

Figure 4.55 : -2.6 kHz frequency noise with LC lilter for submarine and ship platforms.

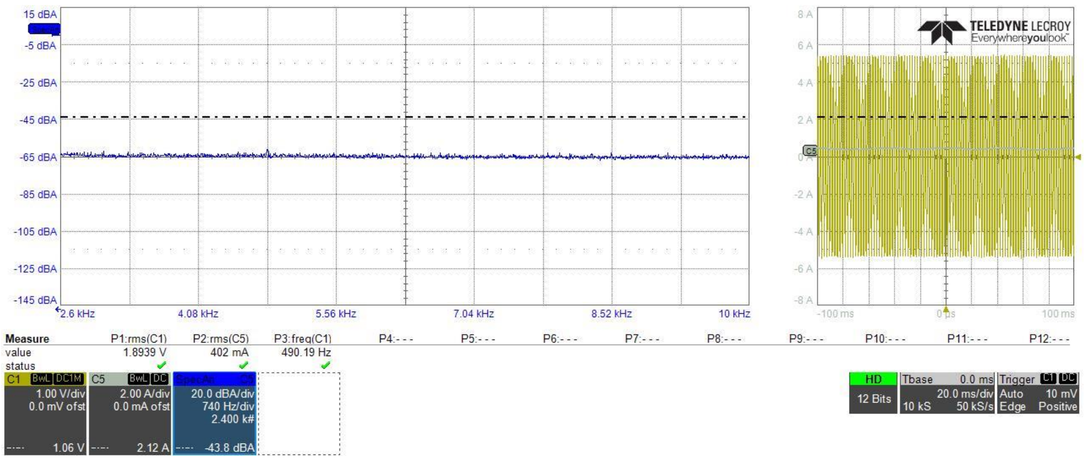

Figure 4.56 : 2.6-10 kHz frequency noise with LC filter for submarine and ship platforms.

4.5 Comments on the Results

In this thesis, sensitive torque control was applied on Permanent Magnet Synchronous Motor. MOSFETs were used in the inverter, and different switching frequencies were applied in order to determine the most appropriate switching frequency. An absolute encoder was used and it was important for exact position information, which was used as feedback in our control algorithm that Field Oriented Control. Also, position information should always be known even if power was cut off. Synchronous Serial Interface (SSI) was used and absolute encoder output data were sent to position manager card thanks to this interface. After the RS485 buffers, output of the position manager card was suitable for SPI communication. Thus, position data was obtained with Simulink via the SPI protocol. SSI protocol has some advantages. One of the most important advantages is that there is no word restriction; that is, there is flexibility for the number of words. Also, serial data transfer has reduced the wiring so the cost can be reduced, and it was easier for implementation. In addition, SPI communication has some advantages. Data transfer rate is high, and it is important for fast response. In this thesis, military standards were respected, and components were selected by taking into account military standards. Temperature and conducted electromagnetic compatibility tests were done, and our design was successful. Some problems were observed at high and low temperatures, such as the clock frequency of the microprocessor distortion, but this problem was solved with an external oscillator. Also, a filter was designed in order to reduce the noise to satisfy EMC standards. Torque ripple and settling time were also examined, and these results were acceptable for our systems.

Actually, Field Oriented Control was applied in this experiment. However, military compatibility and high sensitivity were especially aimed, and these were satisfied. The algorithm was created at Simulink, and implementation was made. A setup was established within the scope of this thesis, and a variety of parameters were tried at actual systems. Our PMSM drivers are intended to produce both native algorithm and hardware structure and use actively in our companies systems instead of exported motor drivers. Thus, dependency on foreign products is aimed to be reduced.

5. CONCLUSIONS AND RECOMMENDATIONS

Electric motors have an important role in the industry, and they are commonly used. The importance of motor drive applications is also increasing day by day because sensitive, efficient, and goal-oriented controls can be done with motor control techniques. Permanent Magnet Synchronous motor drive applications are also crucial. Especially, these applications are developing with the development of semiconductor technology at power electronics.

Speed and torque controls of PMSM can be achieved with varying frequencies, and these controls are applied to military applications. Stabilization systems are one of the applications that torque control of PMSM is done. In this thesis, high sensitive torque control of PMSM for military applications was examined, and military compatibility was ensured in terms of temperature durability and electromagnetic compatibility. The motor drivers that satisfies torque control was imported abroad for military systems. Instead of these imported motor drivers, a national algorithm with the base of field-oriented control was created, and national motor drivers were intended with the scope of this thesis. Performance analyses were done, and military specifications were satisfied. These motor drivers can be used in a lot of platforms by changing the power and torque capacity of hardware components. Aircraft submarine, ship, and land platforms are the platforms that stabilizations systems are used.

Firstly, a literature review was done during this experiment. After the literature review, control techniques and encoder necessity were determined. Absolute position information and determined steady-state characteristics were crucial issues for stabilization systems. Therefore, sensorless control was not appropriate, and position feedback would be used. In the light of these information, field-oriented control was selected, and an absolute encoder was used for sensitive position information. SPI communication was satisfied between the encoder and microprocessor to obtain the position information. Steady-state torque ripple and response time for torque changing were also examined for different MOSFET switching frequencies. The ideal switching frequency was determined. CAN communication infrastructure was used in order to real-time observation. PI tuning was satisfied with real-time trying on the real system. In addition, the switching frequency was changed instantly, and performance analyses could be done fast. This means that steady-state ripple, settling time, etc., were observed in real-time for varying parameters, and optimization was done. Torque ripple at the steady-state was reduced under 2%, whereas the currently used motor driver's torque ripple that was imported from abroad was about 5%. Actually, 1.3% torque ripple was satisfied with 20 kHz switching frequency at room temperature.

In addition, military compatibility was an important issue in this study because these motor drivers could be intended to use military applications. Basically, high and low temperature tests were applied according to conditions that the motor drives could be used. Torque ripple and settling time characteristics were observed between -40°C and +55°C. Torque ripples were observed as 3% at the boundary temperatures. At the boundary temperatures, CAN communication also failed. It was found that the microprocessor's internal clock was corrupted, so an external oscillator was used, and this problem was solved. Furthermore, MIL-STD CE 101 and CE 102 tests were examined for electromagnetic compatibility tests on an electronic card basis. The conducted noise transmitted from the electronic board was observed. An LC filter was designed at the input of the card in order to reduce the noise. Thus, transmitting noise was decreased the acceptable limits. As a result, these temperature and EMC tests were successful.

To conclude, in this thesis, high sensitive torque control was studied for Permanent Magnet Synchronous Motors with military acceptance. The national control algorithm was created with the basis of the field-oriented control for military applications, and steady-state torque ripple performance was improved compared to the foreign equivalent products. For future work, an appropriate product could be produced according to the power and torque requirements of the platform. This means that appropriate hardware could be created for aircraft platforms, land platforms, or submarine platforms.

REFERENCES

[1] Aselsan Satellite Communication System Solutions. <*https://www.aselsan.com.tr/Satellite_Payloads_And_Satellite_Systems_6284.pdf*>,date retrieved 25.06.2021.

[2] Cahill, D. P. M. and Adkins, B. (1962). *The permanent magnet synchronous motor.* Proc. Inst. Elec. Eng., vol. 109, part A, no. 48, pp. 483-491, Dec. 1962

[3] Krishnan, R. and Beutler, A. J. (1985). *Performance and design of an axial field permanent magnet synchronous motor servo drive.* in Proc. IEEE Ind. Appl. Soc. Annu. Meeting, 1985, pp. 634-640.

[4] Richter, E., Miller T. J. E., Neumann, T. W., and Hudson, T. L. (1985). *The ferrite PM ac motor-A technical and economic assessment.* IEEE Trans. Ind. Appl. vol. IA-21 no. 4, pp. 644-650, May/June 1985.

[5] Benhaddadi, M., and Olivier, G. (2008). *Barriers and incentives policies to high-efficiency motors and drives market penetration*. Power Electronics, Electrical Drives, Automation and Motion, 2008. SPEEDAM 2008. International Symposium on. IEEE.

[6] Do-Kwan Hong, Daesuk Joo, Byung-Chul Woo, Yeon-Ho Jeong and Dae-Hyun Koo, (2013). *Investigations on a Super High Speed Motor-Generator for Microturbine Applications Using Amorphous Core.* IEEE Transactions on Magnetics, vol. 49, no. 7, pp. 4072-4075, July 2013.

[7] Zhang, Fengge, Du Guanghui, Wang Tianyu and Liu Guangwei, (2016). *Review on Development and Design of High Speed Machines.* Transactions of china elect, vol. 31, no. 7, pp 1-18, Apr. 2016.

[8] Amin, F., Bin Sulaiman, E., Utomo, W. M., Soomro, H. A., Jenal, M., and Kumar, R. (2017). *Modelling and simulation of field oriented control based permanent magnet synchronous motor drive system.* Indonesian Journal of Electrical Engineering and Computer Science, vol.6, no.2, pp. 387 – 395, 2017.

[9] Capolino, Andre G. (2008). *Recent advances and applications of power electronics and motor drives-advanced and intelligent control techniques.* Industrial Electronics, 2008. IECON 2008. 34th Annual Conference of IEEE. IEEE.

[10] Sathiakumar, S., Biswas, S. K., Vithyathil, J. "Microprocessor based field oriented control of a CSI fed induction motor drive," *IEEE Trans. Ind. Electron*, pp. 33, 39 – 43

[11] Novotny, D. W., and Jansen, P. L. (1991). *Field oriented control of synchronous machines. IETE Journal of Research,* vol. 37, no.1, pp. 46-56, 1991

[12] Chikh, K., Saad A., Khafallah, M., and Yousfi, D. (2011). *PMSM vector control performance improvement by using pulse with modulation and anti-windup PI controller*. in *2011 International Conference on Multimedia Computing and Systems*, 2011, pp. 1–7.

[13] Beladjine, D., Boudana, D., Moualdia, A. and Wira, P. (2020). *Wireless Space Vector Pulse Width Modulation Control of Three-Phase Inverter Using RF-link.* 2020 International Conference on Electrical, Communication, and Computer Engineering (ICECCE), 2020, pp. 1-6, doi: 10.1109/ICECCE49384.2020.9179420.

[14] Biabani, M. A. K. A. and Ali, S. M. (2016). *Control of induction motor drive using space vector PWM.* in *Electrical, Electronics, and Optimization Techniques (ICEEOT), International Conference on*, 2016, pp. 3344–3351.

[15] Sulaimanl, M., Patakorz, F. A., and Ibrahim, Z. (2013). *Dsp Based Implementation of Field Oriented Control of Three-Phase Induction Motor Drives.*

[16] Vas, P. (1998). *Sensorless Vector and Direct Torque Control*. Oxford University Press, Oxford.

[17] Qureshi, M. H. (1993). *The role of electro-optical encoders in digitization of 3-dimensional image on stereo plotter*. *Proc. Opto-electronic Imaging Conf.*, 1993, pp. 369–379.

[18] Doebelin, E. (1990). *Measurement Systems: Applications and Design.* New York: McGraw-Hill.

[19] Wekhande, S. and Agarwal, V. (2006). *High-resolution absolute position Vernier shaft encoder suitable for high-performance PMSM servo drives*. IEEE Transactions on Instrumentation and Measurement, vol. 55, no. 1, pp. 357-364, Feb. 2006, doi: 10.1109/TIM.2005.862020.

[20] Ioakimidis, T. E. and Wexler, R. S. (2001). *Commercial Ku-band SATCOM on-the-move using a hybrid tracking scheme*. *MILCOM Proceedings Communications for Network-Centric Operations:* Creating the Information Force (Cat. No.01CH37277), 2001, pp. 780-784 vol.2, doi: 10.1109/MILCOM.2001.985944.

[21] Fitzgerald, A. E., Kingsley, C., & Umans, S. D, (2003). *Electric machinery*. Boston, Mass: McGraw-Hill.

[22] DC Motor Working Principle, Construction and Diagram Explanation *<https://www.mathworks.com/matlabcentral/fileexch ange/72757-direct-torque-control-dtc-of-induction-motor?s_tid=srch title>*, date retrieved 25.06.2021.

[23] Yildiz, Ali. (2012). *Electrical equivalent circuit based modeling and analysis of direct current motors.* International Journal of Electrical Power & Energy Systems. 43. 1043-1047. 10.1016/j.ijepes.2012.06.063.

[24] Khurram, A. (2001). *Position and speed sensorless control of permanent magnet synchronous motors.* Ph.D. dissertation, Michigan State University, East Lansing, MI.

[25] Valkenburg, V. and Nooger & Neville. (1992). Inc. *Basic Electricity*. Revised ed. Indianapolis, IN: PROMPT Pub.

[26] Muljadi, E. and Green, J. (2002). *Cogging torque reduction in a permanent magnet wind turbine generator*. in Proc. of the 21st Am. Soc. of Mech. Engineers Wind Energy Symp. pp. 1-8.

[27] Flankl, M., Tüysüz, A. and Kolar, J. W. (2017). *Cogging Torque Shape Optimization of an Integrated Generator for Electromechanical Energy Harvesting.* in IEEE Transactions on Industrial Electronics, vol. 64, no. 12, pp. 9806-9814, Dec. 2017, doi: 10.1109/TIE.2017.2733441.

[28] Pillay, P. and Krishnan, R. (1988). *Modeling of permanent magnet motor drives.* in IEEE Transactions on Industrial Electronics, vol. 35, no. 4, pp. 537-541, Nov. 1988, doi: 10.1109/41.9176.

[29] Pillay, P. and Krishnan, R. (1989). *Modeling, simulation, and analysis of permanent-magnet motor drives. I. The permanent-magnet synchronous motor drive.* in IEEE Transactions on Industry Applications, vol. 25, no. 2, pp. 265-273, March-April 1989, doi: 10.1109/28.25541.

[30] Andreescu, G., Coman, C., Moldovan, A. and Boldea I. (2012). *Stable V/f control system with unity power factor for PMSM drives.* 2012 13th International Conference on Optimization of Electrical and Electronic Equipment (OPTIM), 2012, pp. 432-438, doi: 10.1109/OPTIM.2012.6231937.

[31] Chandana Perera, P. D., Blaabjerg, F. J., Pedersen, K. and Thogersen, P. (2002). *A sensorless, stable V/f control method for permanent-magnet synchronous motor drives.* APEC. Seventeenth Annual IEEE Applied Power Electronics Conference and Exposition (Cat. No.02CH37335), 2002, pp. 83-89 vol.1, doi: 10.1109/APEC.2002.989231.

[32] Field Oriented Controller<*https://www.mathworks.com/matlabcentral/fileexchange/73196-field-oriented-control-of-induction-motor?s_tid=srchtitle*>, date retrieved 25.06.2021.

[33] Ocen, **David.** (2005). *Direct Torque Control of a Permanent Magnet Synchronous Motor.* Ph.D thesis, Stockholm, Sweden.

[34] Morales-Caporal, R., Leal-López, M. E., de Jesús Rangel-Magdaleno, J., Sandre-Hernández, O. and Cruz-Vega, I. (2018). *Direct torque control of a PMSM-drive for electric vehicle applications.* International Conference on Electronics, Communications and Computers (CONIELECOMP), 2018, pp. 232-237, doi: 10.1109/CONIELECOMP.2018.8327204.

[35] Wang, X., Liu N., and Na, R. (2009).Simulation of PMSM field-oriented control based on SVPWM," 2009 IEEE Vehicle Power and Propulsion Conference, 2009, pp. 1465-1469, doi: 10.1109/VPPC.2009.5289523.

[36] Direct Torque Controller<*https://www.mathworks.com/matlabcentral/fileexchange/72757-direct-torque-control-dtc-of-induction-motor?s_tid=srchtitle*>, date retrieved 25.06.2021.

[37] Serial Communication Protocols<*https://circuitdigest.com/tutorial/serial-communication-protocols*>, date retrieved 25.06.2021.

[38] Merzoug, M.S. & Naceri, Farid, (2008). "Comparison of field oriented control and direct torque control for PMSM" World Acad Sci Eng Technol. 21. 209-304.

[39] Mishra, A., Makwana, J. A., Agarwal P., and Srivastava, S. P. (2012). *Modeling and implementation of vector control for PM synchronous motor drive.* IEEE-International Conference On Advances In Engineering, Science And Management (ICAESM -2012), 2012, pp. 582-585.

[40] Costa, Cesar & Santin, Christian. (2017). Design and simulation of direct torque control of induction motors using VHSIC Hardware Description Language (VHDL). Scientific Research and Essays. 12. 103-112. 10.5897/SRE2017.6501.

[41] Serial Communication Protocols<Vector Park Transform (armsoftware.github.io)>, date retrieved 25.06.2021.

[42] Yu, L., Wang, C., Shi, H., Xin, R., and Wang, L. (2017). *Simulation of PMSM field-oriented control based on SVPWM.* 2017 29th Chinese Control And Decision Conference (CCDC), 2017, pp. 7407-7411, doi: 10.1109/CCDC.2017.7978524.

APPENDICES

APPENDIX A: CE101 Standards
APPENDIX B: CE102 Standards

APPENDIX A

A.1. CE101, conducted emissions, audio frequency currents, power leads.
A.1.1 CE101 applicability.

This requirement is applicable from 30 Hz to 10 kHz for power leads, including returns, that obtain power from other sources not part of the EUT for surface ships, submarines, Army aircraft& (including flight line) and Navy aircraft*& *For equipment intended to be installed on Navy aircraft, this requirement is applicable only if the platform contains Anti-Submarine Warfare (ASW) equipment, which operate between 30 Hz and 10 kHz, such as Acoustic (Sonobouy) Receivers or Magnetic Anomaly Detectors (MAD). & For AC applications, this requirement is applicable starting at the second harmonic of the EUT power frequency.

A.1.2 CE101 limits.

Conducted emissions on power leads shall not exceed the applicable values shown on Figures A.1 through A.3, as appropriate, for surface ships and submarines; and Figure A.4 for Army aircraft (including flight line) and Navy ASW aircraft.

A.1.3 CE101 test procedure.
A.1.3.1 Purpose.

This test procedure is used to verify that electromagnetic emissions from the EUT do not exceed the specified requirements for power input leads including returns.

A.1.3.2 Test equipment.

The test equipment shall be as follows:
a. Measurement receivers
b. Current probes
c. Signal generator
d. Data recording device
e. Oscilloscope
f. Resistor (R)
g. LISNs

A.1.3.3 Setup.

The test setup shall be as follows:
a. Maintain a basic test setup for the EUT. The LISN may be removed or replaced with an alternative stabilization device when approved by the procuring activity.
b. Measurement system integrity check. Configure the test setup for the measurement system check as shown on Figure A.5.
c. EUT testing.
(1) Configure the test setup for compliance testing of the EUT as shown on Figure A.6.
(2) Position the current probe 5 cm from the LISN.

A.1.3.4 Procedures.

The test procedures shall be as follows:

a. Turn on the measurement equipment and allow a sufficient time for stabilization.

b. Measurement system integrity check. Evaluate the overall measurement system from the current probe to the data output device.

(1) Apply a calibrated signal level, which is at least 6 dB below the applicable limit at 1.1 kHz, 3 kHz, and 9.9 kHz, to the current probe.

(2) Verify the current level, using the oscilloscope and load resistor; also, verify that the current waveform is sinusoidal.

(3) Scan the measurement receiver for each frequency in the same manner as a normal data scan. Verify that the data recording device indicates a level within ±3 dB of the injected level.

(4) If readings are obtained which deviate by more than ±3 dB, locate the source of the error and correct the deficiency prior to proceeding with the testing.

c. EUT testing. Determine the conducted emissions from the EUT input power leads, including returns.

(1) Turn on the EUT and allow sufficient time for stabilization.

(2) Select an appropriate lead for testing and clamp the current probe into position.

(3) Scan the measurement receiver over the applicable frequency range, using the bandwidths and minimum measurement times specified in Table II.

(4) Repeat A.1.3.4c(3) for each power lead.

A.1.3.5 Data presentation.

Data presentation shall be as follows:

a. Continuously and automatically plot amplitude versus frequency profiles on X-Y axis outputs. Manually gathered data is not acceptable except for plot verification.

b. Display the applicable limit on each plot.

c. Provide a minimum frequency resolution of 1% or twice the measurement receiver bandwidth, whichever is less stringent, and a minimum amplitude resolution of 1 dB for each plot. d. Provide plots for both the measurement and system check portions of the procedure.

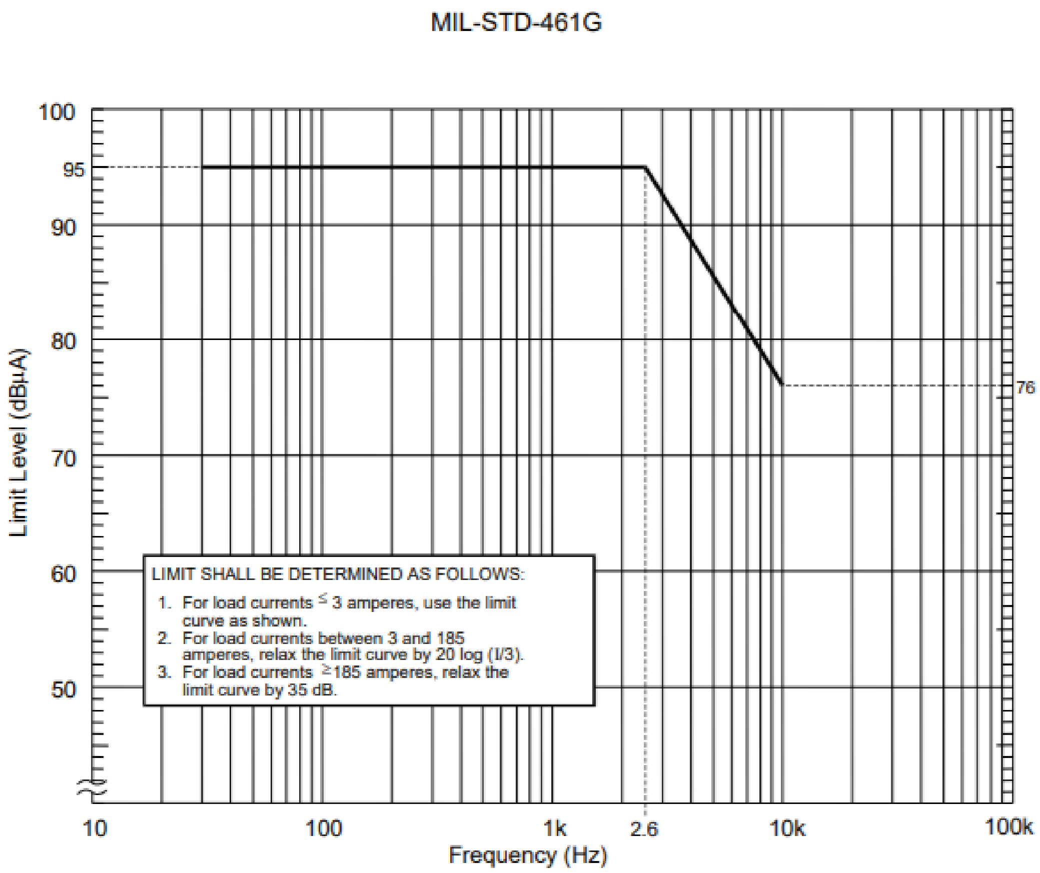

Figure A.1: CE101 limit for surface ships and submarine applications, DC.

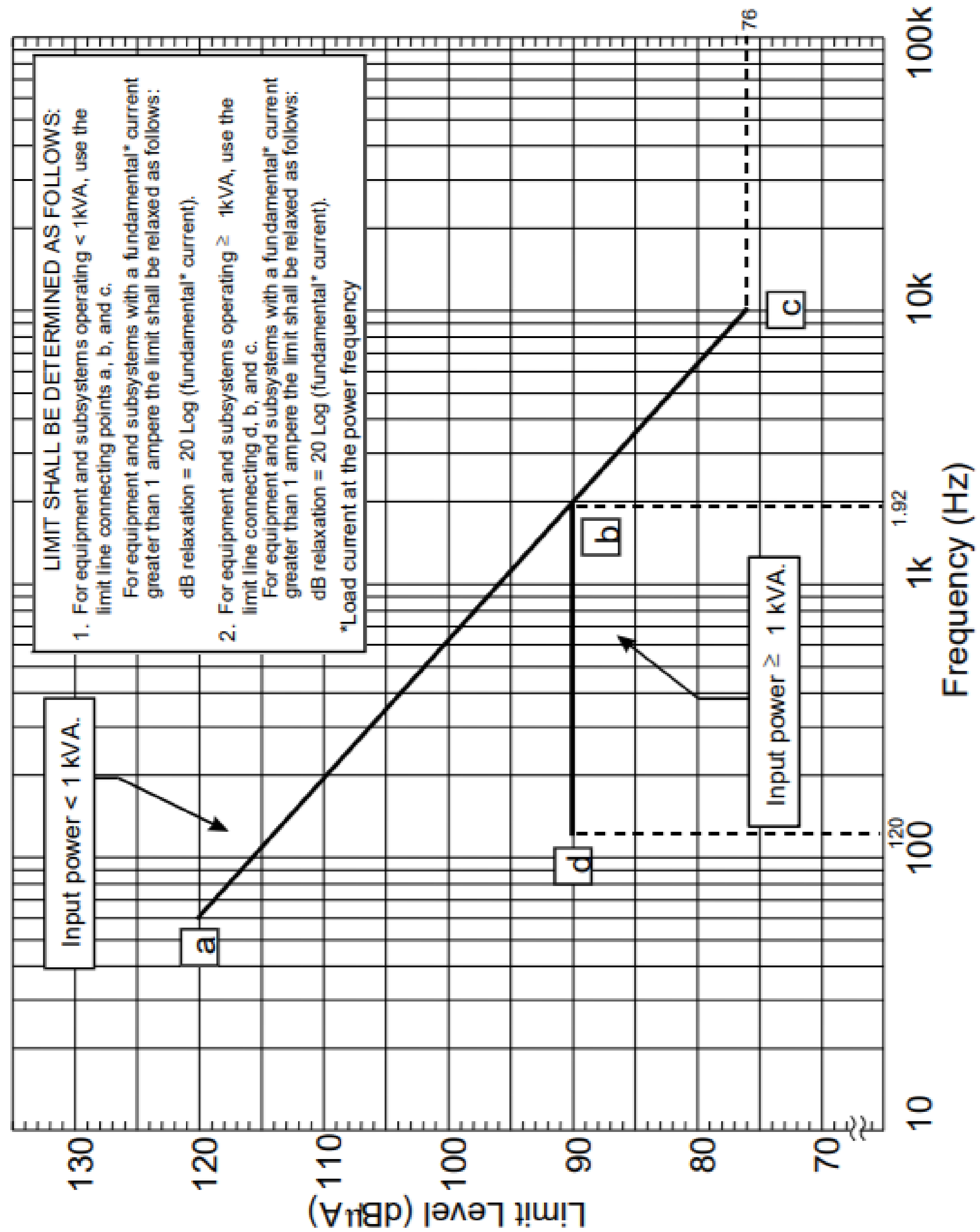

Figure A.2: CE101 limit for surface ships and submarine applications, 60 Hz.

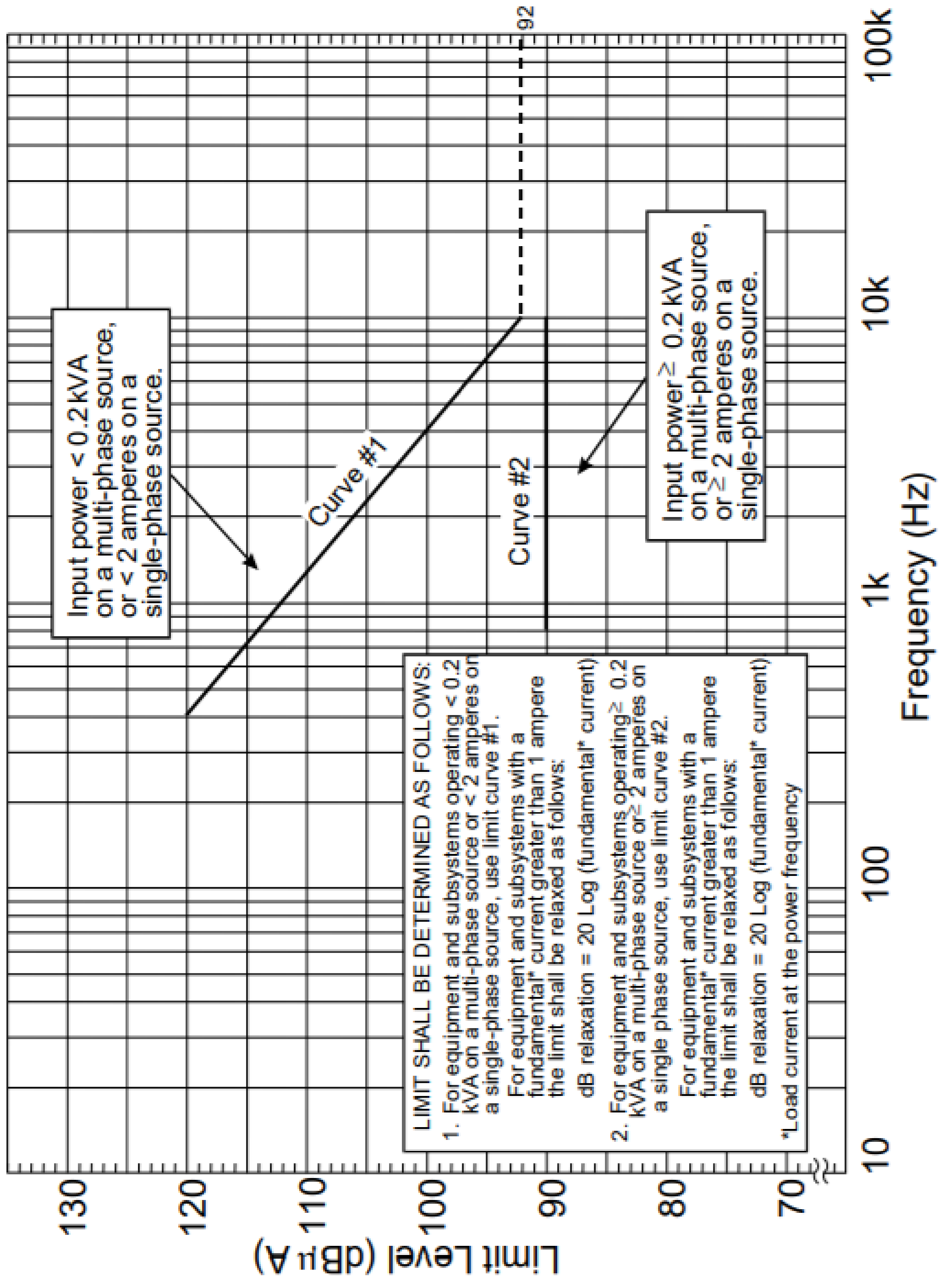

Figure A.3: CE101 limit for surface ships and submarine applications, 400 Hz.

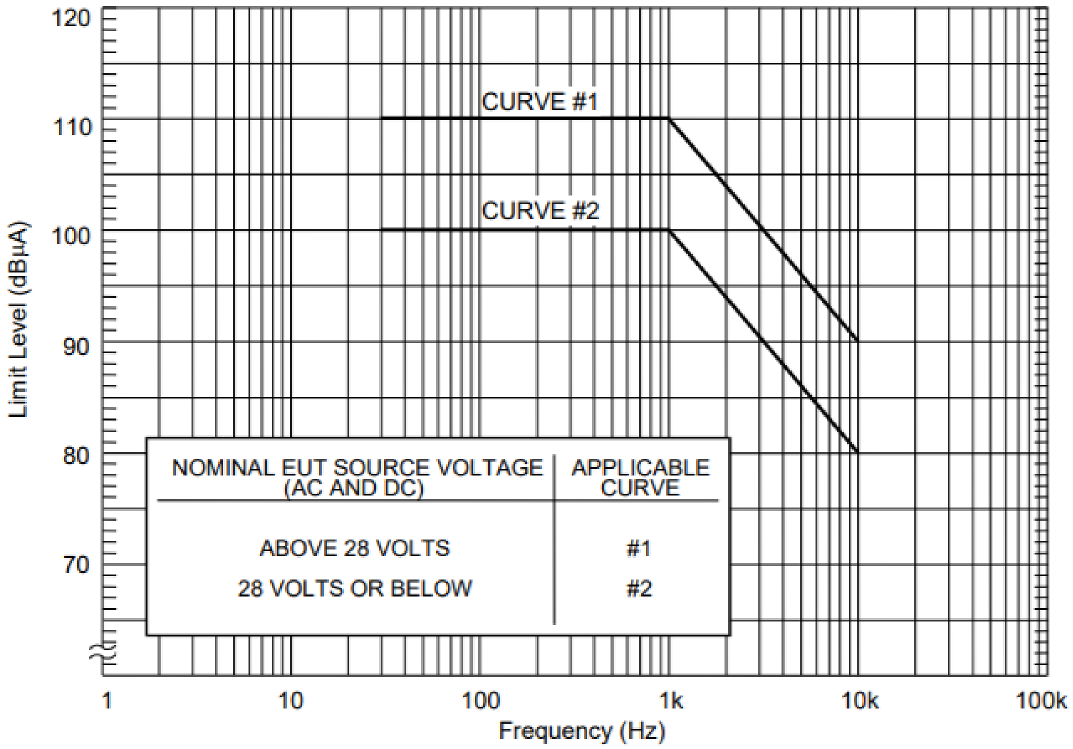

Figure A.4: CE101 limit for Navy ASW aircraft and Army aircraft (including flight line) applications.

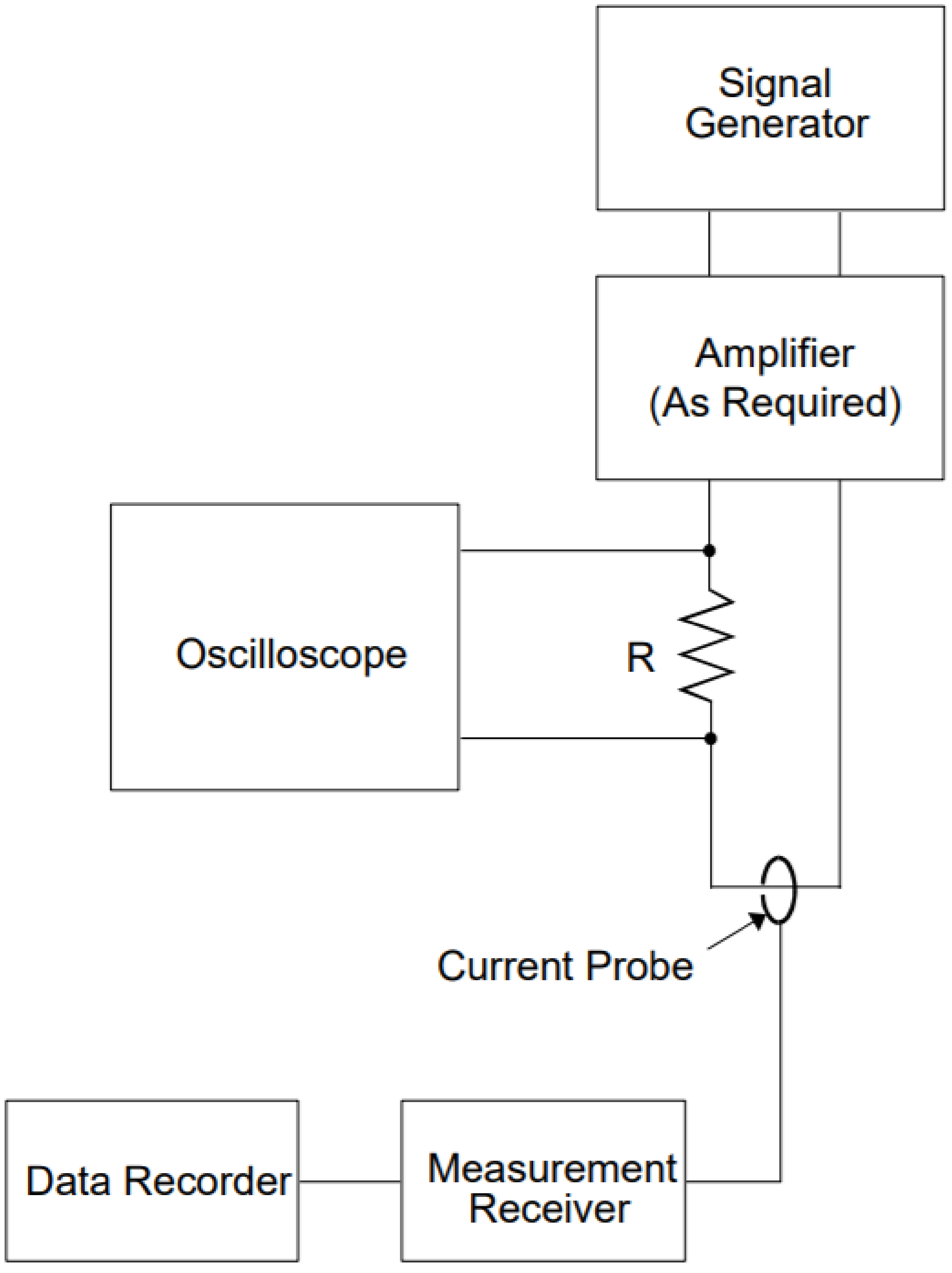

Figure A.5: Measurement system check.

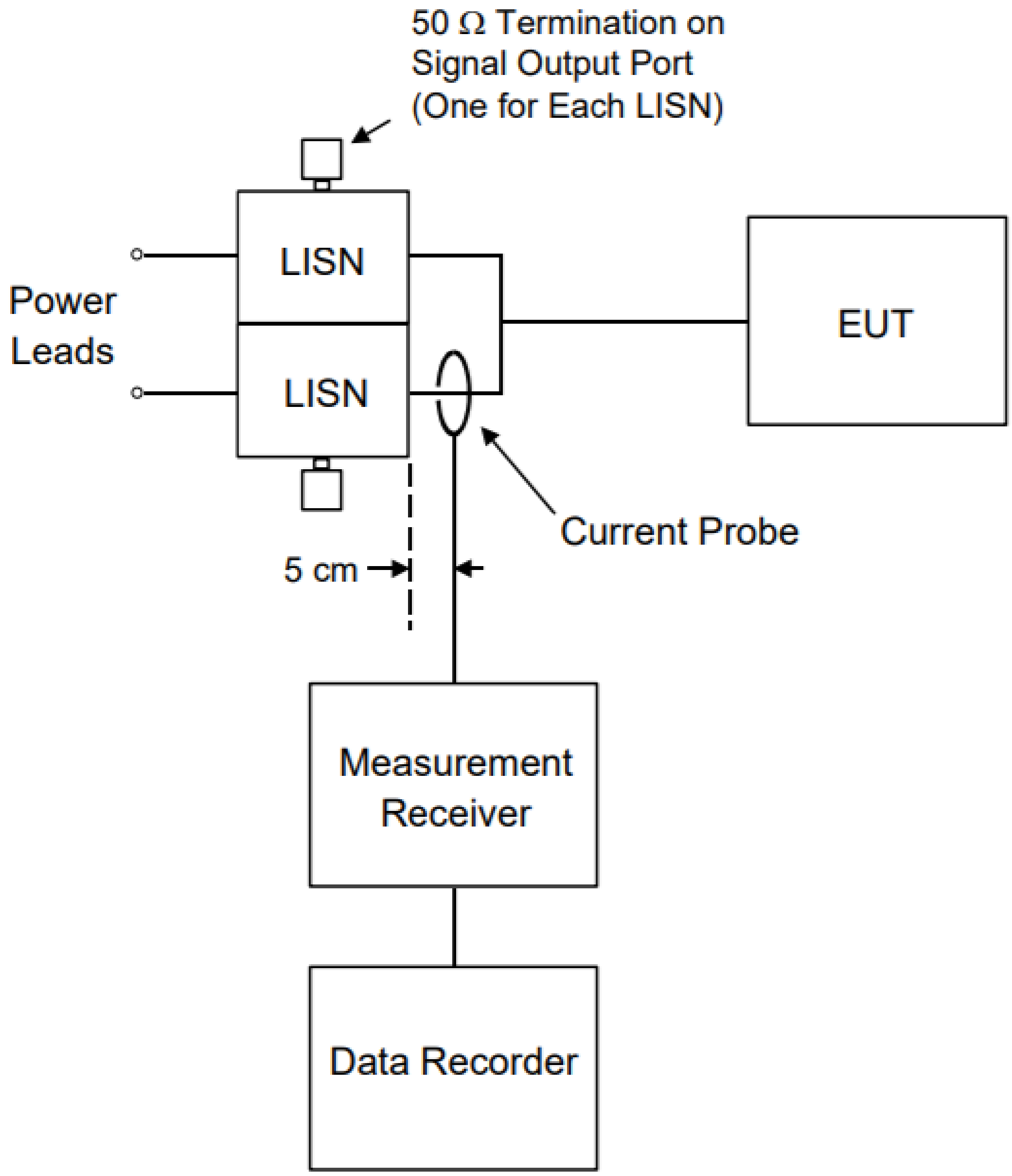

Figure A.6: Measurement setup.

APPENDIX B

B.1. CE102, conducted emissions, radio frequency potential, power leads.
B.1.1 CE102 applicability.

This requirement is applicable from 10 kHz to 10 MHz for all power leads, including returns, which obtain power from other sources not part of the EUT.

B.1.2 CE102 limits.

Conducted emissions on power leads shall not exceed the applicable values shown on Figure B.1.

B.1.3 CE102 test procedure.
B.1.3.1 Purpose.

This test procedure is used to verify that electromagnetic emissions from the EUT do not exceed the specified requirements for power input leads, including returns.

B.1.3.2 Test equipment.

The test equipment shall be as follows:
a. Measurement receiver
b. Data recording device
c. Signal generator
d. Attenuator, 20 dB, 50 ohm
e. Oscilloscope f. LISNs

B.1.3.3 Setup.

The test setup shall be as follows:
a. Maintain a basic test setup for the EUT.
b. Measurement system integrity check.
(1) Configure the test setup for the measurement system check as shown on Figure B.2. Ensure that the LISN power source is disconnected.
(2) Connect the measurement receiver to the 20 dB attenuator on the sign al output port of the LISN.
c. EUT testing.
(1) Configure the test setup for compliance testing of the EUT as shown on Figure B.3.
(2) Connect the measurement receiver to the 20 dB attenuator on the signal output port of the LISN.

B.1.3.4 Procedures.

The test procedures shall be as follows:
a. Measurement system integrity check. Perform the measurement system check using the measurement system check setup of Figure B.2.
(1) Turn on the measurement equipment and allow a sufficient time for stabilization.

(2) Apply a signal level of 90 dBμV at 10.5 kHz and 100 kHz to the power output terminal of the LISN. At 10.5 kHz and 100 kHz, use an oscilloscope, in high impedance mode, to verify that there is a proper signal level at the LISN and verify that it is sinusoidal. After establishing the proper signal at the LISN, disconnect LISN and measure resulting voltage using an oscilloscope with 50 ohm input impedance. The ratio of the LISN voltage to the 50 ohm voltage measurement must be within the following tolerances: at 10.5 kHz = -14 dB (+1 dB/-2 dB) and at 100 kHz = -3 dB (+1 dB/-2 dB).

(3) Apply a signal level that is at least 6 dB below the limit at 10.5 kHz, 100 kHz, 1.95 MHz and 9.8 MHz to the power output terminal of the LISN. At 10.5 kHz and 100 kHz, use an oscilloscope to calibrate the signal level. At 1.95 MHz and 9.8 MHz, use a calibrated output level directly from a 50 Ω signal generator.

(4) Scan the measurement receiver for each frequency in the same manner as a normal data scan. Verify that the measurement receiver indicates a level within ±3 dB of the injected level. Correction factors shall be applied for the 20 dB attenuator and the voltage drop due to the LISN 0.25 μF coupling capacitor

(5) If readings are obtained which deviate by more than ±3 dB, locate the source of the error and correct the deficiency prior to proceeding with the testing.

(6) Repeat B.1.3.4a(2) through B.1.3.4a(5) for each LISN.

b. EUT testing. Perform emission data scans using the measurement setup of Figure CE102-3. (1) Turn on the EUT and allow a sufficient time for stabilization. (2) Select an appropriate lead for testing. (3) Scan the measurement receiver over the applicable frequency range, using the bandwidths and minimum measurement times in the Table II. (4) Repeat 5.5.3.4b(2) and B.1.3.4b(3) for each power lead.

B.1.3.5 Data presentation.

Data presentation shall be as follows:

a. Continuously and automatically plot amplitude versus frequency profiles on X-Y axis outputs. Manually gathered data is not acceptable except for plot verification.

b. Display the applicable limit on each plot.

c. Provide a minimum frequency resolution of 1% or twice the measurement receiver bandwidth, whichever is less stringent, and a minimum amplitude resolution of 1 dB for each plot.

d. Provide plots for both the measurement system check and measurement portions of the procedure.

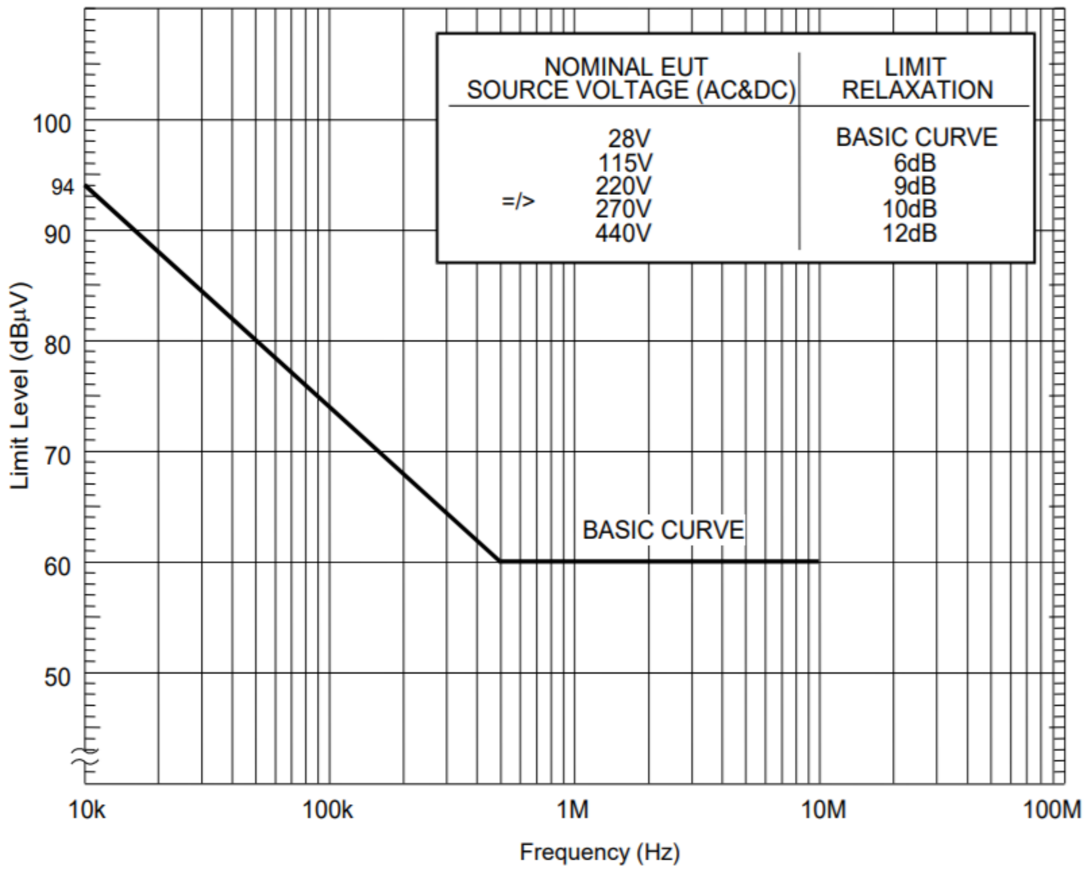

Figure B.1: CE102 limit (EUT power leads, AC and DC) for all applications.

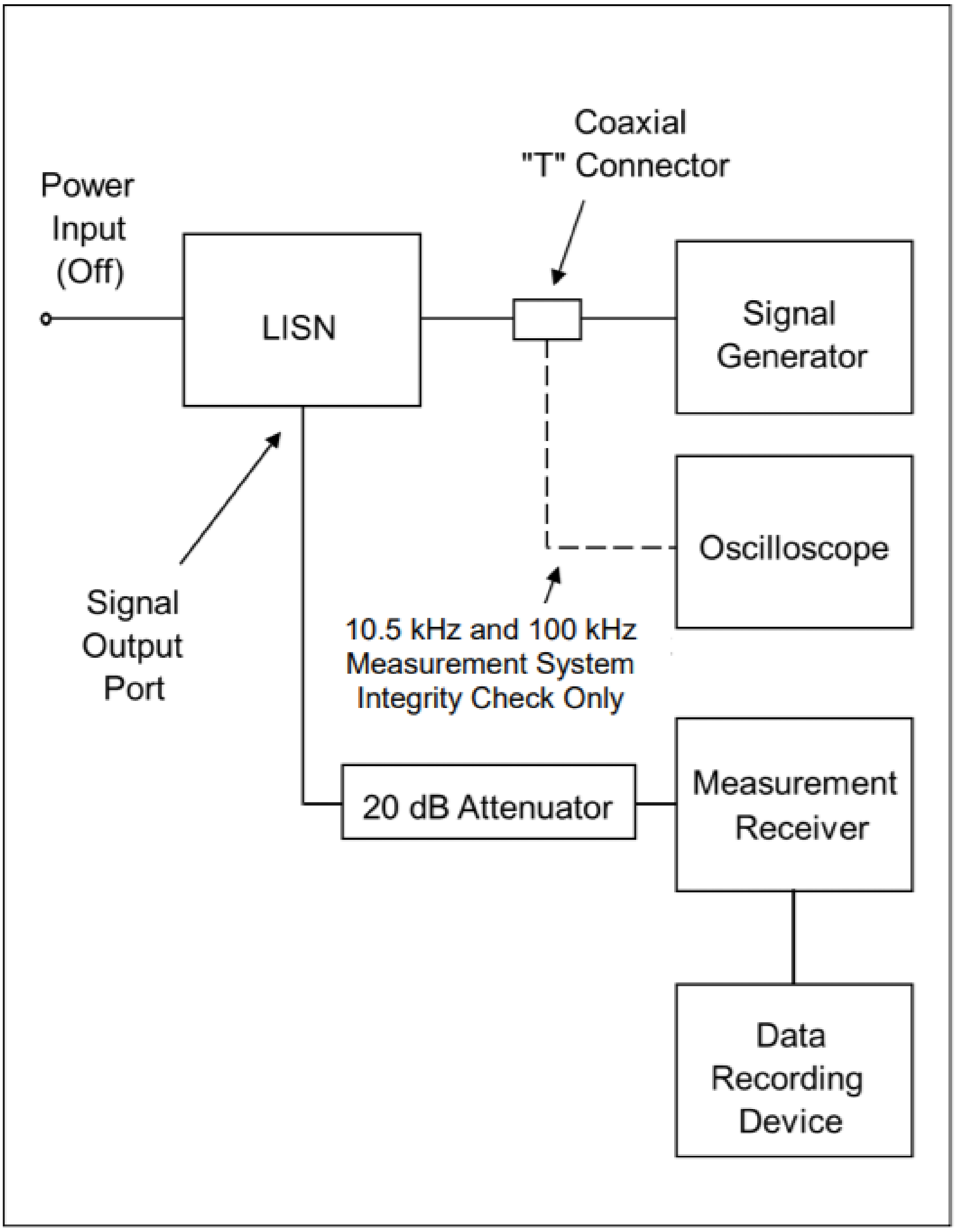

Figure B.2: Measurement system check setup.

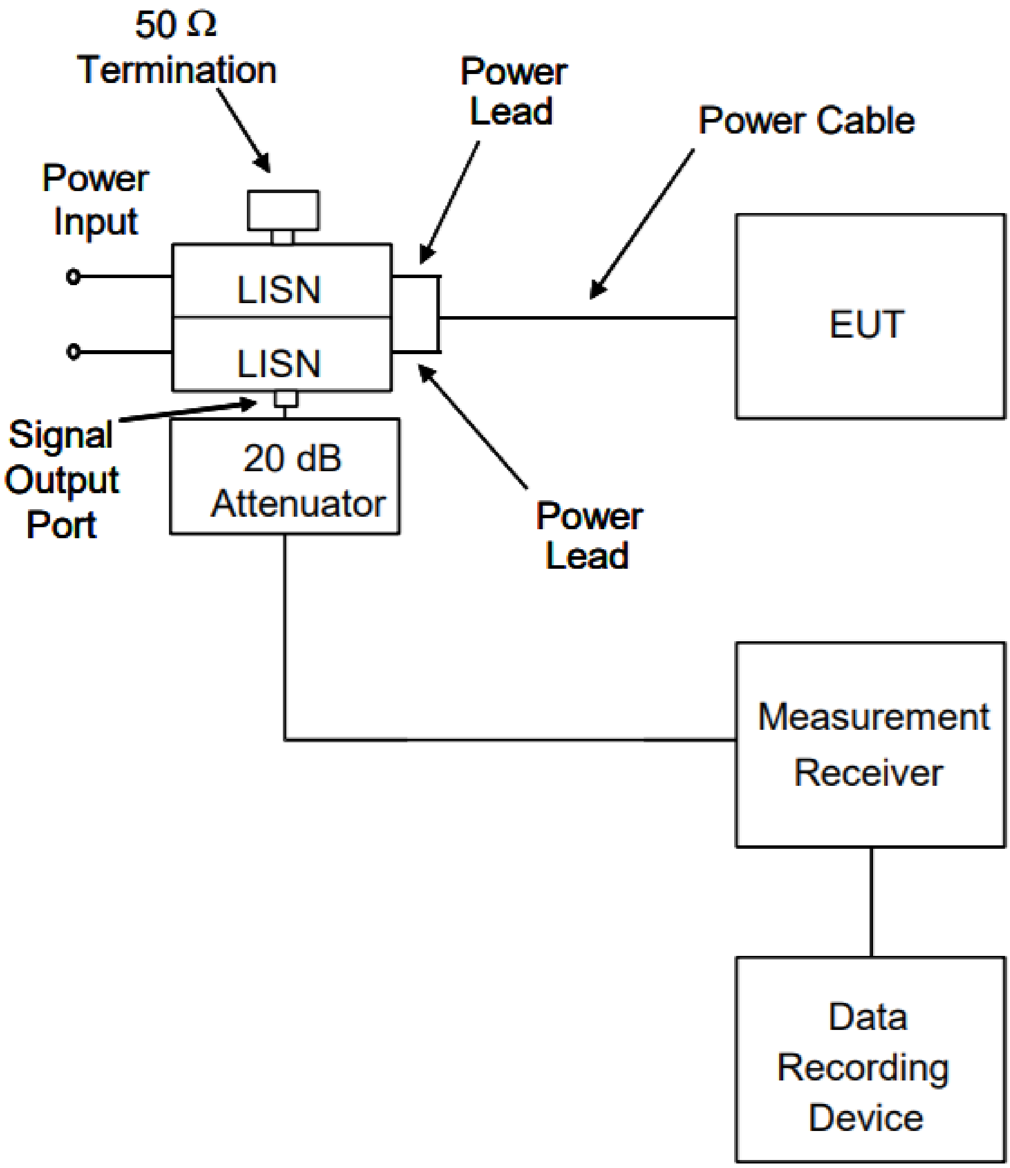

Figure B.3: Measurement system check setup.

CURRICULUM VITAE

Name Surname : Mehmet Eralp KÖSE